UNIVERSITY OF SOUTHAMPTON

FACULTY OF ENGINEERING, SCIENCE AND MATHEMATICS

School of Chemistry

The Production of Nitride Thin Films and Nanocrystalline Composites via a Sol-gel Methodology

by

Andrew William Jackson

Thesis for the Degree of Doctor of Philosophy

September 2007

UNIVERSITY OF SOUTHAMPTON

ABSTRACT

FACULTY OF ENGINEERING, SCIENCE & MATHEMATICS
SCHOOL OF CHEMISTRY

Doctor of Philosophy

THE PRODUCTION OF NITRIDE THIN FILMS AND NANOCRYSTALLINE COMPOSITES VIA A SOL-GEL METHODOLOGY.

By Andrew William Jackson

Metal nitrides are of great interest for the development of new engineering and catalytic applications based on their hardness, chemical and thermal stability. The development of sol-gel production methods for these materials, capable of producing films, powders and monoliths will broaden the range of nitride products possible and yield an important step forward in the general processing of this class of material.

The work presented in this thesis details the synthesis of titanium nitride and carbonitride thin films via sol-gel techniques using primary amines or stoichiometric amounts of ammonia as crosslinking agents. The results using primary amines were found to be the most promising, especially when deposited onto silica substrates. The characterisation and formation of nanocrystalline powders, produced by the ammonolysis of tetrakis(dimethylamino)titanium are also discussed, detailing their suitability for applications requiring ultra-hard composite materials. Finally a novel synthetic route which produced rigid gels made from the precursor amides tetrakis(diethylamino)titanium, tetrakis(diethylamino)hafnium or tetrakis(diethylamino)zirconium and stoichiometric amounts of ammonia in THF will be discussed. The potential to produce monolithic metal nitride gels suitable for supercritical extraction of the solvent, enabling the 'dried' product to be heated with a reduced risk of sintering, is also proposed.

TABLE OF CONTENTS

LIST OF FIGURES

LIST OF TABLES

ACKNOWLEDGEMENTS

I would like to thank the EPSRC (grant number GR/S/10155/01) for financing my research and paying me for three years! I would also like to thank Epichem, for their generous donation of TDMAT; the CCLRC and Fred Mosselmans and the SRS in Daresbury for the award of beamtime for my research under grants 40249 and 43057; Andy Wright at Thermo Electron Corp. and Rob Palgrave and Ivan Parkin at UCL for the XPS analysis of samples; Paul McMillan and Olga Shebanova for their help with analysis on nanocrystalline compounds; Barbara Cressey and Shuncai Wang, for their help when I had problems at the microscopy centre; Dr Baishakhi Mazumder for her assistance when it was required and for her continual good humour and I would also like to thank all those people who willingly helped me without question at the drop of a hat, even if it was just to hold the front of the glovebox on whilst I screwed it back together (again)!

I would also like to reserve a special thank you for my supervisor Dr Andrew L Hector. Without his patience, commitment, friendship and guidance I surely would not have managed to get here and owe him a debt of gratitude. Thank you, Andrew.

In my personal life a handful of people have steadfastly remained by my side offering me unwavering support and kind words of encouragement when I needed it most. My good friend Steve whose deprecating humour, passion for cars and unquestioning friendship ensured that I always had someone to turn to when I needed a friend; my sister Claire, who has helped me in more ways than I can remember and without her, my time in Southampton would surely have been that much more difficult. I would also like to thank my Dad for his unwavering support and words of encouragement which seem to pass his lips with every conversation we have had since I embarked upon this journey. I would also like to take the opportunity to thank both my Dad and my Mum, who sadly is no longer with us, for their insistence that I stay in school and strive to be the best I could be, I hope I've achieved all you hoped I would and that I've made you proud.

Finally, I would like to thank my girlfriend Jinny. I have never known anyone with such limitless depths of love and support. She has been my rock, standing by me when all I could do was act ill-tempered and stressed-out! Thank you, Jinny. I really couldn't have done it without you.

DEFINITIONS

2-2' Bipyridyl	BiPy
Ammonia	NH_3
Atmospheric Pressure Chemical Vapour Deposition	APCVD
Caesium Iodide	CsI
Centipoise	cP
Chemical Vapour Deposition	CVD
Concentric Hemispherical Analyser	CHA
Debye-Waller	DW
Degrees Celcius	°C
Electron Diffraction	ED
Electron Spectroscopy for Chemical Analysis	ECSA
Electronic-Grade	ULSI/BiP
Elemental Analysis	EA
Energy Dispersive X-ray Analysis	EDX
Extended X-ray Absorption Fine Structure	EXAFS
General Structure Analysis System	GSAS
Gigapascal	GPa
Gram	G
Infra-Red Spectroscopy	IR
Ionisation Constant	pKa
Kilo-electron-volt	keV
Low Pressure Chemical Vapour Deposition	LPCVD
Mass Spectroscopy	MS
Metal-Organic Chemical Vapour Deposition	MOCVD
Millilitre	ml
Millimetre	mm
Millimol	mmol

Molecular Equivalent	Mol
Nanometre	nm
Nuclear Magnetic Resonance	NMR
Oxygen Free Nitrogen	OFN
Physical Vapour Deposition	PVD
Aerosol Assisted Chemical Vapour Deposition	AACVD
Plasma Enhanced Chemical Vapour Deposition	PECVD
Potential of Hydrogen	pH
Powder X-ray Diffraction	PXD
Scanning Electron Microscopy	SEM
Silicon Tris(Disilylamide)	TDSA
Solid-in-Liquid	Sol
Tetrahydrofuran	THF
Tetrakis(diethylamino)hafnium	TDEAH
Tetrakis(diethylamino)titanium	$Ti(NEt_2)_4$
Tetrakis(diethylamino)titanium	TDEAT
Tetrakis(diethylamino)zirconium	TDEAZ
Tetrakis(dimethylamino)titanium	TDMAT
Tetrakis(dimethylamino)titanium	$Ti(NMe_2)_4$
Tetrakis(dipropylamino)titanium	TDPAT
Thermogravimetric Analysis	TGA
Titanium Nitride	TiN
Transition Metal Nitrides	TMNs
Transmission Electron Microscopy	TEM
Trifluoromethylsulphonic Acid	Triflic Acid
X-ray Absorption Near-Edge Structure	XANES
X-ray Absorption Spectroscopy	XAS
X-ray Photoelectron Spectroscopy	XPS
X-ray Photoelectron Spectroscopy	XPS

Table 1. Definitions

1 INTRODUCTION

Transition metal nitrides (TMNs) have attracted much interest in coatings research. The ability to deposit a ceramic coating onto a substrate, enabling it, for example, to become chemically, thermally and mechanically resistant to extreme conditions is important in order to utilise fully the bulk properties of many materials. In addition to the more established coating methods, such as chemical vapour deposition (CVD) and physical vapour deposition (PVD), there is an interest in sol-gel synthesis of nitrides. This is because of its potential to deposit films which, when annealed, form nitrides. Deposition by dip- or spin-coating would increase the range of applications in which they are viable and contribute to the inherent versatility of the synthetic method; it would represent an important step toward general sol-gel processing of nitride materials.

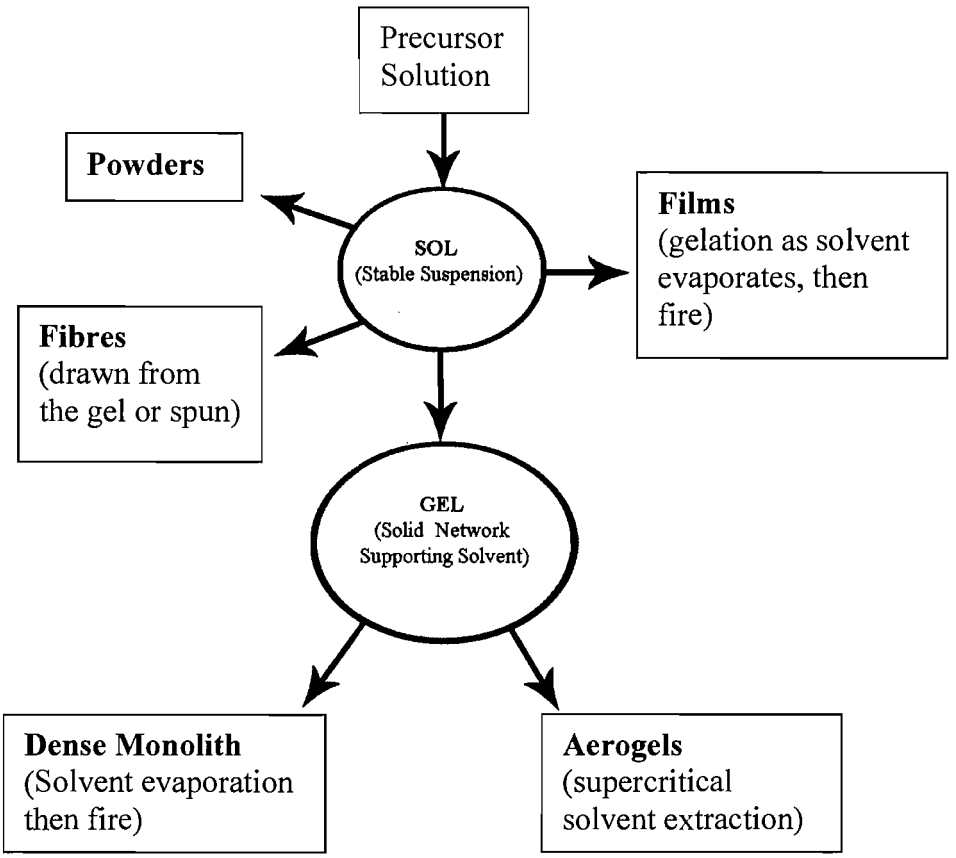

Figure 1.1: Examples of the products possible by sol-gel.

With transition metals, the ammono based analogue of the well established alkoxy route to gels is inherently difficult to control due to the basicity of the system. The overwhelming tendency is for the starting materials to favour particle growth which results in precipitation rather than a stable emulsion, unless both environment and synthetic pathway are carefully controlled. Hence reports to date of sol-gel routes to nitrides largely describe production of powders[1,2,3].

This thesis concerns the area of sol-gel processing of TMNs and reflects upon what is required to successfully produce various forms of nitridic material from solution based syntheses.

1.1 Transition Metal Nitrides

1.1.1 Physical Characteristics

Transition metal nitrides form a class of materials with unique physical properties[4]. These range from high temperature resistance[5], superconductivity[6] and hardness[7] to catalytic activity. Initial studies in the 1960s by D. C. Bradley *et al.* revealed that ammonolysis of amides with primary amines led to the formation of a variety of subtly different compounds.[8,9] In particular tetrakis(dimethylamino)titanium (TDMAT) (see Figure 1.2) was extensively studied.[9]

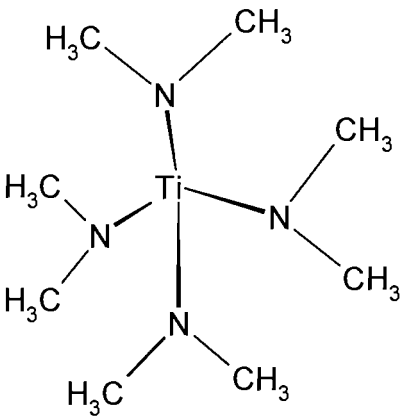

Figure 1.2: Tetrakis(dimethylamino)titanium.

Curiously, the annealing of these compounds was not apparently undertaken in the initial studies undertaken by Bradley *et al.* These compounds and similar amide precursor

complexes were subsequently proved to thermally decompose to form their respective nitrides[10,11].

1.1.2 Previous Research

Interest in the area was not resumed until the late eighties and mid nineties when the research groups of Brown and Maya[12], and Chisholm *et al.*[13] further investigated the properties of these precursor systems. The studies of Brown and Maya involved the reaction of a variety of transition metal amides with liquid ammonia and the study of the gaseous species yielded through the subsequent annealing of the solid products via mass spectroscopy. In their conclusions they stated that: "The general course of the thermal process in which the ammonolysis products are converted to refractory materials is dependant on the reaction conditions and the identity and valence of the metal". They also speculated on the formation of the Ti^{4+} spinel phase compound (Figure 1.3). The Ti_3N_4 was justified by ESCA binding energies of their titanium containing products that were 'characteristic' of Ti^{4+}. Chisholm *et al.* followed this research with a comprehensive study of amide precursor pyrolysis whilst again using MS, IR and also TGA in order to elucidate the composition of the materials produced pre- and post-pyrolysis.[13] They speculated that nitrogen rich Ti_3N_4 had been formed at lower annealing temperatures, this time relying on TGA and EA to endorse their conclusion, however, the existence of such a material has never been conclusively demonstrated; a Ti_3N_4 phase has been predicted *theoretically* to be stable in the spinel structure[14] although no material to date has been published conclusively identifying a titanium nitride spinel structure *via* a structural technique such as X-ray diffraction or EXAFS.

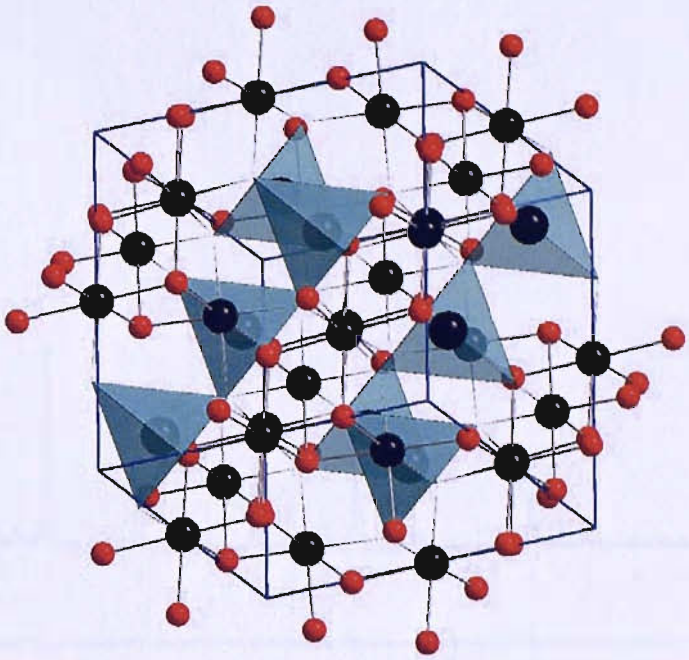

Figure 1.3: Spinel-type unit cell illustrating the structure of Si_3N_4/Ge_3N_4. Octahedral sites are in black and polyhedra are highlighted in cyan.

Ti_3N_4 is of great interest since the discovery of γ-Si_3N_4/Ge_3N_4[15,16] and the striking physical characteristics that were shown by these materials in comparison to α/β-Si_3N_4 (25% increase in density, a significant increase in elastic moduli and a microhardness of 30 – 43 GPa). Further investigation of the possibility of group 4 spinel phase nitrides by A. Zerr *et al.* led to the discovery of the Th_3P_4-type Zr_3N_4/Hf_3N_4[17] which were produced at 2,800 K and 18 GPa using a 'diamond anvil'[18]. Their findings indicated that the physical characteristics of the products were very similar to those of γ-Si_3N_4 (e.g. 30 GPa hardness value). TEM indicated that the material contained hafnium and nitrogen, and powder diffraction data indicated for hafnium, the presence of several new lines which could not be attributed to any currently known "subnitrides" such as Hf_3N_2 or Hf_4N_3 (see figure 1.4). Th_3P_4-type structures allow Raman-active vibrational modes (see figures 1.5 and 1.6) and these combined with the diffraction studies enabled the identification of the new phases.

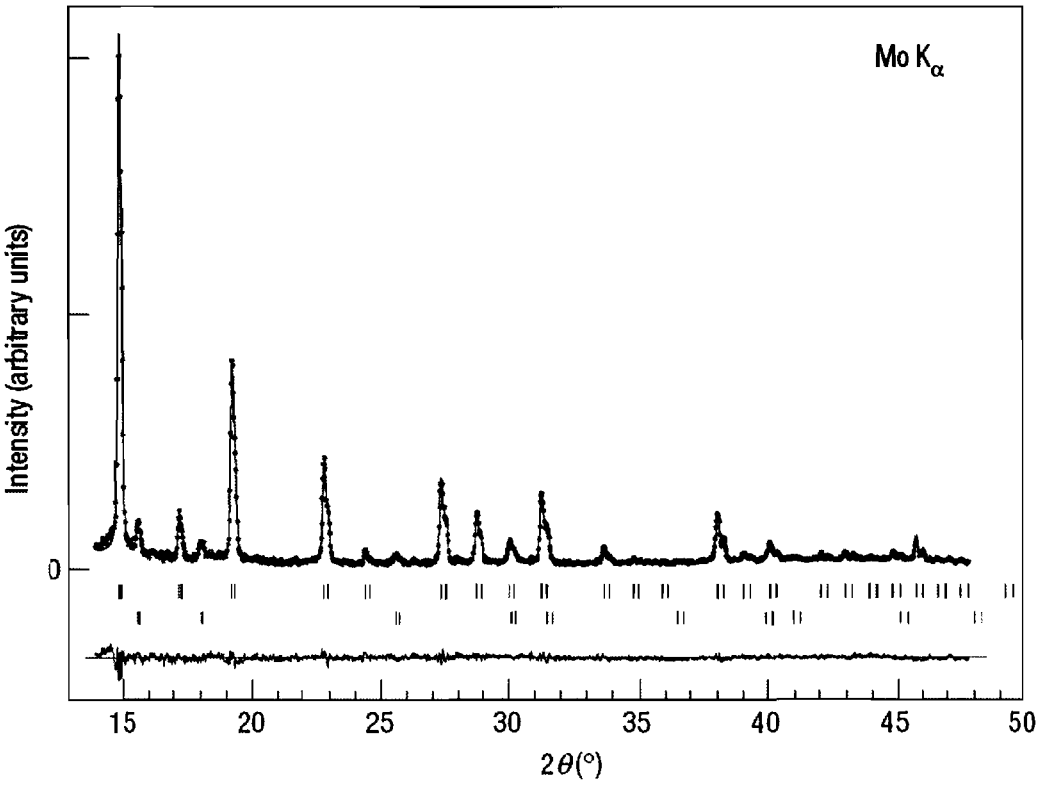

Figure 1.4: Diffraction pattern displaying c-Hf_3N_4 with an admixture of δ-HfN. Reprinted from reference 17, with permission from Nature Materials.

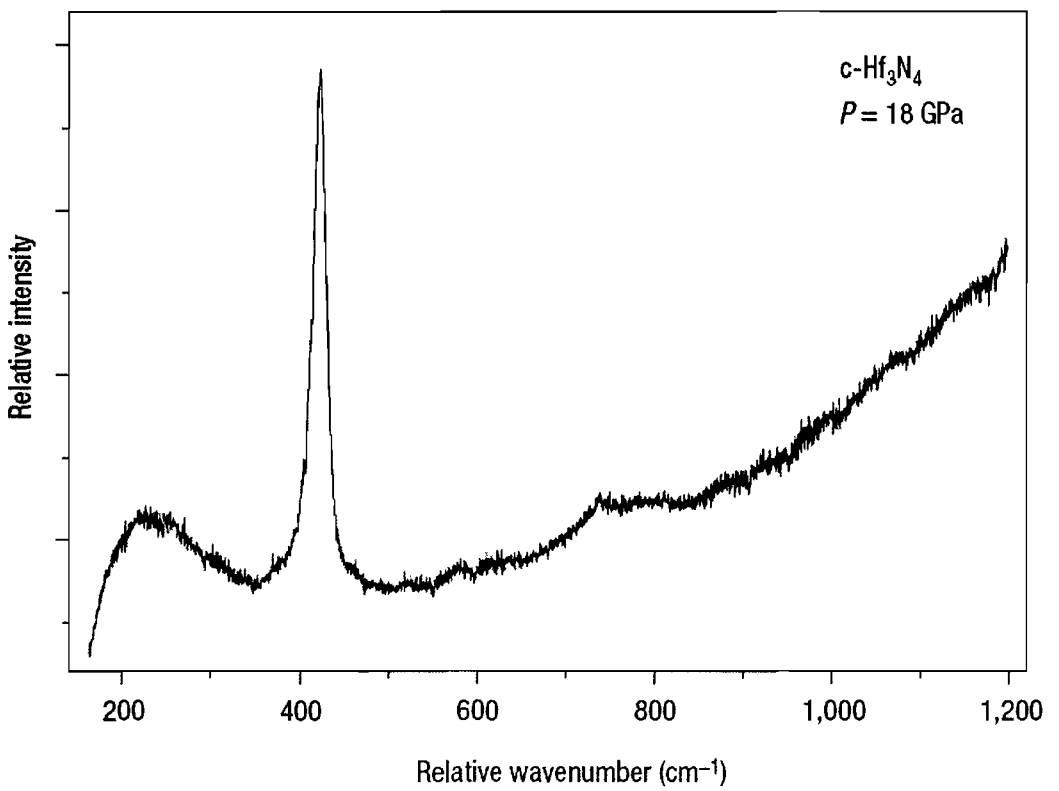

Figure 1.5: Raman spectrum of c-Hf_3N_4 synthesised at 18 GPa. Reprinted from reference 17, with permission from Nature Materials.

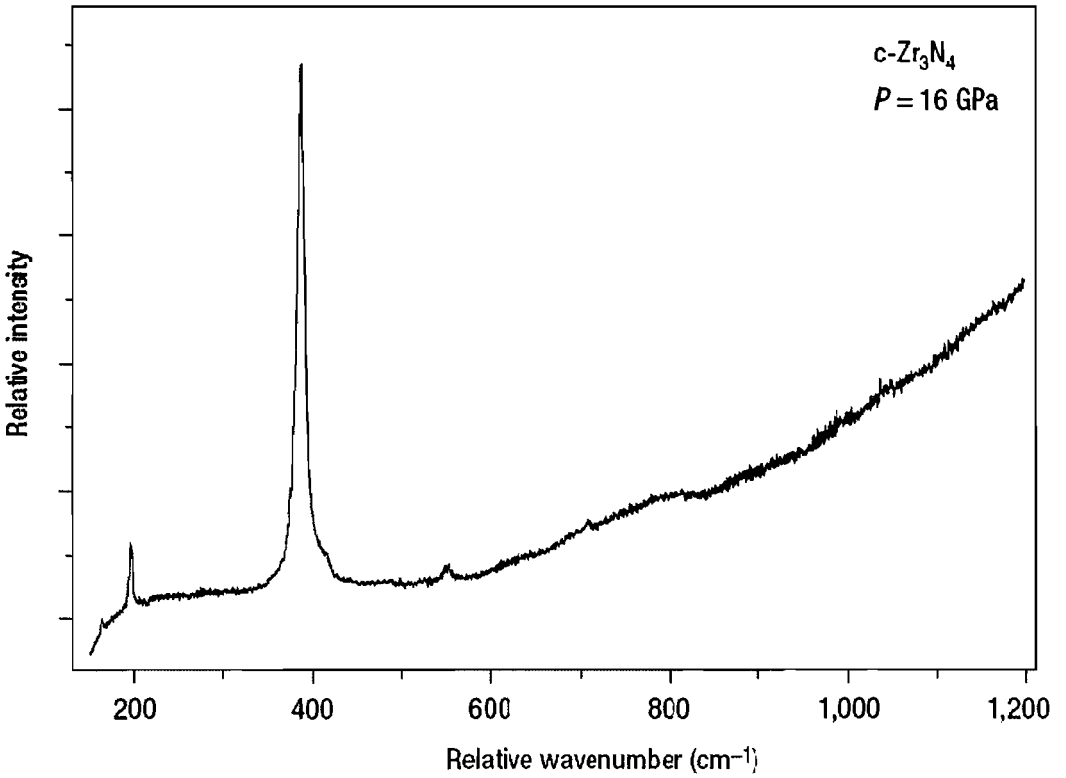

Figure 1.6: Raman spectrum of c-Zr_3N_4 synthesised at 16 GPa. Reprinted from reference 17, with permission from Nature Materials.

However, when the formation of Ti_3N_4 was attempted at conditions between 17.5 – 25 GPa and 1500 – 3000 K only cubic rocksalt-type TiN was produced (see figure 1.7); Ti_3N_4 had been theoretically predicted to be stable at pressures below 35 GPa[14]. Clearly it would seem that that the synthetic conditions are not currently understood sufficiently in order to successfully synthesise Ti_3N_4, however this does not rule out the possibility of its formation and it would certainly be of potential interest as a narrow band-gap semiconductor and as a high-hardness material.

1.1.3 Nitride Production Methods

Non-oxide ceramics can be produced in a variety of different ways. Solid state methods such as direct reaction of elements or carbothermal reduction[19] – wherein oxidic species are annealed at temperatures *circa.* 1200 °C with carbon and nitrogen or ammonia – are the commonest methods. Problems such as incorrect stoichiometry, unsuitable grain size, a lack of homogeneity due to agglomeration of the product material, or lack of complete

reaction within the reactive species are commonplace unless great care is taken during the numerous heating stages. The drawbacks of this method are compounded by the inherent high temperature stability of nitrides; once formed TiN has a melting point of circa. 3000 °C and the resultant products can be highly-agglomerated large-grained particles. To combat the unfavourable grain sizes mechanical grinding of the product, at intervals during the heating process, can be introduced to maintain a homogenous particle size distribution although this can cause the introduction of impurities from the apparatus and therefore is detrimental to the purity, and consequently the properties, of the product[20].

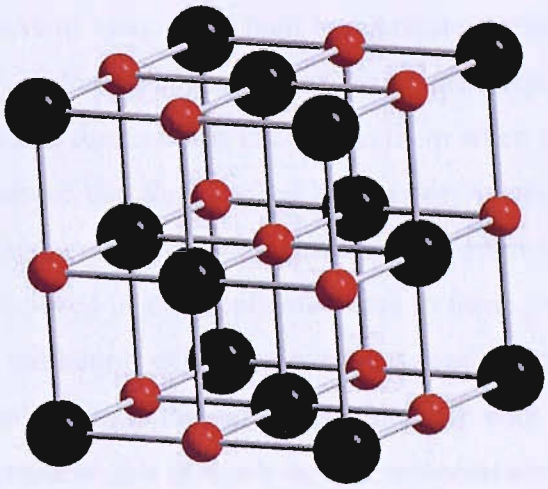

Figure 1.7: The cubic 'rock-salt' type structure exhibited by titanium nitride, with cations shaded in black and anions shaded in red.

Therefore developing new routes to transition metal nitrides which avoid these problems is an attractive area of research[4,6,21,22]. An approach that can potentially address these issues is the synthesis of ceramic precursors via sol-gel methods[19,23]. Using a sol gel method, solid material can be formed from a homogenous solution with all required constituents present, removing the need for grinding as the pre-annealed material is both finely divided and contains all or almost all constituents required for controlled decomposition to the target product.

Whilst sol-gel processes for the formation of oxides are highly developed and can deliver thick or thin films, precise monoliths, powders, grains, spheres, fibres, composites, porous gels and membranes, only a handful of precursor routes are used to any great extent in the synthesis of TMNs[24,25,26,27]. An ideal route would involve the production of a precursor

material from non-oxide materials which, when heated, would form the desired product without any additional heating or modifying steps.

1.2 Coating with Nitrides

A variety of coating methods for metal nitrides have been developed over the years which allow the modification of a substrate's physical and chemical performance. The physical requirements of the coating can differ markedly, for example being required to maintain chemical stability or structural integrity at high temperatures, resist high rates of wear, or be chemically inert; in motorsport, suspension parts are required to withstand high temperatures due to frictional forces being exerted on them when being used on-track. The coating is employed to ensure that the expelled heat-energy is efficiently conducted away from the suspension components in order to maintain optimum performance[28]. Titanium nitride has been frequently used in this application due to these properties and in addition to its practical abilities, marketing departments have seized on the aesthetic qualities of nitride coated parts and sold them to the public, as is the case with TiN coated parts, on the strength of their gold appearance just as much as their technical abilities[29].

1.2.1 Vapour Deposition Methods

Chemical vapour deposition (CVD) processes been developed to meet the high-performance demands of nitride coated substrates, with the earliest reports utilising metal halides, nitrogen and hydrogen at high temperatures[30]. CVD is a highly developed deposition method which is exemplified by the range of subtly different deposition methods currently used, all of which provide advantages to the application in which they are used. An example of such a variation is "aerosol assisted" chemical vapour deposition or AACVD. In this technique the precursor is atomised usually by ultrasound to produce a gas/liquid aerosol that can then be effectively transported to the target substrate. This is usually performed with non-volatile precursor materials.

The CVD process involves a precursor being deposited from a gaseous state inside a reaction chamber (see Figure 1.8); precursors must be volatile, but at the same time stable enough to be able to be delivered to the reactor, for example

tetrakis(dimethylamino)titanium, along with a reactive gas, such as ammonia. Both are usually diluted in a carrier gas and are pumped into a reaction chamber, at which point they are exposed to a heated substrate.

The action of coming into contact with the heated substrate causes the gaseous precursors to react or decompose onto the surface of the substrate forming a solid layer. The substrate temperature is critical and can influence the qualities of the deposited film.

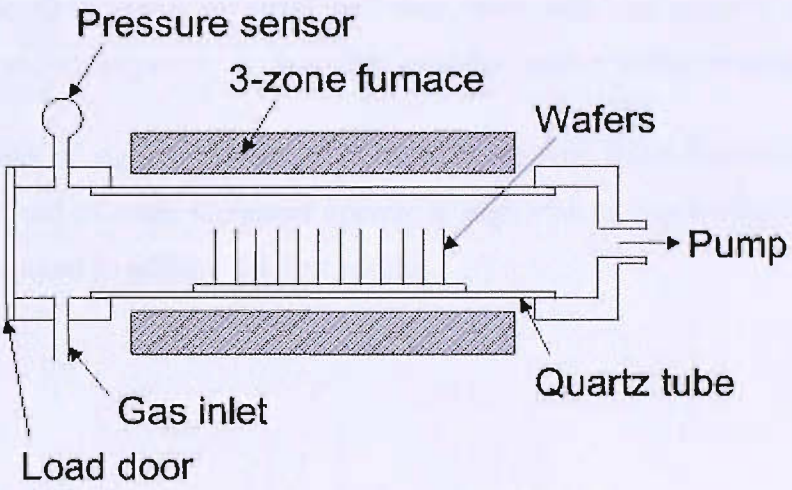

Figure 1.8: A typical CVD reactor.

A major consideration of CVD is the by-product of the deposition process; the reagents used usually produce toxic, volatile or corrosive gases so must be treated appropriately. However, by analysing the exhaust gases via a method such as mass spectroscopy the reaction mechanism can be better understood and the information used to refine the process.

1.2.2 Physical Vapour Deposition

Physical vapour deposition (PVD) is a vaporisation coating technique, involving transfer of material on an atomic level. The process is similar to chemical vapour deposition except that the raw materials/precursors start out in solid form and are evaporated, whereas in CVD, the precursors are introduced to the reaction chamber in a gaseous state.

During evaporation, a 'target' consisting of the material to be deposited is bombarded by a beam of electrons or ions. This dislodges atoms from the surface of the target, or 'vapourises' it and is then transported to a reaction chamber by action of a pressure gradient. As this process is a 'line-of-sight' technique, the electron beam and reaction chamber is in series so consequently the 'target' substrates can only be flat.

In the instance of metal nitride coatings, the target will consist of the metal, whilst an ammonolytic or N_2 atmosphere provides the nitrogen containing aspect of the coating layer. The vapourised atoms of metal will then react with the reactive gas during the transport stage and subsequently be deposited onto the surface of the substrate.

As PVD is a line of sight technique, it is difficult to coat three-dimensional objects or surface features and as some processes operate at high vacuums and temperatures, skilled operators are required to achieve the best results.

1.3 Sol-Gel Processing

1.3.1 The Development of Sol-Gel Techniques and Science

A sol is a colloidal chemistry term which is an abbreviation for 'solid-in-liquid'. More accurately it can be defined as a dispersion of colloidal particles suspended in Brownian motion, within a fluid matrix. At normal temperatures thermal motion and convection currents are sufficient to counteract any tendency for sedimentation and provided the colloidal particles remain stable, a uniform suspension will be observed.

The earliest recorded uses of 'sols' dates back to the Lascaux cave paintings (see figure 1) in France, *circa* 15,000 BC[31] where finely ground carbon, clay and iron ore were used as pigments and dispersed into water, with natural oils being used as surfactants to keep the suspension stable. Further references throughout history are present, examples include: building products used in the bible[32]; silicate glazes for porous containers from 4000-2000BC[33] and cements for structural applications[34].

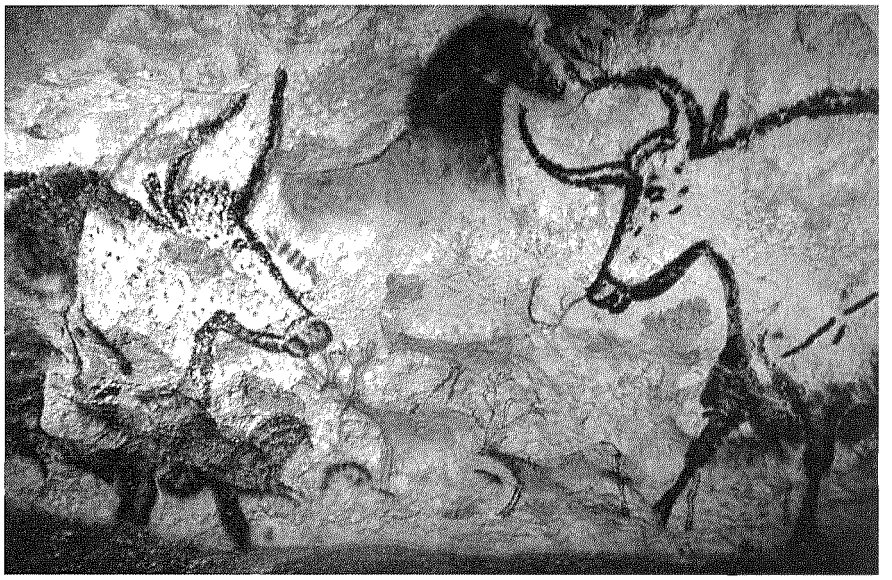

Figure 1.9: The Lascaux cave paintings, thought to have been created using basic 'sols' *circa.* 15,000 BC.

'Sol-gel' science was first recorded in 1644 by von Helmot[35] when, upon acidification of dissolved silicate materials in alkali, a precipitate equal in density to that of the original

silicate dissolved was observed, this was taken a step further in 1779 by Bergman[36], when he discovered that if the correct amount of acid was used in a sol, rather than precipitate being formed the mixture would gel. In the 19th century oxide materials were produced from hydroxide gels[37], however, it was not until the early 20th century when sol-gel techniques would capture the scientific community's interest; W.A. Patrick demonstrated how a homogenous silica gel could be fired to make a highly porous form of silica[38], he went on to develop the material as an effective catalyst support. Interest in the area was now huge[39] and the modern sol-gel technique was born.

1.3.2 Utilisation of Sol-Gel Methods for Oxide Materials

Sol-gel processing takes a sol and through interaction with a reactive species, induces gelation and thus can be used to form a film or monolith. However, the biggest strengths of sol-gel processing lie in its versatility, as there can be a large variation in the physical and structural appearance of the end-products simply by adjusting concentrations of the starting materials. The development of the 'modern' sol-gel technique is based upon the processing of silicate materials from gels[40] created from silicon alkoxides.

A typical mechanism for the gelation of an oxide based silicon system involves the nucleophilic substitution of a silicon alkoxide group with a hydroxide group.

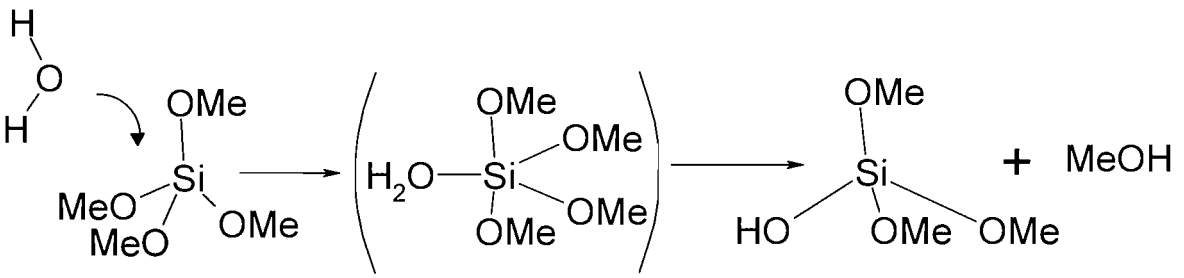

Figure 1.10: A typical mechanism for the gelation of an oxide based silicon system.

Due to the low nucleophilicity of water and the steric unfavourability of forming a 5 – coordinate transition state, the rate of substitution and molecular cross-linking is very slow. Therefore, the reaction is almost always catalysed with either a small amount of acid or base. The effect of the acid is to protonate the alkoxide groups, increasing the effective positive charge at the silicon by reducing the polarisation of the bond. A base catalyst deprotonates the water and increases its nucleophilicity. These methods of catalysis

continue throughout the process of condensation, with acid-catalysed reactions promoting fast nucleation throughout the sol followed by slower particle growth, leading to cross-linking and a long-chain polymeric network, whilst base-catalysed reactions lead to the formation of highly substituted clusters with fewer cross-links.

Taking into consideration the differences in the products from either route, it is possible to tailor a product for a desired end-use by using a specific synthetic route, for example, a catalyst bed would require homogenous pore size and a uniform repeat structure on a macromolecular scale, something which the acid catalysed process could feasibly produce, whereas an application requiring nanocrystalline powders with a high compressive strength, could utilise the base catalysed route which produces amorphous or crystalline particles, often with high performance mechanical properties[41].

When these mechanisms are transposed to a system involving metals another factor needs to be considered; the reactivity of the starting materials can be substantially different. If the central metal atom has a greater nucleophilicity or has a larger co-ordination sphere the propensity for substitution of ligands or addition is much greater and can lead to difficulties in the preparative steps of sol generation, resulting in the precipitation of materials, or a lack of gelation altogether.

Control can be sought through the use of more sterically hindered alkoxides or, if reaction modifiers are included in the reagent mixture, blocking potential reaction sites and thus reducing the availability of free sites which would otherwise contribute to unwanted addition reactions.

An example of a method which utilises the ammonolysis of oxidic precursors was developed by Nakane *et al.* In this method, a transition metal oxide is produced via a sol-gel methodology and then heated under an ammonolytic atmosphere at high temperatures[42]. (see Figure 1.11) offers an example of how the ammonolysis would most likely proceed:

$$Ta_2O_5 + 2C + 2NH_3 \longrightarrow 2TaN + 3H_2O + 2CO$$

Figure 1.11: The ammonolytic process followed by tantalum oxide in the formation of tan.

Whilst this method proves to be successful at producing Tantalum Nitride there are two inherent problems with a method such as this. Firstly, as the precursor is an oxide, it can never be assumed that all oxygen is eliminated after the nitridation process is complete; the potential for oxygen to either be trapped within the macro-molecular structure or to be unreacted due to insufficient penetration by the reactive gas is always going to be a problem. This is due to the refractory nature of the nitride; as the material is synthesised from the oxide, it effectively becomes a thermal barrier for any unreacted oxide material deeper inside the substrate. Secondly, due to the very high temperatures which are required to convert the oxide to its nitride analogue, morphological changes can occur to the structure of the product, thus, if a nitride were required in a specific morphology, this methodology would be inadequate for such a purpose; oxides can readily sinter at lower temperatures than the conditions which are required to effect the transformation of the oxide to the non-oxide analogue.

1.3.3 Utilisation of Sol-Gel Methods for Non-Oxide Materials

The basic principle of sol-gel synthesis is the controlled hydrolysis, or in the case of ammono systems *ammonolysis*, of a metallo-organic compound in an organic solvent (ideally aprotic and of medium polarity). The reaction proceeds via a sequential series of ammonolysis, condensation and addition steps which firstly form colloidal agglomerates and then coagulate to form a gel. The rate of condensation can be controlled by factors such as reagent, solvent, reaction temperature, concentration and the presence of reaction modifiers. Once the gel is formed, removal of the solvent and organic fragments (achieved by ventilation of the gel containing vessel under an inert atmosphere, followed by 'mild' heating ~200 $^{\circ}$C) results in a powder which, depending on the concentrations/solvents used, should be of specific morphology, pore size etc. These factors also affect the physical characteristics of the gel and thus can be exploited to design a sol suitable for dip coating.

Non-oxide ceramic materials can be synthesised via a number of different reaction pathways such as the ammonolysis of silicon amides developed by Bradley *et al.* which has spawned a variety of hybrid routes wherein, the ammonolysis of $Si(NMe_2)(NH_2)$ *via* acid catalysis has produced a translucent semi-rigid gel[1,3,21]. It was initially thought that the role of the acid catalyst in this reaction was to act as a protonating species for the bridging

nitrogen of the dialkylamine branches of the amide, in order to promote the dialkylamine as the favourable leaving group and thus be more susceptible to transamination with the ammonia, due to the increased positive charge. However, now it is thought that in the case of CF_3SO_3H, the dimethyl amide groups are protonated and subsequently ejected from the metal amide, whilst the triflate remains attached to the central metal giving the amide an ideal leaving group for both the ammonolysis and condensation stages.

Another method involves the co-ammonolysis of alkylamides developed by Jansen *et al.* [23], here, using two "elementalylamide" reagents which possess similar ammonolysis rates, reactions can produce tertiary silicon nitrides by solvating the two amides in a common solvent at low temperature and ammonolysing the solution to create a polymetallosilazane precipitate. It is thought to follow the general reaction described below.

$$\text{M-NRR'} + NH_3 \longrightarrow \text{M-}NH_2 + \text{HNRR'} \qquad \text{(Ammonolysis)}$$

$$\text{M-}NH_2 + \text{M-NRR'} \longrightarrow \text{M-NH-M} + \text{HNRR'} \qquad \text{(Condensation)}$$

$$\text{M-}NH_2 + \text{M-NRR'} \longrightarrow \text{M-}NH_2\text{-NRR'M} \qquad \text{(Addition)}$$

Figure 1.12: The three stage process by which it is thought co-ammonolysis of alkylamides proceeds.

The solid powder precursor yielded from the reaction was then annealed under anhydrous ammonia at 1000 °C to give a mixed metal nitride.

The direct reaction of *B*-trichloroborazene with bis(trimethylsilyl)carbodiimide[43] is a very different approach, delivering a single-source precursor which could be annealed under an inert atmosphere to yield a tertiary nitride via the following general reaction scheme:

$$RSiCl_3 + (SiMe_3)_2NCN \xrightarrow{\text{Pyridine}} RSi(NCN)_{1.5} + 3(CH_3)_3SiCl \xrightarrow{\text{Heat}} R(C,N)_z$$

Figure 1.13: The carbodiimide-based sol-gel route, illustrating the production of silicon carbo-nitride.

1.3.4 Sol-Gel Processing for Nitrides

Sol-gel processing involves the generation of colloidal suspensions (sols), their subsequent conversion to viscous gels and then to a solid material. This process occurs in 4 stages; gelation, ageing, drying and densification. The method used in the work presented here

takes the relatively well established alkoxy route, which generally involves the reaction of a metal alkoxides with an alcohol and water, and re-applies the theory with nitrogen containing analogues, namely transition metal amides and amines. The successful production of a sol or sol-gel is dependant upon many prerequisites such as reagent solubility, concentration gradients, viscosity, steric factors and impurity inhibition, however, if all these factors can be correctly controlled or expelled from the reaction scheme, production of a gel should – in theory – be possible.

1.3.5 Condensation

Condensation reactions involve the substitution of the dialkylamine 'branches' with NH_2 groups. These groups can then cross-link with other tetrakis(dimethylamino)titanium molecules creating dimers with an NH bridge.

The key to successfully producing a gel is in the initial production of the colloidal particles. The initial step requires 'supersaturation' (the maximum concentration of reagent that can be solvated into the reaction media without observing precipitation) of the transition metal amide with the chosen amine. Due to the various basic values of the different amine, amide and THF constituents, the mechanisms by which the reactions take place can only be base catalysed. This means that due to inductive and steric effects, the nucleation reactions self-propagate as the target material becomes more substituted leading to tight clusters with few cross-linkages (see Figure 1.14), the opposite of acid-catalysed which does not self-propagate, allowing for the generation of cross-links (see Figure 1.15) and if this remains uncontrolled, precipitation can occur. However, if controlled correctly, successful gelation is possible albeit dependant on the nature of the method of catalysis, see below.

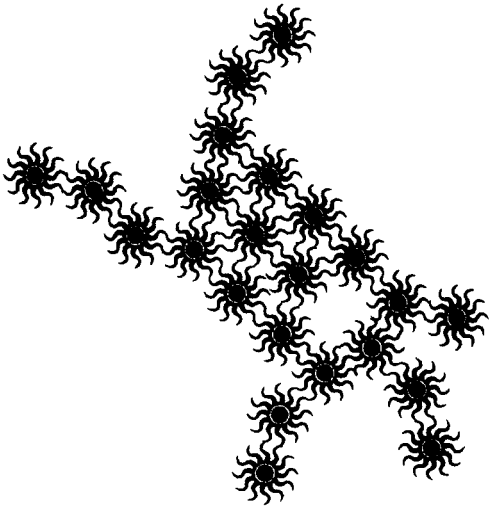

Figure 1.14: The product of base-catalysed condensation reactions; branched, highly agglomerated clusters.

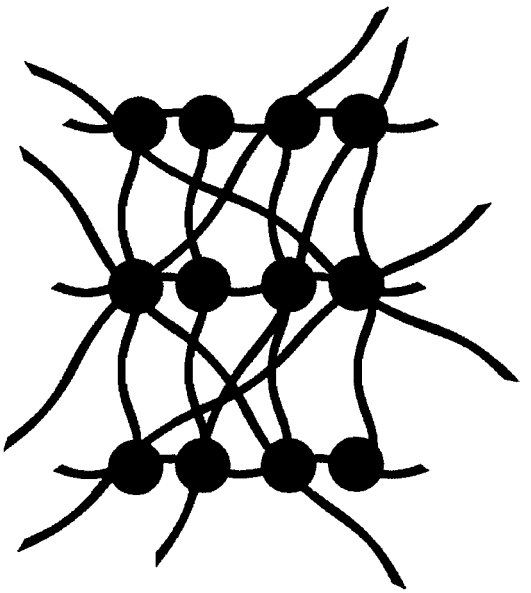

Figure 1.15: The product of acid-catalysed condensation; linear, randomly branched polymers.

An explanation of base-catalysed gelation using ammonia is as follows:

The initial dialkylamine groups on TDMAT are less electron donating than the incoming NH_3 groups being used to transaminate the amide. However, due to the steric hindrance of the dialkylamide groups the ammonia is unable to easily transaminate with the existing dialkylamine groups. Once the displacement of one dialkylamine group is achieved the

transition state is destabilised as there is less steric hindrance, exposing the central metal to a greater number of attacks from the NH_3 groups. Subsequently the rate of transamination increases. This is an iterative cycle and increases in speed proportionally with substitution and thus gives rise to the problem of the reaction favouring particle growth.

Restrictions are required in order to achieve a rate of nucleation sufficient to compete with the overwhelming tendency toward particle growth; reduced concentrations of starting material is an option which can result in the reduction of particle growth, through the starvation of starting materials which could be ammonolysed. Reducing the reaction temperature is another method which can suppress the rate of transamination, potentially increasing the chance of nucleation.

1.3.6 Gelation

Gelation occurs when the amide sols crosslink to such an extent that a 'framework' spans the containing vessel. The viscosity of the material increases dramatically, although the gel is not fully formed, with the framework trapping sols. This is embodied physically by the solution displaying viscosity but not elasticity. Eventually, when the entrapped sols crosslink with the existing framework, the gel then gains elastic properties too.

1.3.7 Syneresis

Syneresis is the continued cross-linking and 'trans-pore' condensation reaction of the newly formed gel. The rate of syneresis is dependant upon pH, temperature and gel composition. The overall result of this process is a gradual shrinking of the gel due to weak interactions being replaced by newer stronger bonds of a finite length. This shrinkage leads to expulsion of liquid from the gel and manifests itself with the transition of the homogeneous gel to a shrunken monolith immersed in liquid.

The final effect that may happen is phase transformation. This occurs only when gelation has occurred very quickly or where several precursors of differing solubility have been used. Generally the resultant material has a varied structure and composition, localised in the areas which have reacted in a different manner to the reaction media as a whole. The

result is a material which appears phase separated with discoloured areas. This phenomenon can only be removed by modification of the reaction rate, or substitution of co-solvents.

Possible Advantages of Sol-gel Processes for Nitrides

- These are low temperature processes therefore thermal degradation and high stoichiometry can be achieved
- Highly porous and nanocrystalline materials can be produced
- Pore sizes can be tailored by the modification of reagents or the control of initial nucleation and/or condensation.
- Templating of pores can be achieved by the entrapment of species into the gel
- Due to the material being a gel, the casting of complex shapes can be achieved without the need for melting or machining
- Synthesis is below the materials crystallisation temperature, thus amorphous analogues can be produced.

Limitations

- The amide precursors are expensive and highly sensitive to moisture
- These are time consuming processes
- Scale-up may be difficult
- Ageing and drying are difficult to control
- Densification can involve dimensional change

1.4 Summary and Aim of Thesis

Due to the analogous nature of nitrides versus oxides, sol-gel presents itself as an ideal technique to be employed for the synthesis of nitride coatings. Sol-gel techniques can already access a variety of morphologies which would be of great interest if nitride materials could be manipulated in the same manner, for example, templating methods

which can produce ordered mesoporous and macroporous arrays are of great interest for catalytic and filtration applications[44]. The aforementioned problems with the high-temperature ammonolysis of oxidic species could be avoided also, if the precursor were to already possess a nitrogen-rich composition requiring either and inert or ammonolytic atmosphere and high temperature to finish the synthetic process.

Ultimately the ability to create a sol precursor which could then be applied to a substrate by either simple dip- or spin-coating would open the door to a range of new possibilities and applications for nitrides which have otherwise remained closed due to technical or synthetic difficulties.

This project aims to give a solution to this situation, firstly, by understanding the dynamics of the ammonolysis of transition metal amides, and then working systematically to provide a number of possible methods which can be used to create ammonolytic sols, which can either be used to coat substrata or be allowed to gel to produce monolithic nitride materials.

2 INSTRUMENTAL METHODS OF ANALYSIS

2.1 Introduction

The following chapter details the techniques used for the characterisation of the films and powders which were produced throughout the study for this thesis. For powders the techniques included PXD, IR, EA, TGA, SEM, EXAFS and EDX, and they focused on the characterisation of chemical composition and atomic structure. For films deposited onto silica and alumina substrates SEM, XRD, EDX, XPS and TEM were used to characterise their thickness, composition, quality and atomic structure.

2.1.1 XAS

X-ray Absorption Spectroscopy (XAS) experiments were performed in order to establish inter-atomic bond distances, atomic composition and bonding geometry of the samples analysed and required a high intensity beam of polychromatic X-rays to perform the analyses. This could only be produced by the means of a 'synchrotron' which employs the use of bending magnets to amplify the energy of a beam of X-rays in accordance with the equation in Figure 2.1where EC is the critical energy of the X-ray photons, B is the strength of the magnetic field bending the electron beam and E is input energy.

$$EC = 0.667\, BE^2$$

Figure 2.1: The equation for the production of synchrotron X-ray radiation.

When a photon of a particular wavelength interacts with an atom, it may be absorbed. This 'excitation event' causes the ejection of a core electron of energy equal to that of the X-ray photon minus the binding energy of the departing electron. This causes the emission of a photoelectron wave from the absorbing atom, which consequently interacts with the surrounding atoms in the local environment of the excited atom (termed as backscattering, see Figure 2.2) and consequently a spectrum is produced from the interaction between these photoelectrons and the incoming beam of monochromated X-rays.

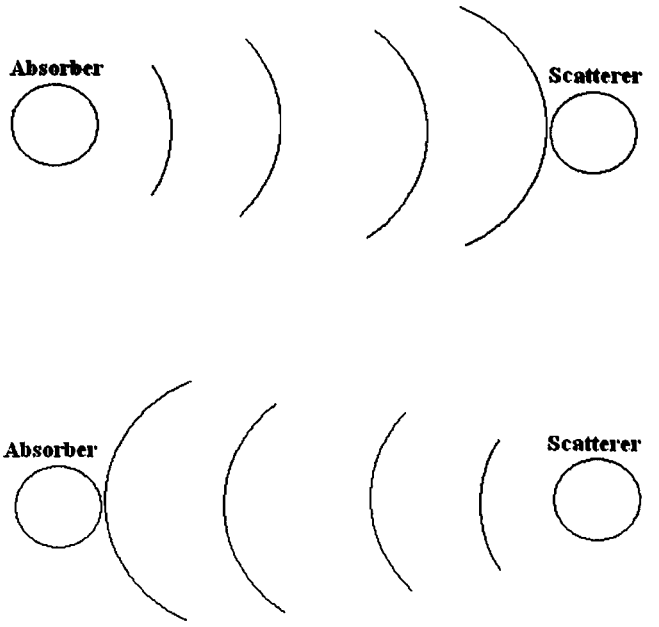

Figure 2.2: An illustration of back scattering.

Further to the phenomenon of backscattering, multiple scattering occurs when an ejected photoelectron encounters more than one backscattering atom before returning to the absorbing atom, and can affect the overall spectra collected substantially. Multiple scattering is particularly common in high symmetry molecules, simply due to the ordered arrangement of atoms within the matrix and the subsequent likelihood of the photoelectron interacting with more than one atom during its excitation.

X-ray absorption spectroscopy was performed at the SRS at daresbury laboratories on station 7.1 to ascertain local structural information about the titanium nitride products yielded from various precursor experiments. Station 7.1 was designed for X-ray absorption spectroscopy in the region of 4-12 KeV which is ideal for the titanium-based ceramic materials whose K-edge occurs at ca. 4977 eV. The beam size was 2.5 mm in diameter enabling small sample sizes to be analysed which again was ideal for the quantities of sample being produced in the laboratory.

All samples to be analysed were prepared in a nitrogen atmosphere glovebox, using boron nitride as an inert media in which the samples were diluted. This was done in order to ensure that the target sample did not absorb too many X-rays and thus give too strong a signal which would have been unrefinable. These samples were then sealed inside a brass washer sandwiched between two pieces of mylar film. This was done to prevent any

hydrolysis or oxidation of the sample from occurring; as XAS is sensitive to the oxidation states of the constituent elements any metal oxide or hydroxide would affect the structural data acquired.

Samples were pre-annealed in sequential 100 °C steps from 400 to 1000 °C, in order to establish the structural changes that occurred during the pyrolysis of the titanium precursor material. As crystallinity was only expected at the highest annealing temperatures, in line with the densification and crystallisation which is commonly observed in the thermolysis of ceramic precursors, it was expected that the 'low' temperature annealed samples would exhibit disorder throughout the atomic structure.

As high levels of long-range order were present in the high temperature annealed TiN samples, structural vibrations caused by the action of the impacting X-rays during analysis could be accounted for during the modelling of the resultant spectra. However, as the 'lower temperature' samples possessed no such order the task of resolving the structure was made proportionally more difficult. Therefore a cryostat was incorporated into the analysis technique to assist in arresting the atomic vibrations and enable the disordered ceramic to be structurally characterised.

EXAFS Data Analysis

Inelastic scattering background interference was removed from the X-ray data using the software 'PAXAS'[45]. Once this was achieved structure refinement of the data could be performed using 'EXCURV98'.

Curved wave theory was used in all refined structures as this suits structures which contain 'light' backscatterers (i.e. nitrogen). The principles of the theory are based on the path of an X-ray being a wave. Sometimes to enable approximate calculations on lower powered machinery, the simpler 'small atom theory' is used (wherein the path of the X-rays is linear).

In a structure containing 'light' backscatterers – atoms which have a lower density and thus are more susceptible to the incoming incident radiation – the structure is more likely to display apparent disorder, due to the ease at which motion can be incited within the

structure; using curved wave theory serves to counter this phenomenon as a more accurate model of the scattering can be calculated.

XAS was useful for the structural characterisation of the samples. The most useful aspect of the technique was the ability to elucidate structural information from amorphous materials.

2.1.2 XANES

X-ray absorption near edge structure (XANES) occur as part of EXAFS in the 'near-edge' region of the X-ray absorption spectra; within a proximity of +/- 40 eV.

When X-rays pass through a material, a proportion of the photons are absorbed, measuring the amount of absorption whilst increasing X-ray energy can reveal so-called edge structures; the point at which the level of absorption suddenly increases (see Figure 2.3).

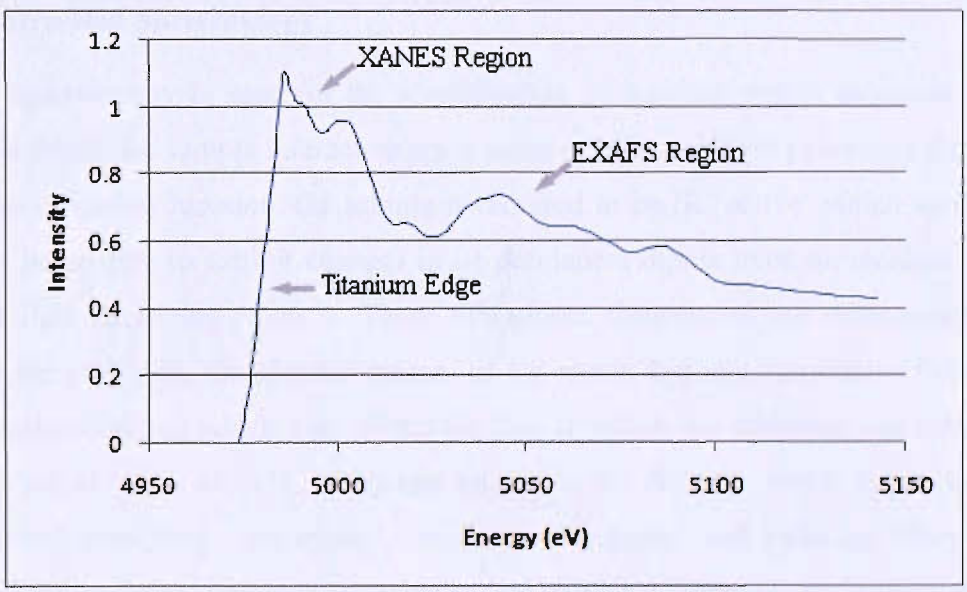

Figure 2.3: A graph illustrating the edge-, XANES- and EXAFS-region of titanium nitride.

This happens when the incoming incident X-rays have sufficient energy to free or excite a bound electron within the material but, in addition to this, small oscillations can be seen superimposed on the edge step, these oscillations which occur close to the edge region, are known as XANES.

Analysis of these XANES oscillations in the spectrum of a particular sample can provide information about vacant orbitals, electronic configuration and the site symmetry of the absorbing atom. Theoretical multiple scattering calculations can be compared with the experimental spectrum to determine the geometrical arrangement of the atoms surrounding the absorbing atom. The absolute position of the edge also contains information about the oxidation state of the absorbing atom.

XANES were used to differentiate samples in a qualitative rather than quantitative manner; the information required from the spectra was basic and required purely as a complementary technique. Pre-edge features of precursor samples annealed at various temperatures were examined for s-d transitions, which are not allowed in centrosymmetric sites, and hence could assist in the characterisation of the structure of the lower temperature annealed materials.

2.1.3 Infra-Red Spectroscopy

Infrared spectroscopy is used for the identification of bonding within molecules via the manner in which the sample interacts when a beam of infra-red light penetrates the sample. For the technique to function, the sample is required to be IR 'active' which involves the molecule being able to exhibit changes in its permanent dipole upon an incident beam of infra-red light impacting upon it. These vibrational frequencies are determined by the shape of the molecule, the specific masses of the atoms and any associative forces other than covalent bonding which may affect the rate at which the molecule can vibrate. For example, the atoms in an NH_2 group can vibrate in six different ways, symmetrical and asymmetrical stretching, 'scissoring', 'rocking', 'wagging' and twisting. They can be characterised by their vibrational frequencies and plotted in terms of the wavelength of the vibration versus the percentage absorption of the infra-red light. These wavelengths appear as a series of 'peaks' signifying the level of absorption and are referenced by simply comparing them with tables of known compounds[46].

Infra-red spectroscopy was performed using a PerkinElmer *Spectrum One* FT-IR spectrometer in conjunction with PerkinElmer's analytical software *Spectrum* v3.05

Due to the pyrophoric nature of the precursor, samples had to be prepared inside a nitrogen filled glovebox. A typical analysis would involve approximately 1 mg of the precursor material being ground in approximately 150 mg of dry caesium iodide (CsI) powder using a pestle and mortar; the sample and CsI were ground to reduce the particle size to less than 5 μm in diameter, otherwise the larger particles would scatter the infrared beam causing a sloping profile in the baseline of the spectrum. Caesium iodide was used because of its wider transmission range than potassium bromide, thus allowing the analysis of the far-infrared range of the spectrum too without interference from the media. CsI was also used as the apparatus' 'cell' used CsI disks between which the sample was held, any contributions from these disks were background subtracted, thus making the media "transparent".

The sample was then mounted between the two CsI disks in an IR 'cell' with a teflon spacer (see Figure 2.4). The entire unit was placed inside a resealable bag, in order to offer further protection towards oxidation during transportation to the spectrometer which was not housed in a protective-gas environment.

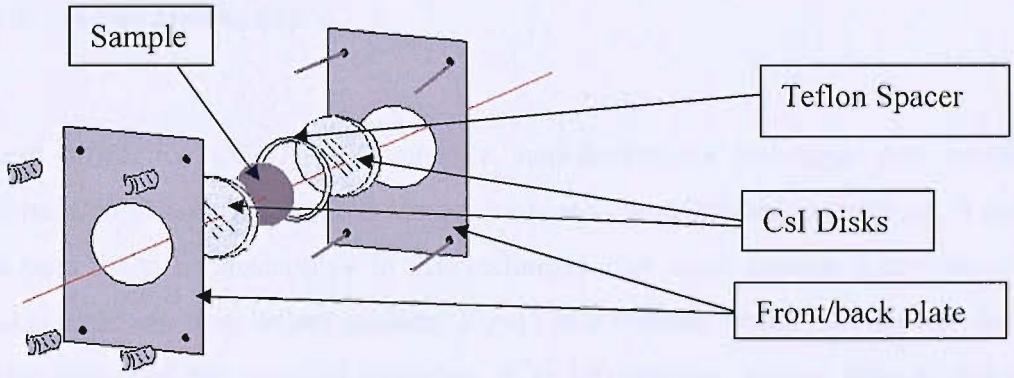

Figure 2.4: An exploded diagram of an ir sample holder.

The samples were analysed to determine the functional groups present and to identify similarities between the precursors; the presence of any oxygen derived vibrations, such as –OH stretching, would be clear indication of contaminated precursor material. The technique was used to elucidate if the different preparative methods yielded significant changes in the chemical composition of the precursor in terms of functional groups which could be beneficial to the formation of nitrogen-rich nitrides upon annealing.

2.1.4 Microanalysis

Microanalysis was performed by Medac Ltd, Egham, Surrey. Precursor materials and annealed nitrides were sent for analysis; information on the quantities of carbon, hydrogen, and nitrogen were collected. This information was used to establish carbon content within the analytes and the nitrogen content of each sample could be used as a guide to its stoichiometry compared to calculated percentages from 'ideal' materials.

Microanalysis was used to compare the C, H and N concentrations of the precursors thermolysed under either ammonia or nitrogen as well as the annealed products of the various different precursors produced via the preliminary work undertaken for the investigation of nanocrystalline TiN. However, due to the highly refractory nature of TiN and its composites, it is possible that unless the grain size of the analyte material is homogeneous and the particle size is sufficiently small, there can be parts of the sample which would not fully decompose thus giving low carbon and nitrogen analyses.

2.1.5 X-ray Diffraction

X-ray diffraction (XRD) is a versatile, non-destructive technique that reveals detailed information about the chemical composition and crystallographic structure of samples. For the samples to be susceptible to this technique they must possess a crystalline structure. The sample can then reflect incident X-rays in a manner which is unique to the elemental composition of the material allowing it to be indexed against known reflections and consequently identified.

The process of X-ray generation involves electrons being excited from a cathode and accelerated through a strong electrical potential, usually in the region of 30-40 kV. The electrons collide with a metal plate, usually copper; due to its high thermal conductivity and ability to produce strong K_α and K_β X-rays; the radiation used to interact with the powdered target sample.

The radiation possesses a mixture of different wavelengths and to simplify the crystallographic data it is monochromated. This is done by placing a 'monochromator' in series between the radiation source and the target analyte. The monochromator is a single crystal, which is mounted in a given orientation to diffract X-ray photons of specific wavelengths only. This not only simplifies the data analysis, as only one series of reflections are recorded, but also removes radiation that degrades the sample without contributing useful information.

The monochromated beam is then collimated to a single direction, by using either mirrors or a physical barrier, before they are allowed to strike the sample. Upon the radiation impacting the analyte, the resultant signatures are scattered according to Bragg's law (see Figure 2.5). Where d is the atomic distance between lattices; θ is the angle between the incident x-rays and the scattered x-rays; n is an integer and λ is the wavelength of the incident radiation.

$$2dSin\theta = n\lambda$$

Figure 2.5: Bragg's law.

These signatures are then collected in the detector area of the diffractometer, where computer software plots the information as 2-dimensional cartesian coordinates of intensity (y-axis) versus 2θ, the angle of diffraction (x-axis). See Figure 2.6 for a schematic diagram of the path of diffraction.

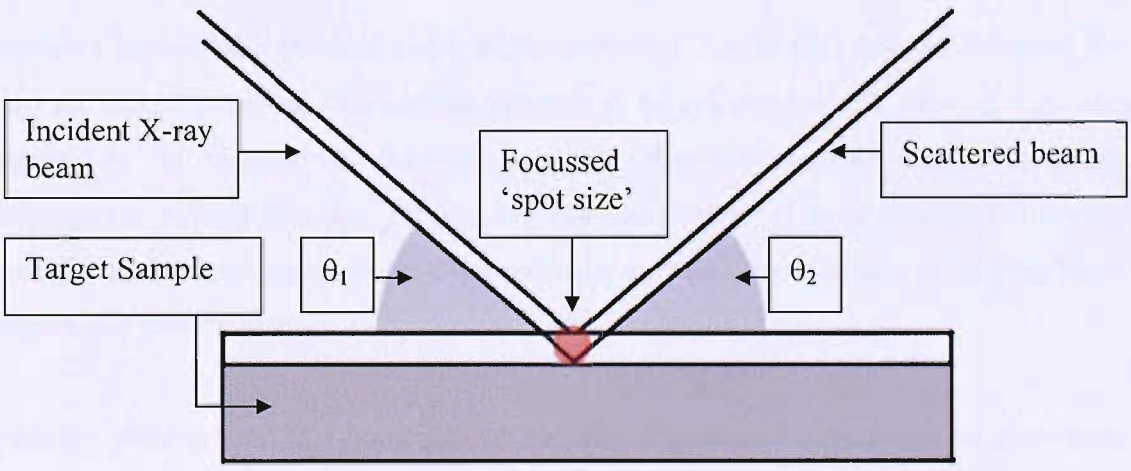

Figure 2.6: A schematic diagram of the path of reflection of a beam of X-rays upon hitting a powdered sample. Where θ_1 is the angle between the incident X-rays and the speciemen and θ_2 is the angle between the incident X-ray and the defracted beam.

Powder X-ray diffraction (PXD) data was collected using a Siemens D5000 diffractometer, in Bragg-Brentano geometry, commonly used for the study of inorganic solids since it minimises absorption by high atomic elements (see Figure 2.7) and a Bruker D8 advance C2 diffractometer (Figure 2.9), both using Cu-$K_{\alpha 1}$ radiation. Structural analysis of the data was performed by Dr Andrew Hector using the refinement software GSAS[70].

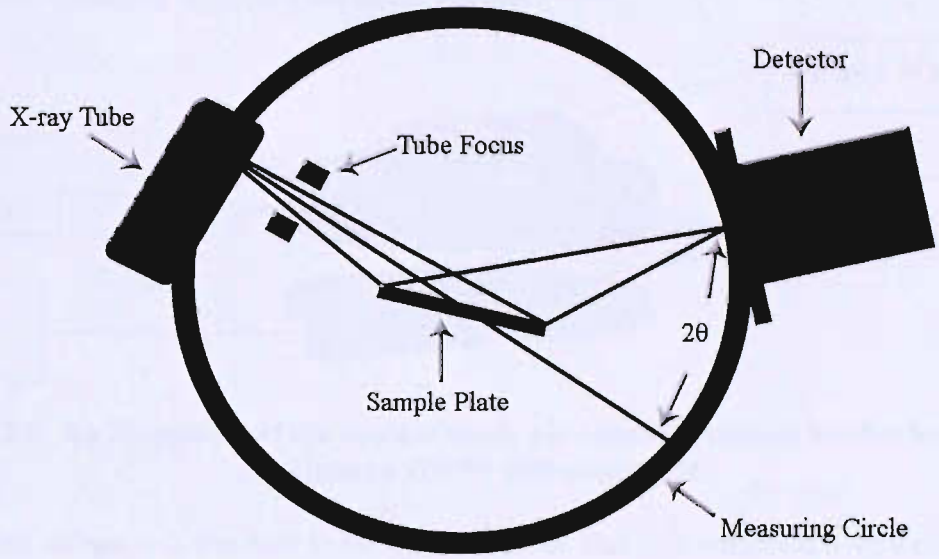

Figure 2.7: A basic schematic diagram of the bragg-brentano-type layout of a diffractometer.

The D5000 was used for the majority of routine characterisation work and was also used for collecting data for Rietveld analysis. This setup was used for the characterisation of the powders because the incident angle of the incoming X-rays (θ_1) and the reflected X-rays (θ_2) are linked allowing symmetrical patterns to be collected which were of high enough quality to be refined via Rietveld analysis. Rietveld analysis elucidates structural information from diffraction patterns beyond verification of peak locations. Information specific to the specimen can be obtained such as lattice parameters, bond lengths, bond angles and particle size.

Samples were ground to a homogenous particle size inside a nitrogen filled glovebox, the resultant powder was then mounted in a suitable air-sensitive sample holder and sealed, in order to safeguard against any potential surface oxidation.

The sample holder used was custom made (see Figure 2.8). The base unit was identical to a standard "open air" sample holder – a round disc with a recess at its centre for the specimen. A custom made cover was placed over this, which consisted of an aluminium cover with a perspex window, and where the two parts met, they were sealed with a ring of silicone grease. A nylon zip-tie was then used to hold the unit together and it was mounted into the diffractometer in the conventional manner.

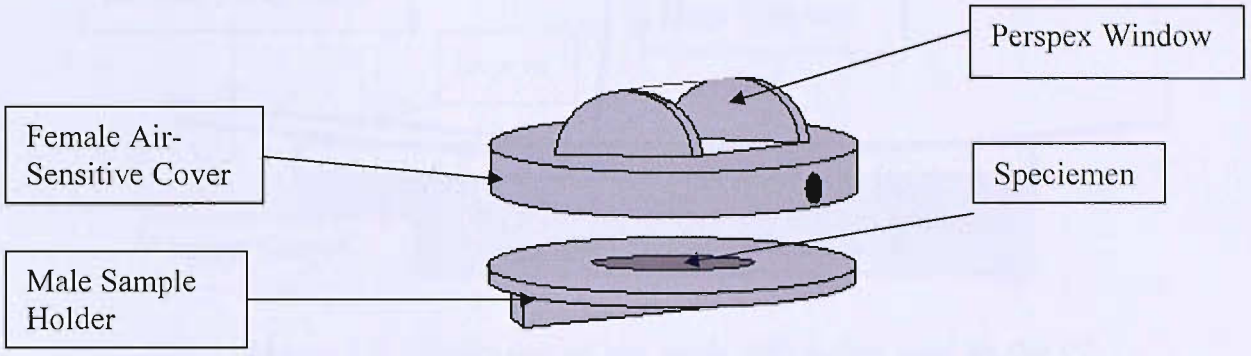

Figure 2.8: An illustation of the custom made air-sensitive sample holder for use on the Siemens D5000 diffractometer.

The sample holder was attached to the diffractometer and data collected over a range of 20 to 70 2θ. Titanium nitride displays peaks at approximately 37, 42 and 62 2θ. The phases present were identified by comparison with the JCPDS database through the Bruker "Eva" software package.

The C2 diffractometer was used to analyse both powders and films *in situ.* on the substrate surface *via* low angle diffraction. The advantage of the 'C2' was the small spot size it could offer. This allowed for physically small quantities of sample to be analysed which was vital when considering that the average yields from some preparations were <0.1g.

Another advantage of using the C2 for analysis of the coatings was the ability to configure the equipment to project a low angle incident beam of X-rays which increased the effective thickness of the coating, increasing the possibility of recording data on the sample and reducing contributions from the substrate. A drawback was the effective increase in spot size of the X-rays during low-angle diffraction and the additional broadening of reflections which it contributes. This led to characteristic broadening of the peaks.

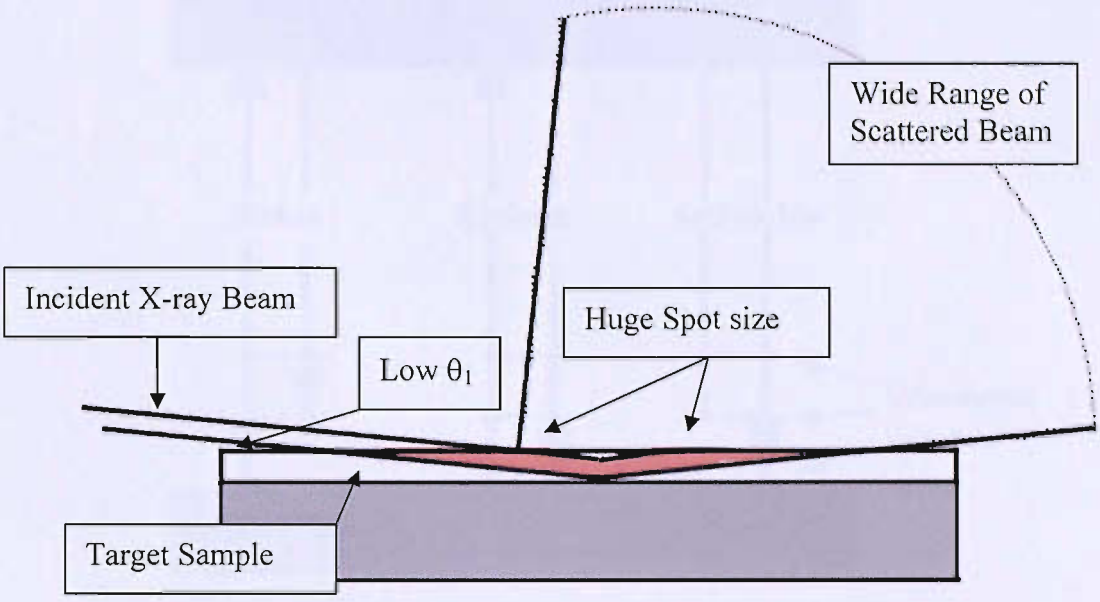

Figure 2.9: Illustration of low angle diffraction used on the C2.

Further, the data collected by the C2 was unrefinable due to the broad asymmetric peaks. It was however possible to 'fingerprint' the materials being analysed in order to index the ring pattern transmitted by the sample.

2.1.6 Raman spectroscopy

Raman spectroscopy is used to study vibrational, rotational, and other low-frequency modes in a system, in a similar manner to infra-red spectroscopy. The major difference however is that Raman relies on the inelastic scattering of photons and comprises a very small fraction, about 1 in 10^7, of the incident photons. The incident light interacts with phonons or other excitations in the system, resulting in the energy of the photons being shifted up or down and it is this shift that gives information about the phonon modes in the system. For a molecule to be Raman active its polarisability must change with vibrational motion. Thus, Raman spectroscopy complements IR spectroscopy as more information can be extracted from the samples in a similar fashion. Raman spectroscopy was used due to the vibrational information, which is very specific to chemical bonding, that could be extracted from analysed samples. A simplified energy diagram that illustrates these concepts is given below.

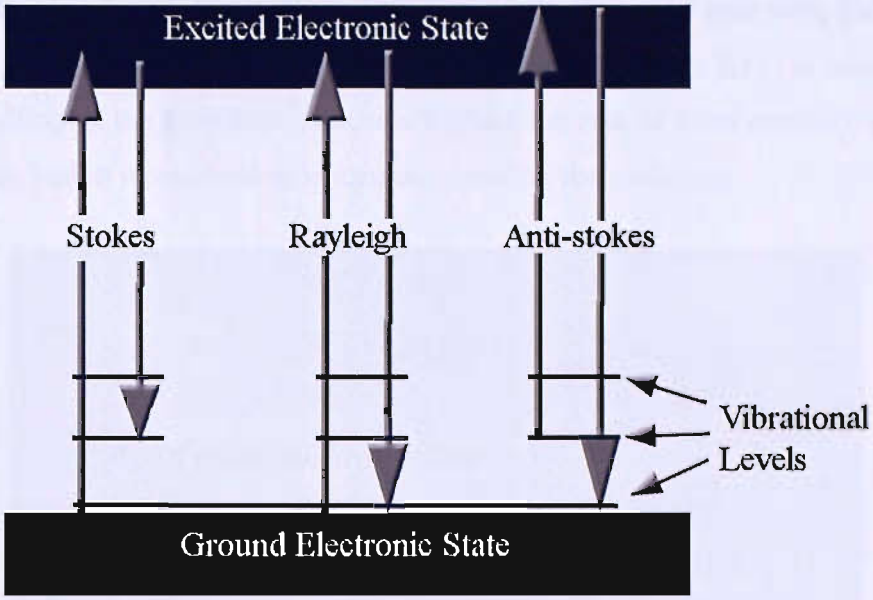

Figure 2.10: A simplified energy diagram illustrating the differences between Stokes, Rayleigh and Anti-Stokes scattering.

This inelastic scattering gives information on the population of a given phonon mode in the ratio between the Stokes (downshifted) intensity, and anti-Stokes (upshifted) intensity. This is directly related to the vibrational energy spacing in the ground electronic state of the sample which therefore means the wavenumber of the Stokes and anti-Stokes lines are a direct measure of the vibrational energies of the molecule.

Raman spectroscopy was performed at UCL by Olga Shebanova and used during the analysis of nanocrystalline nitrides and carbonitrides largely as a "fingerprinting" technique. It was also employed to identify the presence of any oxide material within titanium nitride samples as TiO_2 phases have strong characteristic Raman features.

2.1.7 Thermogravimetric Analysis

Thermogravimetric analysis is a technique in which, a thermally sensitive sample can be pyrolysed under a reactive or inert gas – which can be either oxidative or reductive – and is used to measure changes in the mass of a sample as a function of temperature and/or time; TGA was performed using a Mettler Toledo 'TGA851e'thermogravimetric analyser.

Due to the highly air-sensitive nature of the precursors that were analysed, the equipment had to be mounted inside a nitrogen atmosphere glovebox (Figure 2.11) in order to enable the free handling of the precursor materials without the risk of them partially oxidising or decomposing, which would lead to inaccuracies during their analysis.

Figure 2.11: Mettler Toledo TGA851e being used inside a nitrogen-filled glovebox.

Some reactions required powders to be annealed under oxygen-free conditions using nitrogen. Rather than setting up a furnace rig catering for these requirements the built-in furnace of the equipment was used, as it was connected to a supply of electronic grade nitrogen (either BOC "ULSI" or Air Products "BiP" grade nitrogen) and was sealed in an oxygen-free environment.

Samples were loaded into a dry crucible and then placed onto the balance arm within the analyser. The sample was then heated to a pre-programmed temperature and allowed to decompose. The balance assembly measures the initial sample weight and then continuously monitors any change in weight, either losses or gains, as a function of temperature and time. Electronic-grade, high purity nitrogen was used for the pyrolysis of the precursor at a variety of temperatures (Air Products or BOC variants), as there was the risk of oxidation when using standard grade oxygen-free-nitrogen (OFN). This was due to trace amounts of oxygen which were present within the supplier's industrial grade OFN blend gas.

Sample analysis involved the determination of the temperature at which phase change between amorphous TiN_x and TiN occurred and the quantity of organic species specific to the sample. Oxygen gas was also used as a reactive gas in order to oxidise the samples, this enabled the titanium content to be quantified by measuring the amount of oxidation that occurred when the sample was heated to temperatures of 1000°C. The precipitate was heated at various temperatures under ULSI-grade nitrogen (70 cm^3min^{-1}); a typical weight loss profile is illustrated in Figure 2.12.

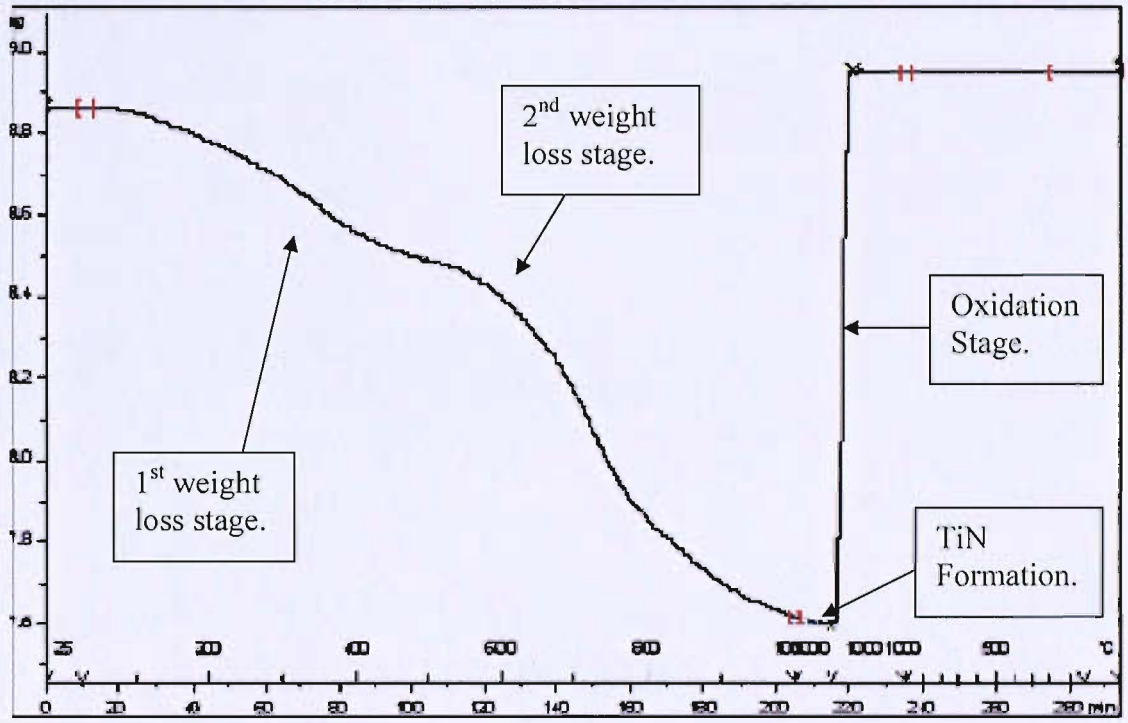

Figure 2.12: A typical TGA trace of a ti precursor pyrolysed under high-purity nitrogen and then oxidised at 1000 °C.

This technique was used to compare the different reaction conditions used to produce the precursor powders. As part of the initial research was to establish if a precursor material could be produced which enabled the production of nitrogen-rich nitrides, TGA was integral to the analysis of these materials.

Whilst TGA was able to ascertain the metal content of any of the precursors analysed it was severely limited in offering any other *quantitative* information. Whilst the TGA trace can indicate the percentages of weight loss in a compound, this information only becomes meaningful if the material pyrolysed is already known. Without this knowledge the TGA

trace can only offer a simple indication of the relative concentration of the volatile constituents. Addition of a mass spectrometer to the TGA exhaust would enable the real-time analysis of the volatilised fragments as they were released from the sample and allow the characterisation of both the molecular mass as density of the fragments of the sample as it was pyrolysed.

2.1.8 XPS

X-ray Photoelectron Spectroscopy is a quantitative analysis technique which measures the chemical and electronic state of the constituent elements of the material being analysed. Spectra are obtained by irradiating a material with a beam of X-rays while simultaneously measuring the kinetic energy and number of electrons that escape from the top 1 - 10 nm of the sample.

The detected elements are characterised by their 'binding energy' following the equation developed by Ernest Rutherford in Figure 2.13:

$$E_{binding=} E_{photon} - E_{kinetic} - \phi$$

Figure 2.13: Ernest Rutherford's equation explaining binding energy.

Where E_{photon} is the energy of the incident photon; $E_{kinetic}$ is the energy required to eject an electron from the target atom and Φ equals the "working distance" (the energy expelled after the photons have left the source and before they hit the target specimen) of the spectrometer used. This allows the elemental constituents of the sample to be identified as each possesses a unique binding energy dependant on their electronic and chemical environment and thus can be identified against an index of known elemental binding energy values.

XPS was performed by Robert Palgrave at University College London using a GE 205 X-ray photoelectron spectrometer and courtesy of Thermo using a '*Theta Probe*', both with a Al Kα source, on titanium nitride samples to establish binding energies of the constituent atoms in the samples and therefore their chemical environment. This was done in order to elucidate the oxidation state of the titanium and to establish what the chemical composition could be in the powdered samples. The oxidation state of the titanium was of particular interest as samples annealed at lower temperatures (circa. 450 °C) were being investigated to establish whether the formation of Ti_3N_4 was possible. XPS would clearly have shown data correlating the titanium environments to Ti^{4+} if that were the case.

As XPS is a surface sensitive technique with a very short penetration depth compositional analysis was also performed in conjunction with argon ablation in order to remove surface

contamination which had either been deposited through handling or occurred due to oxidation, in an attempt to gain an accurate assessment of the composition of the samples. However, the loading procedure could not be performed in controlled atmospheric conditions and therefore the samples were exposed to the atmosphere. Thus surface oxidation of the samples could have occurred and this resulted in the inability to establish whether oxygen detected in the samples was present due to the exposure during loading or the method of synthesis.

2.1.9 SEM

As a primary goal of the project was to produce good quality films, a highly resolved visual technique was required; the JSM 5910 scanning electron microscope possesses a resolving power of 3 nm and was used to establish the thickness, quality and continuity of the coatings deposited via the various methods described herein.

A general explanation of how an SEM functions follows:

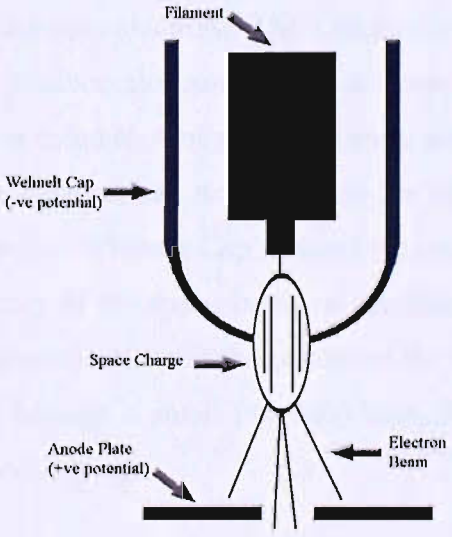

Figure 2.14 The electron gun.

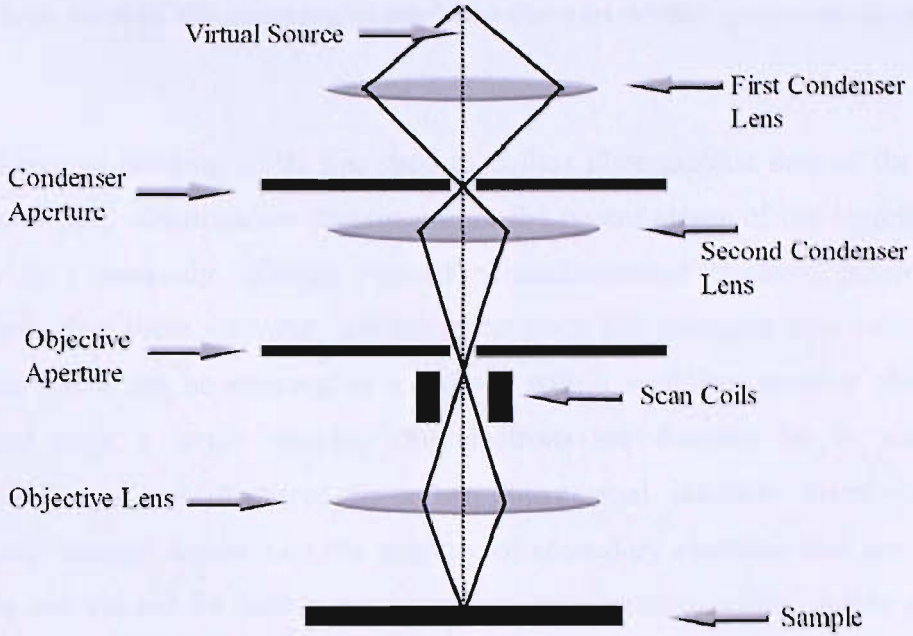

Figure 2.15: A graphical representation of the SEM focussing process.

The electron gun in Figure 2.14 is represented as a virtual source in Figure 2.15. This produces a stream of monochromatic electrons. The Thermionic Electron Gun possesses a cathode, which is heated to produce electrons which are then accelerated by a positive potential applied down the gun column. A negative electrical potential (~500 V) is applied to the 'Whenelt Cap' and as the electrons move toward the anode any emitted from the filament's side are repelled by the 'Whenelt Cap' toward the optic axis (horizontal center). A collection of electrons occurs in the space between the filament tip and Whenelt Cap (called a space charge) and those electrons at the bottom of the space charge nearest to the anode can exit the gun area through a small (<1 mm) hole. These electrons then move down the column to be used in imaging.

Once the stream of electrons is allowed out of the gun, the stream is condensed by the first condenser lens, usually controlled by a 'coarse' focus control. This lens is used to both form the beam and limit the amount of current in the beam. It works in conjunction with the condenser aperture to eliminate the high-angle electrons from the beam. The beam is then constricted by the condenser aperture, eliminating some high-angle electrons and the second condenser lens forms the electrons into a thin, coherent beam. The final or

'objective' lens focuses the scanning beam onto the part of the specimen desired to be analysed.

Secondary Electron Imaging (SEI) was used to collect photographic data of the samples analysed. Secondary electrons are present within the parent atoms of the targeted nuclei and behave in a markedly different manner to backscattered electrons when excited. Relatively speaking, these secondary electrons are much less energetic than backscattered electrons and hence can be attracted to a cathode with a sufficient positive charge after being ejected from a target sample. The electrons are detected by a 'scintillator-photomultiplier' and are displayed in a two-dimensional intensity distribution. The brightness and contrast depends on the quantity of secondary electrons that are detected; lighter areas are caused by higher concentrations of electrons whilst darker areas are caused by lower concentrations. This intensity distribution can be viewed and saved as a Digital image.

Scanning Electron Microscopy (SEM) was carried out at the University of Southampton Microscopy Centre using both JEOL JSM-5910 and JSM-6500F instruments to give surface analysis of coatings and powders produced throughout the course of research. Samples were prepared inside a nitrogen filled glovebox and mounted onto aluminium stubs using conductive carbon pads. As the technique was non-destructive samples could be repeatedly analysed if required, therefore edge-on analysis of the coatings was performed in order to establish the range of thicknesses that were produced by the variety of different coating sols. In order to analyse the thickness, the tiles were cleaved and mounted perpendicular to the aluminium stub in conductive putty. However, as the silica substrate was not conductive the shear face of the tile was coated with carbon in order to ensure that charging was minimised and well resolved images could be collected. As EDX had already been performed on the face of the tile and was not to be performed on the edge, the carbon coating was not an issue.

Whilst SEM was extremely effective at providing detailed imagery of the solids and films analysed, the mounting and topography of the substrate was critical to the generation of good quality results. This was because the beam had to enter the sample perpendicular to the surface, allowing the region emitting secondary electrons to be uniform about the axis of the beam. If the angle of incidence were to increase, the emission distance of one side of

the beam would decrease and more secondary electrons would be emitted leading to areas of increasing brightness as opposed to a flat surface.

2.1.10 EDX

Energy Dispersive X-ray Analysis was used in conjunction with SEM and is not as surface sensitive as XPS, possessing a penetration depth in the region about 2 microns. EDX was used to qualitatively analyse coatings and solids as it was necessary to establish that the materials produced were in fact nitrides and not oxynitrides or oxides. Its capabilities are due to the principle that each element of the periodic table has a unique electronic structure and thus, a unique X-ray emission spectrum.

The detector used in EDX was a lithium drifted silicon detector operated at liquid nitrogen temperatures. When X-ray photons strike the detector, photoelectrons are generated within the body of the Si and as the photoelectrons travel through the Si, they generate electron-hole pairs which are attracted to opposite ends of the detector with the aid of a strong electric field. The size of the current pulse thus generated depends on the number of electron-hole pairs created, which in turn depends on the energy of the incoming X-ray photon. Thus, an X-ray spectrum can be acquired giving information on the elemental composition of the material under examination.

As the materials produced were inherently conductive, EDX was a particularly well suited technique; the samples did not require either gold or carbon coating prior to analysis, which meant that accurate elemental analysis could be performed, without corruption of the materials due to any additional conductive coating. However, in situations where surface charging effects were too strong (due to very thin film thicknesses) carbon coating was performed to give better images.

Samples were mounted on stubs inside a glovebox and treated as air-sensitive in order to minimise any potential surface oxidation.

Whilst EDX was used for elemental analysis, nitrogen was difficult to detect. This was because the SiLi detector was protected by a Boron Nitride window and hence any

nitrogen contained within the samples was rendered 'invisible'. Additionally in situations where carbon coating was required to enhance the conductivity of the samples this removed the ability to quantify the presence of any carbon in the sample itself. Also, as the penetration depth of the electron beam is in the region of 2 microns, in thin films the detection of the substrate beneath the surface of the coatings was a regular occurrence and led to the detection of silicon and oxygen in all samples. This meant that additional characterisation techniques were required in order to establish that the source of oxygen was only due to the contributions of the substrate and that the films themselves were oxygen-free.

2.1.11 TEM

In transmission electron microscopy, a thin specimen is irradiated with an electron beam of uniform current density. Electrons are emitted from the electron gun and illuminate the specimen through a two or three stage condenser lens system. The objective lens provides the formation of either an image or a diffraction pattern of the specimen. The electron intensity distribution behind the specimen is magnified with a three or four stage lens system and viewed on a fluorescent screen. The image can be recorded digitally by a CCD camera.

Transmission electron microscopy (TEM) was carried out using a 300kV JEOL JEM-3010 transmission electron microscope in combination with energy dispersive X-ray microanalysis. Either powdered samples or fragments of a coating film were ground in deuterated benzene and deposited onto carbon grids using a Pasteur pipette. The technique was used to obtain visual information on the nanostructure of coatings produced throughout the research, approximate particle sizes and also to utilise electron diffraction to obtain structural information.

Whilst Electron diffraction proved to be a vital technique in the characterisation of the coatings' crystallinity it was subject to several important limitations as the sample had to be 'electron transparent'(the sample thickness had to be in the order of 100 nm or less.) Also, whilst the diffraction rings could be indexed to known crystal structures the refinement of the data to extract more in depth dimensional characterisation was not possible.

3 NANOCRYSTALLINE NITRIDES AND CARBONITRIDES

3.1 Introduction

Due to their desirable properties, titanium nitride films are gradually expanding their field of application. This is because the hardness, chemical and thermal stability[7,5,47] that the compound possesses makes it ideal for applications involving extreme environmental conditions which demand a surface that is resistant to mechanical wear. Examples of such applications include drilling equipment or bearing surfaces in turbines[48,49,50,51]. These types of coatings have historically been deposited via vapour-deposition methods such as CVD or PVD.

The process of chemical vapour deposition of titanium nitride involves the use of titanium dialkylamides and ammonia[24] in a reaction that proceeds via the transamination of the amide with the eventual formation of $Ti_{1+x}(NH_2)_2(NMe_2)_{4x}$ 'cage' intermediates which collapse when heated to form cubic rocksalt-structured TiN[25].

It has been suggested that another intermediate compound 'Ti_3N_4' could exist if the correct conditions for thermolysis can be identified[14], this has never been conclusively demonstrated, although if possible, Ti_3N_4 could be of potential use as a semi-conductor material. The 'spinel' phase is the suggested extended structure for Ti_3N_4 due to the existence of spinel-phase Si_3N_4 and Ge_3N_4[15,52,14].

The history of research into the ammonolysis of dialkylamides dates as far back as 1962 when Bradley investigated the effects of a variety of reagents on dialkylamides[9]. Due to the primary aim of their research being to study the amides themselves, the products yielded from the ammonolysis reactions were not studied beyond simple characterisation and it was not until further research was undertaken by Brown and Maya[6] and Baxter *et al*[13] into the products of ammonolysis, that it was realised that it could be a useful route to the production of nitride materials. The reaction of $Ti(NMe_2)_4$ with ammonia was found to produce a brown precipitate with a stoichiometry of $TiC_{1.2}N_{1.2}H_4$ which upon heating in helium produced TiN powder. The TGA analysis of this powder revealed that weight loss occurred in 2 discreet stages with a plateau between 400 and 600 °C. Upon performing

decomposition analysis on a sample made following the Baxter methodology[13] we found the decomposition profile to be essentially identical to the aforementioned research group's reported findings (see Figure 3.1). However, the previous research[13] concluded that the product possessed a stoichiometry of $TiN_{1.2}$ 'with a trace of carbon', consequently declaring that the material was effectively Ti_3N_4.

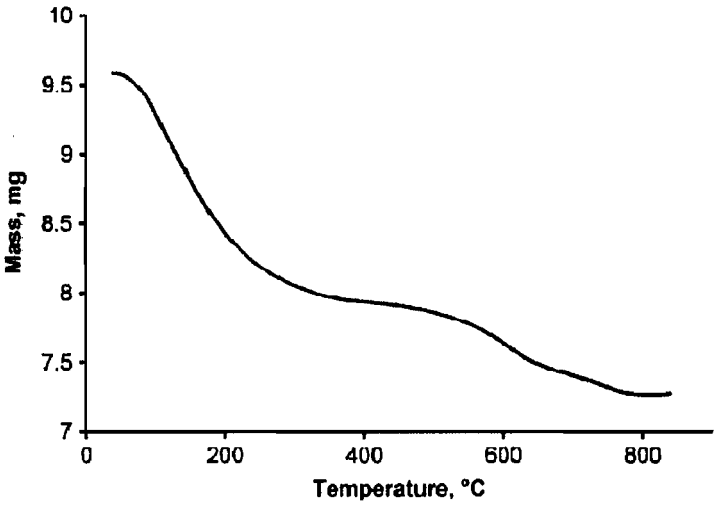

Figure 3.1: TGA curve showing the two-stage thermal decomposition of the titanium-based precursor synthesised using the Baxter methodology[13].

Our studies led us to review these findings and carry out our own analysis using a variety of techniques including: XAS, EXAFS, TEM, Raman, FTIR and TGA.

3.2 Experimental Section

2 cm^3 of $Ti(NMe_2)_4$ was dissolved in 50 cm^3 of sodium dried THF and continually mixed using a standard stirrer/hotplate and exposed to an excess of NH_3. The $Ti(NMe_2)_4$, was used in a variety of concentrations; 2.0, 1.0, 0.5 or 0.1 ml, over three different temperature conditions; 25 °C (room temperature), -78 °C (attained by using dry ice in an icebath with acetone) and -20 °C (using an ethylene glycol filled coolbath). These conditions were implemented in order to establish if there were 'ideal' parameters in which a nitrogen rich precursor material could be synthesised.

The premise was to transaminate the amide precursor with ammonia in order to give a carbon free intermediate compound, via the following reaction:

$$Ti(NMe_2)_4 + nNH_3 \xrightarrow{stirring} Ti(NMe_2)_{4-n}(NH_2)_n + n(HNMe_2)$$

3.2: Predicted route of ammonolysis for tetrakis(dimethylamino)titanium with excess gaseous ammonia.

Upon annealing, this could then be thermolysed to make a carbon-free nitride ceramic powder.

The amide used (tetrakis(dimethylamino)titanium, 99.99%) was sourced from Epichem. TiN powder used for comparative testing was purchased from Aldrich (>99%), electronic grade ammonia (99.99%) was purchased from Air Products and ULSI grade nitrogen (99.999%) was procured from BOC Edwards to be used for the thermolysis of the products of ammonolysis.

All reagents were highly air and moisture sensitive and in the case of the amides used, highly flammable. The products of the reactions with ammonia were pyrophoric and therefore all reactions and handling of materials were carried out in controlled environments under nitrogen, using either a Schlenk line or a glovebox.

THF was the solvent in all reactions and was dried using a combination of sodium metal as the drying agent and benzophenone as the indicator; denoted by a purple colour once satisfactory dryness had been achieved.

The ammonia atmosphere was maintained over the solution for one hour to ensure total precipitation of amide; corroborated by the solvent becoming colourless upon settling of the precipitate. Once this time period had elapsed, the source of NH_3 was removed and the precipitate separated from the solution using a customised class 3 sinter attached to a Schlenk line, in order to protect the product from oxidation. The solid was dried under vacuum.

TGA analysis of the precipitate was undertaken using a Mettler-Toledo TGA851e thermogravimetric analyser mounted inside a nitrogen-filled glovebox. The sample was thermolysed to 1000 °C under an atmosphere ULSI grade nitrogen (99.999%), procured from BOC Edwards. The principle aim was to monitor the decomposition profiles to see if

the material decomposed in discrete steps, which could indicate thermal conditions suitable for the synthesis of Ti_3N_4.

TEM data were recorded using a 'JEOL 3010' microscope with an 'Oxford Inca 100' energy dispersive X-ray (EDX) microanalysis probe with a 300 kV accelerating voltage. Additional images and diffraction data were obtained using a 'JEOL 100cx' 100kV microscope. A Bruker 'IFSv-66' infra-red spectrometer was used to gain reflectance spectra and conductivity measurements of pressed samples of pure product were carried out using a standard multimeter.

Raman spectra were obtained using a home built high-throughput system[53], comprising of Kaiser 'Supernotch' filters, an 'Acton 300' spectrograph system and a liquid-nitrogen cooled, back-thinned Si CCD detector. The 514.5 nm line of an Ar laser or the 633 line of an He-Ne laser were used to excite the samples using a 50 mm working distance Mitutoyo objective lens. The scattering was collected using an 1801 geometry through the same lens. Laser power was kept to a minimum of 1 mW in an effort to minimise heating of the sample in order to prevent the onset of surface oxidation; spectra obtained were collected in a nitrogen filled "diamond-anvil" cell, loaded cryogenically with nitrogen and maintained at a pressure of 1-3 GPa.

Powder x-ray diffraction (PXD) data was collected using a Siemens D5000 diffractometer, in Bragg-Brentano geometry, using Cu-$K_{\alpha 1}$ radiation. Structural analysis of the data was performed by Dr Andrew Hector using the refinement software GSAS[70]. As the samples being analysed were annealed, their respective specimens were treated as air-stable and therefore no special conditions were required for analysis, such as the use of an air-sensitive sample holder (see Figure 2.8).

X-ray absorption spectra were collected at Daresbury laboratories using station 7.1 (in transmission mode) of the SRS; a Si-111 monochromator was used. Samples were pressed into 13 mm disks using boron nitride as a diluting media, inside a nitrogen-filled glovebox. These disks were then sealed inside 6 μm Kapton film to avoid air exposure. Background subtraction was carried out using PAXAS[45]; EXAFS analysis and curve fitting was done using the programme 'Excurve'[54].

3.3 Results and Discussion

After a delay of several seconds the yellow solution began to darken and a precipitate formed on the surface and then throughout the solution. The precipitate was a brick-red in colour, highly pyrophoric and found to have a representative composition of $TiC_{0.49}N_{1.10}H_{2.32}$ *via* elemental and thermogravimetric analysis. Brown precipitates were obtained from the reaction method were analysed using IR, and TGA. Individual samples were then annealed from 400 °C to 1000 °C under either electronic grade ammonia or ULSI grade nitrogen. Once annealed, the speceimens were then analysed via Raman, TEM, PXD and EXAFS.

3.3.1 Compositional Studies

IR spectra of the precipitate were obtained and as would be expected, only minor variations were observed in the profiles and therefore did not indicate any substantial difference in the chemical composition of each sample. Rather than the reactions producing major variation in composition, the nuances of each preparation were likely to be the only major contributing factor to the composition of the analyte.

There were strong similarities between all spectra which can be summarised in Figure 3.3.

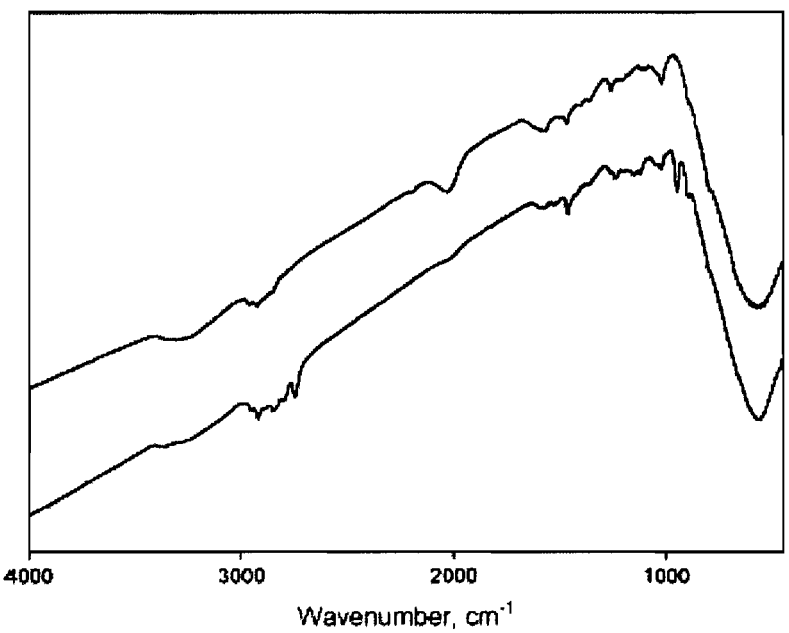

Figure 3.3: Representative infrared spectra of precursor materials, showing variation in the composition immediately after precipitation.

The spectra are dominated by a prominent stretch at 560 cm^{-1} which is attributed to the excitation frequency of a covalent M-N bond. Weaker bands were also always observed at 3250 cm^{-1}, 2920-2740 cm^{-1}, and 1590 cm^{-1} which are attributed to ν(NH), ν(CH) and $\delta(NH_2)$ respectively.

This type of spectrum corresponds to a polymeric sol-gel material possessing imide groups, amide termini and a small number of unreacted dimethylamide groups. As mentioned previously, differences were observed between spectra. Most notable was the occurrence of a feature observed at approximately 2030 cm^{-1} which can be tentatively assigned as being a Ti-H vibration as Jansen *et al.* observed a similar peak within the Si/N system[23].

As with the previous research carried out by Baxter *et al*[13], the TGA trace of the brown precipitate was found to possess two discrete weight losses which centred around 200 °C and 700 °C. As with the IR spectra, a broad variation of results were observed for the decomposition profiles of each precursor material. All samples tested exhibited the same basic characteristics of two 'steps' in the decomposition of the precursor material, although some were more pronounced than others, see Figure 3.4 and Figure 3.5.

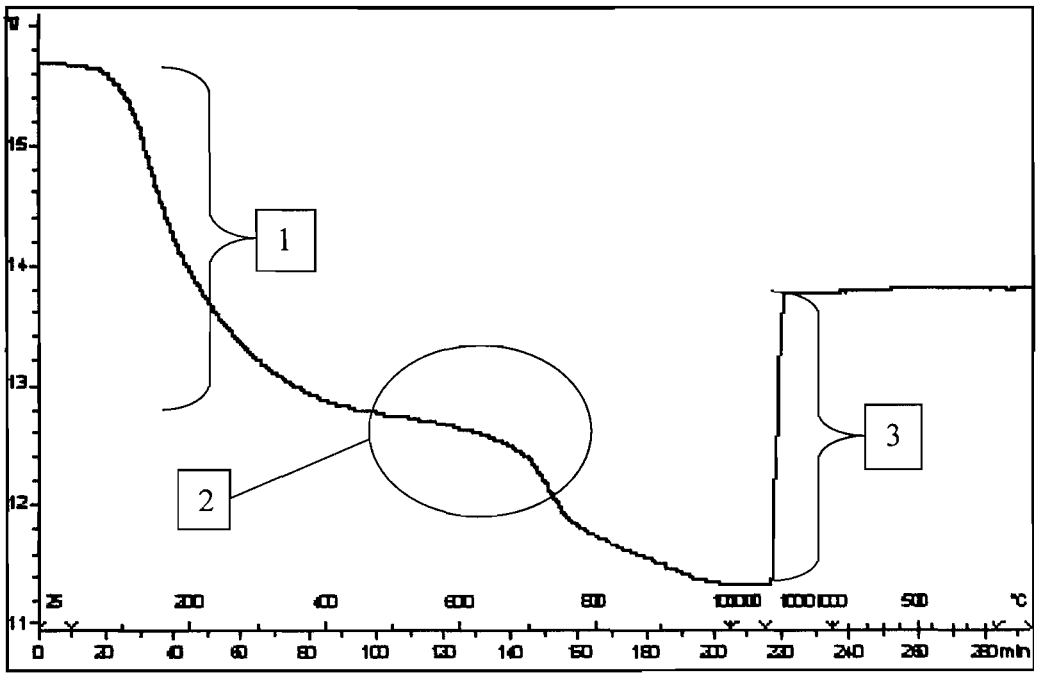

Figure 3.4: A TGA decomposition profile of the precursor material synthesised using 2.0ml $Ti(NMe_2)_4$ and 20.0ml THF, annealed to 1000 °C under ULSI grade nitrogen and then oxidised under industrial grade oxygen. This sample demonstrates a more pronounced plateau.

Figure 3.4 illustrating the two discrete weight losses which centred around 200 °C and 700 °C. The initial step involving the loss of organic residues and carbonaceous material and is witnessed at 100 – 500 °C (1). This is followed by a plateau (2) which indicates the onset of crystallisation and the loss of excess carbon and nitrogen which typically occurred between 700 °C – 1000 °C. Step (3) displays the introduction of oxygen at 1000 °C and the subsequent weight gain through the replacement of nitrogen within the system with oxygen.

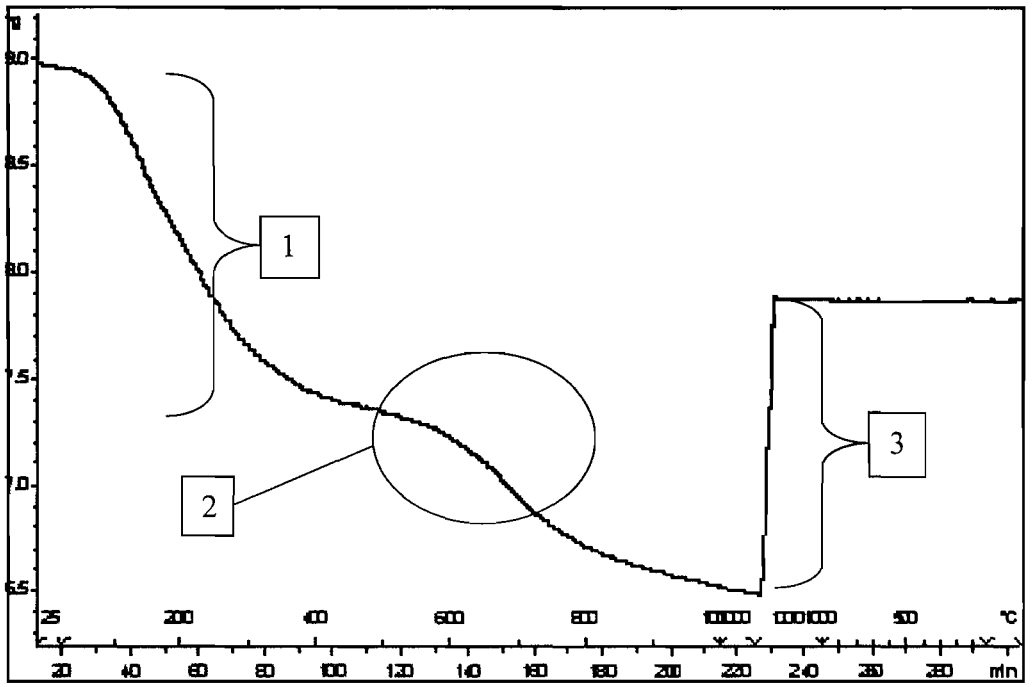

Figure 3.5: A TGA decomposition profile of the precursor material synthesised using 2.0ml $Ti(NMe_2)_4$ and 25.0ml THF, annealed to 1000 °C under ULSI grade nitrogen and then oxidised under industrial grade oxygen. This sample illustrates a less pronounced plateau.

Figure 3.5 illustrates again the same the same profile of a two stage weight loss that was seen in all TGA analysis that was performed. It should be noted that the plateau observed in this sample (2) was not as defined as in other syntheses (such as that seen in figure 3.4). Due to the less pronounced plateau given, this signified that the reaction conditions were less suitable for the generation of a precursor material capable of forming an intermediate – and potentially nitrogen-rich – compound.

Annealing studies were carried out on the precipitated material under atmospheres of either high-purity nitrogen or ammonia in order to investigate whether different phases of titanium nitride could be synthesised depending on the conditions used. Table 2 displays the chemical compositions and results of analysis of the PXD data obtained from the various materials analysed. Products annealed at and above the second stage weight-loss temperature was found to possess a crystalline TiN or Ti(C,N) cubic rocksalt structure depending on whether it was annealed under an atmosphere of ammonia of nitrogen respectively.

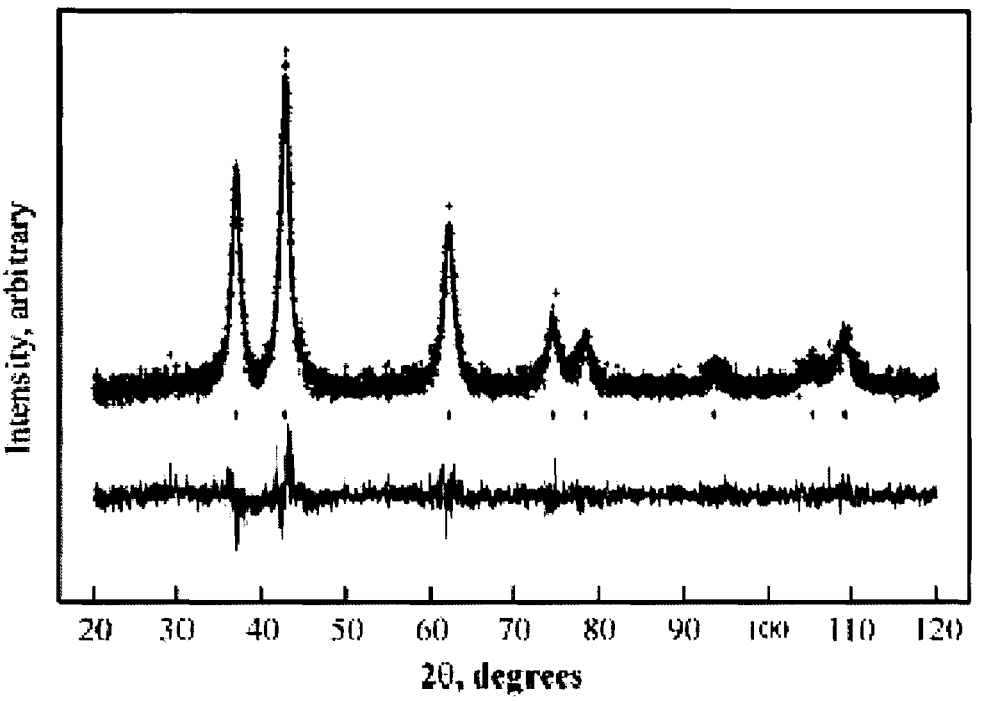

Figure 3.6: Refined PXD pattern of sample annealed at 850 °C for 2 hours, crosses mark the data points, upper solid line; the profile fit and lower solid line; the difference.

Presumably the lower occurrence of carbonaceous species within the product annealed under ammonia is due to the aggressively reductive nature of the reactive gas used.

Sample Preparation			Composition			PXD		
Atmosphere	Temp. (°C)	Duration (hours)	C (%)	H (%)	N (%)	a (Å)	Crystallite Size (nm)	Ti–N bond length (Å)
Nitrogen	450 °C	2	4.04(2)	0.11(2)	21.80(5)	Amorphous		2.05 Å
Nitrogen	1000 °C	2	4.04(3)	<0.1	18.86(2)	4.2382(12)Å	12 nm	2.10 Å
Ammonia	850 °C	2	0.80(2)	0.20(2)	20.93(5)	4.2274(9)Å	8 nm	2.11 Å
Ammonia	850 °C	8	0.17(1)	<0.1	19.89(1)	4.2269(10)Å	9 nm	2.11 Å
TiN Standard			<0.1	<0.1	21.36(6)	4.2251(6)Å	27 nm	2.12 Å

Table 2: Composition and crystallographic data on products of annealing the precipitate under N_2 at 450 °C for 2h, sample preparation, composition (%C, %H, %N) and PXD data.

The lattice parameters resulting from the structural refinement of the diffraction data indicated that the lattice size was slightly larger than that of stoichiometric TiN; 4.227 – 4.238Å as opposed to 4.225Å[56].The observed variation in bond length was likely due to the variation in composition and annealing conditions. This could potentially lead to materials possessing vacancies, due to the lack of homogeneity leading to localised nitrogen deficiency in the precursor material which would translate into a product possessing areas deficient in nitrogen. Also, the substitution of carbon for nitrogen in the annealed product could occur due to the less aggressive nature of the nitrogen atmosphere being used in the annealing stages; products annealed using gaseous ammonia were discovered to be virtually carbon free.

Fitting of PXD patterns for materials annealed between 850-1000 °C indicated that the average particle size was in the region of 8 to 12 nm (see Table 2); TEM corroborated that this was the case (see Figure 3.7, Figure 3.8 and Figure 3.9).

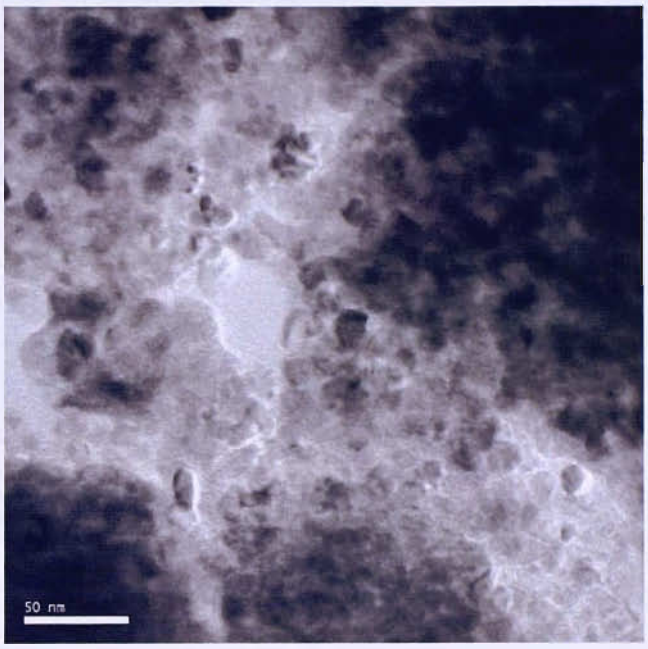

Figure 3.7: Transmission electron micrograph of $TiC_{0.18}N_{0.83}$ obtained by heating the precipitate at 1000 °C for 2 hours.

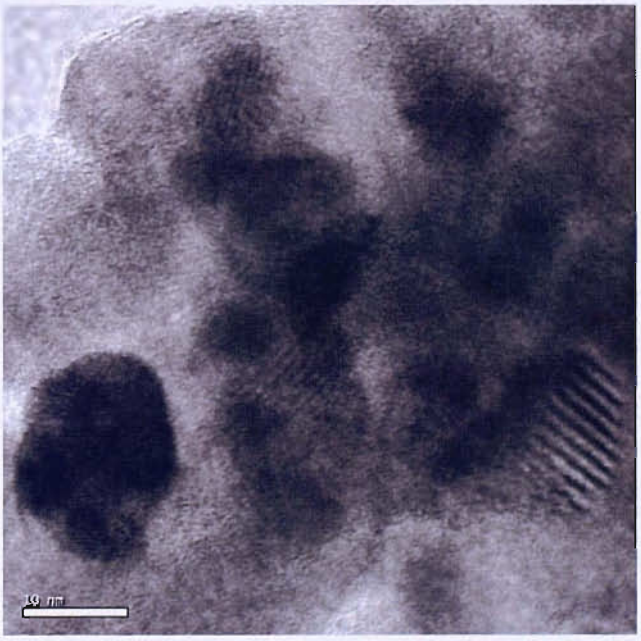

Figure 3.8: Close-up transmission electron micrograph of $TiC_{0.18}N_{0.83}$, obtained by heating the precipitate at 1000 °C for 2 hours; illustrating crystallite size being in the region of 5 – 10 nm.

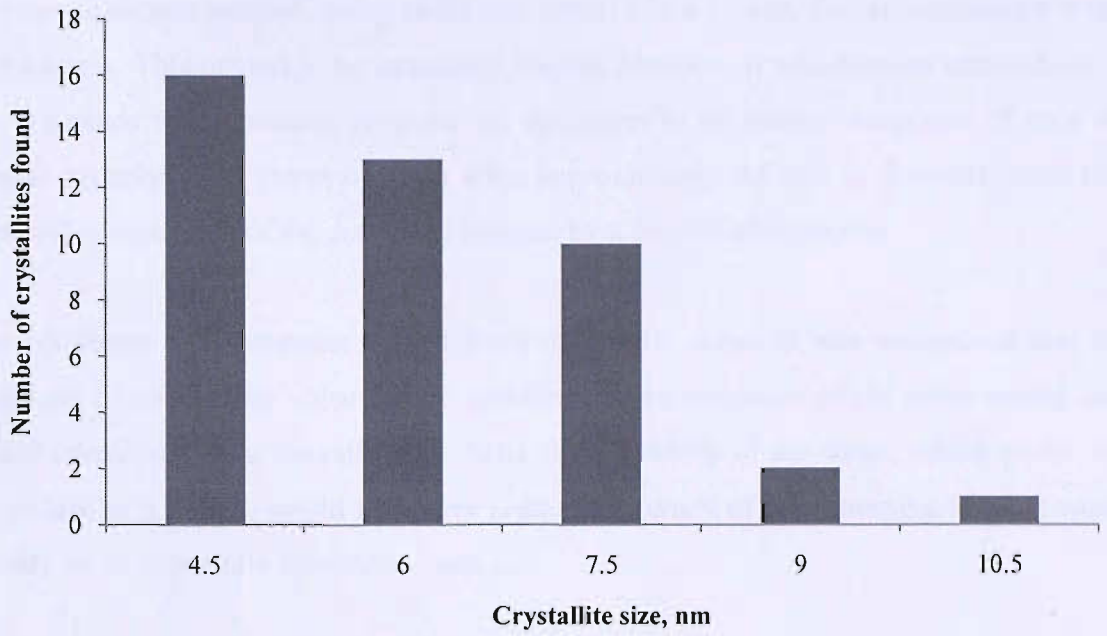

Figure 3.9: Crystallite size distribution of $TiC_{0.18}N_{0.83}$ obtained by heating the precipitate at 1000 °C for 2 hours.

Precursors annealed at 1000 °C under atmospheric nitrogen for two hours displayed particle sizes ranging from 4.5 nm to 10.5 nm with very few exceeding 10 nm and were carbon rich; the carbon content did not change as the annealing temperature was varied from 450 °C to 1000 °C.

These results are of potential interest for the creation of nanoparticle composites; useful nanocomposite materials based on TiN require a particle size of less than 10 nm in order to attain optimum hardness[41]. Additionally the introduction of C into TiN increases its hardness[55]. The speculated Ti_3N_4 phase which *should* have been obtained by heating the precursor at 450 °C in nitrogen in fact yielded a black, X-ray amorphous powder.

Chemical analysis of the material indicated a relatively high level of carbon was present. Nitrogen was also detected. The analyte's composition corresponded to $TiC_{0.22}N_{1.03}H_{0.07}$, or $Ti_3(C_{0.17}N_{0.78}H_{0.05})_{3.96}$. The material was black in colour and discovered to be electrically conductive when having a voltage applied across a pressed-disk sample by testing the conductivity of the material using a standard off-the-shelf electronic multimeter.

The specimen was pressed, using an IR disc press, into a 13 mm disc approximately 1 mm in thickness. This proved to be extremely fragile, however, it was deemed unavoidable as the resistance measurements required the specimen to be purely composed of only the sample material. Two pieces of silver wire, approximately 0.5 mm in diameter, were then attached to either end of the disc; each secured by a droplet of superglue.

The resistance measurements ranged from 0.1 to 0.3 ohms. It was recognised that this could not be an accurate value for the specimen as the resistance of the silver wiring used would contribute to the overall value. Also, the sensitivity of the meter, which could only go as low as 0.1 ohm, would also have reduced accuracy of measurement to what would already be an inherently inaccurate value.

However, as the silver wires were separated by approximately 10 mm of specimen and a resistance value was recorded. This clearly indicated that whilst the actual value was not necessarily known, the sample itself *was* electrically conductive.

Infrared reflectance spectroscopy was performed on the material. The IR active zone centre optic phonon TO mode (Ti-N or Ti-C stretching vibrations) of a highly crystallised TiN or TiC molecule occurs near 500 cm^{-1}; the LO mode[57] extends up to 800 cm^{-1}. The sample prepared at 450 °C yielded a strong peak at 480 cm^{-1} and a shoulder region which extended to 800 cm^{-1}; the spectrum was strongly reminiscent of rocksalt-structured Ti(C,N) prepared by annealing at 1000 °C (Figure 3.10). However there was also a small feature at *c.* 2000 cm^{-1} which corresponded to Ti-H vibrations and were absent in the material that was prepared at 1000 °C.

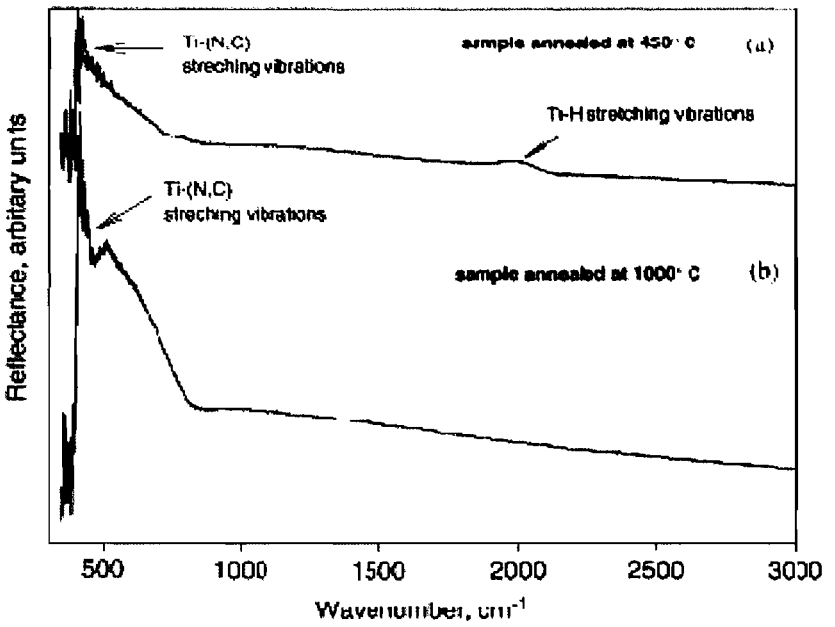

Figure 3.10: Reflectance IR spectra of $Ti(C,N)_X$ materials annealed in N_2.

TEM analysis of the sample indicated that nanocrystalline particles were present, however they were embedded into an amorphous matrix. (see Figure 3.11) The particles gave an fcc diffraction pattern with a unit cell of 4.23Å, comparable to TiN and Ti(C,N)[56]. These particles were approximately 5 nm in dimension, however they were all polycrystalline, indicating that individual crystallite sizes were infact smaller.

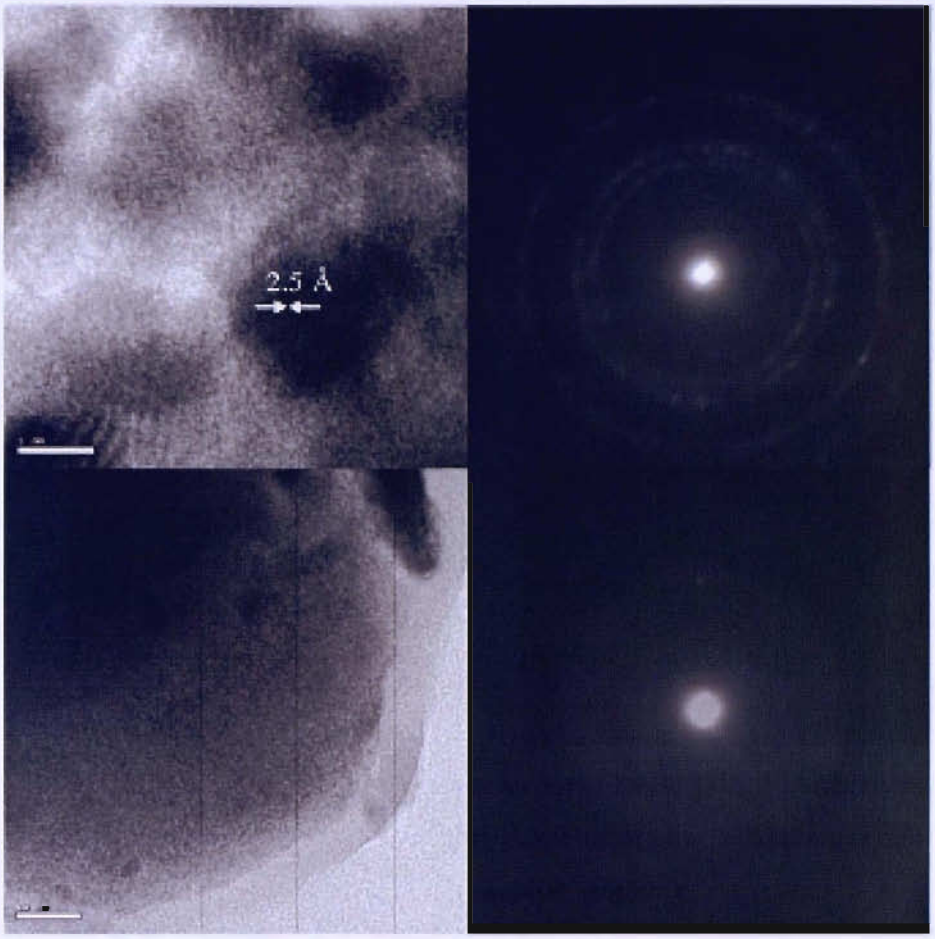

Figure 3.11: Transmission electron micrographs (left) and electron diffraction patterns (right) of polycrystalline (top) and amorphous (bottom) regions of the material annealed at 450 °C.

Lattice fringes of approximately 2.5Å were observed for some particles which corresponded to the (111) reflection of cubic rocksalt structured TiN_x (2.47Å[56]) or Ti(C,N) nanoparticles.

Electron diffraction patterns of the amorphous regions indicated d-spacings similar to the (200) and (220) reflections of crystalline TiN, albeit the rings were diffuse, suggesting that the short range structural correlations present within the amorphous material were associated with an underlying rocksalt structure.

EDX showed titanium and nitrogen in both the nanocrystalline and amorphous regions of the analyte.

Raman spectroscopy was used to characterise Ti(C,N) materials which should, if possessing a stoichiometric TiN or TiC composition, exhibit an *Fm3m* symmetry and possess no first order raman-active vibrations. As expected, samples analysed which were highly crystalline and of ideal stoichiometry exhibited only weak second-order scattering in the spectra garnered[57]. However, it was found that if the analyte possessed defects or vacancies on the cation/anion sites, the spectra developed strong acoustic branches in the regions of 250 and 350 cm^{-1}. Spectra of materials prepared at 450 and 1000 °C related to $Ti_3(C,N)_4$ and nanocrystalline Ti(C,N) respectively and were almost identical.

Both generally resemble the spectrum obtained for highly defective TiN_x (x = 0.59) (see Figure 3.6)[57]. At 600 cm^{-1} there is a broad band present in all spectra which corresponds to a combination of acoustic and optic modes (Ti-N/Ti-C stretching vibrations) and a weaker feature at lower wavenumber (200-400 cm^{-1}) due to acoustic vibrations (see Figure 3.12).

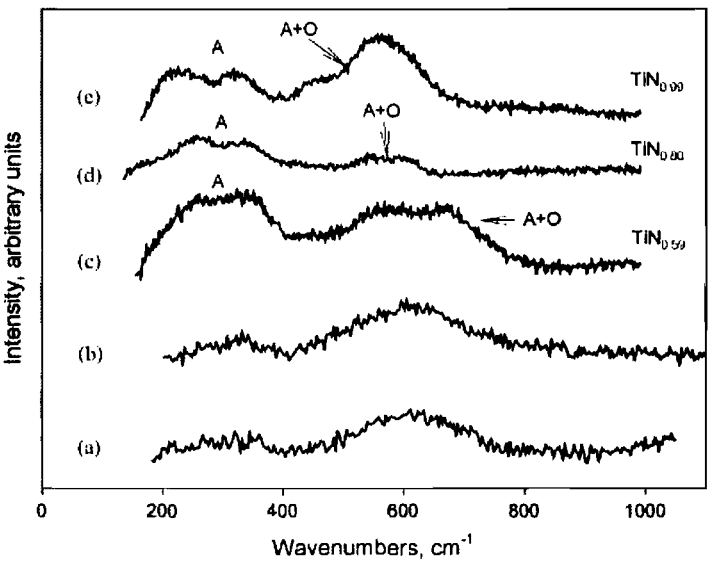

Figure 3.12: Raman spectra of $Ti(C,N)_X$ materials annealed at (A) 450 °C or (B) 1000 °C and TiN_x materials with different compositions (C, D, and E). "A" represents acoustic branches; "A+O" represents combinations and overtones of acoustic and optic branches.

The spectra indicate that both of the carbonitride materials prepared have a similar local structure and can be correlated with the underlying cubic structure of TiN/TiC, however they possess large scale defects.

3.3.2 X-Ray Absorption Spectroscopy

Titanium K-edge XAS data were obtained from the samples annealed in N_2 at temperatures from 400 to 1000 °C. The absorption edge of titanium in the XAS occurs at 4977.6 eV when the sample is annealed at 400 – 700 °C, this shifts to approximately 4979.2 eV when the sample is annealed at 900 – 1000 °C (see Figure 3.13 and Figure 3.14).

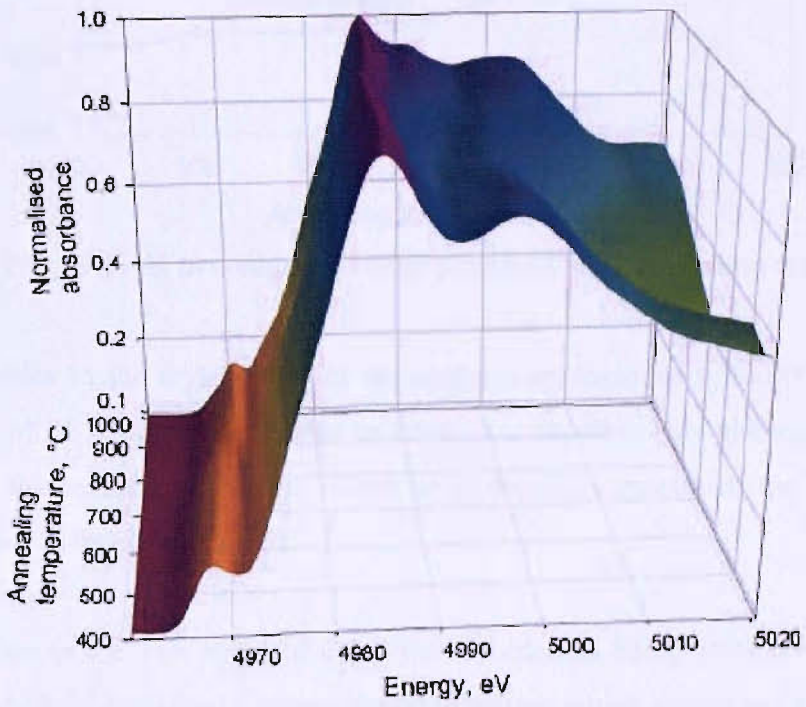

Figure 3.13: Plot of the variation in the XAS spectra, in relation to annealing temperature.

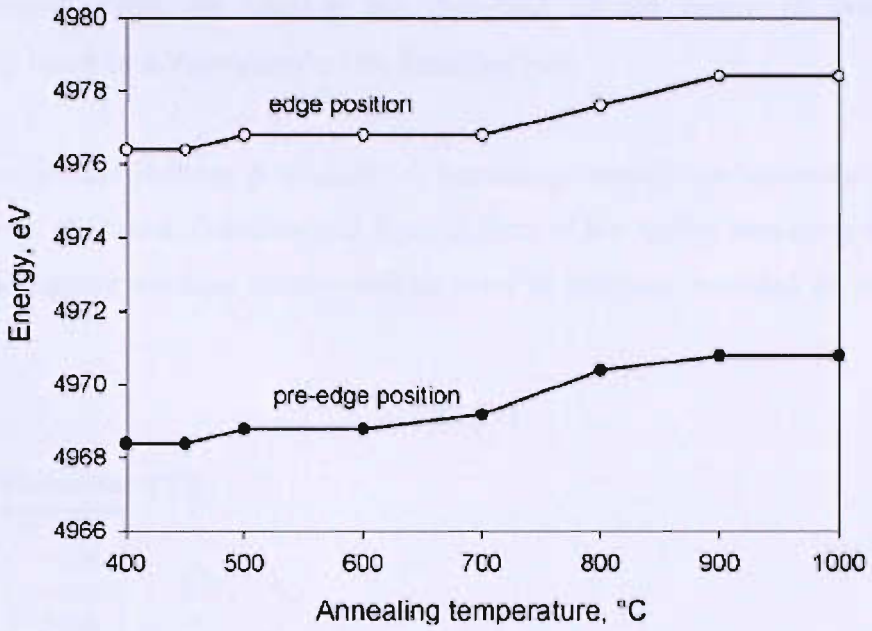

Figure 3.14: Plot of Ti–K pre-edge and edge positions with annealing temperature.

This change relates to the crystallinity of the analyte; approximately 800 °C is a critical temperature at which the material begins to crystallise rapidly. This phenomenon is also represented by the second weight-loss observed in the TGA spectra of the material (see Figure 3.1, Figure 3.4 and Figure 3.5).

The edge position of the TiN standard used was recorded as being 4978.0 eV. The near-edge region (XANES) contained a strong pre-edge feature which accounted for 14% of the edge jump, by measure of intensity, at 4968.4 eV for samples annealed between 400 - 700 °C. This feature moved to 4970.8 eV for samples annealed at 800 – 1000 °C.

The Ti pre-edge feature is attributed to s-d electron transitions that are not formally allowed for centrosymmetric sites. These types of feature have been attributed to the presence of 4- or 5- coordinate Ti in titanium bearing oxide systems, where it is known to be very weak or absent in materials that have 6-coordinated Ti^{4+} sites[58]

Cubic rocksalt-structured titanium nitrides or carbides should not exhibit any form of Ti K pre-edge feature as all the metal sites are centrosymmetric however, vacancies within the structure or the substitution of carbon/nitrogen within the coordination sphere around the

titanium central metal can lead to the distortion of the centre of symmetry and consequently result in a 'relaxation' of the selection rule.

The pre-edge feature reduces in intensity as annealing temperature increases, presumably as the material collapses, densifies and loses defects at the higher annealing temperature, although the feature remains clearly visible, even in samples annealed at 1000 °C (see Figure 3.15).

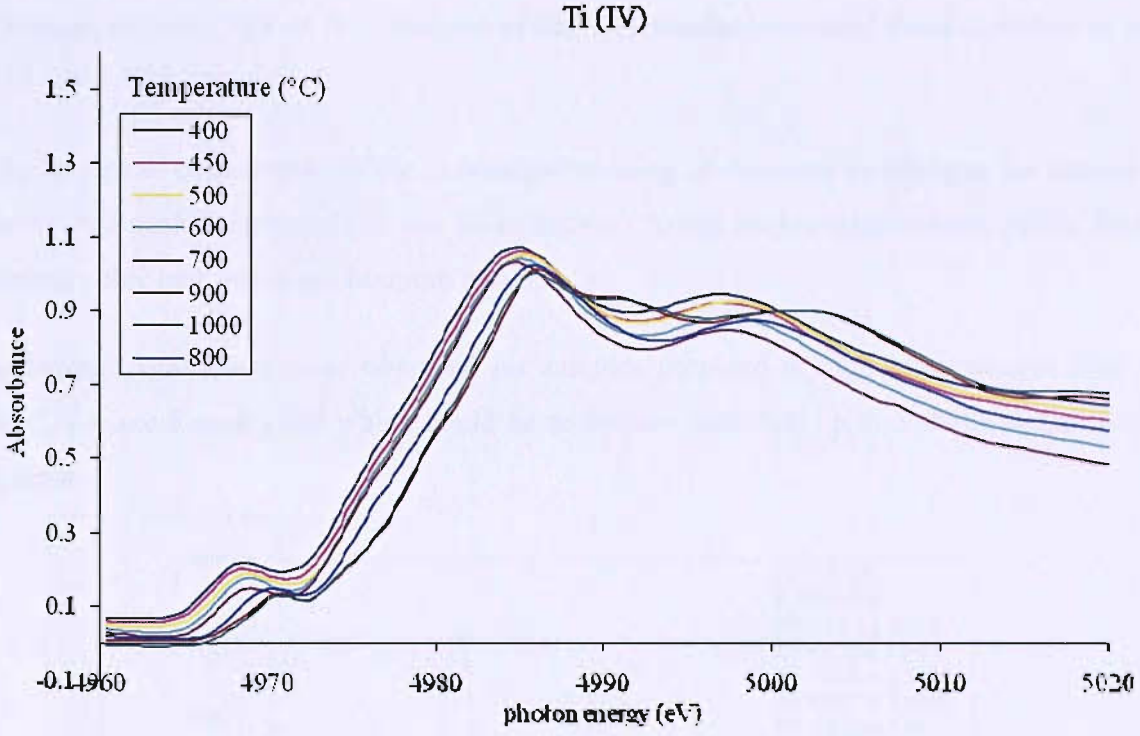

Figure 3.15: Stack-plot of near-edge XAS, illustrating the reduction in intensity of the pre-edge, against temperature.

Interestingly it was discovered that a similar pre-edge feature was present in the TiN standard used which, when analysed, was attributed to defects present within the compound, as the composition was established to be $TiN_{0.95}$.

The TiN standard possessed a pre-edge peak at around 4917.2 eV. On the strength of these data collected from the control standard, it can be concluded that the high temperature annealed samples (800 – 1000 °C) possess pre-edge features due to the presence of vacancies or disorder on the anionic sites within the structure and not due to the presence of oxide containing material.

The pre-edge feature in the amorphous Ti-C-N samples obtained from the annealing temperatures between 400 – 700 °C could potentially be due to the same reasons as for the high temperature annealed samples. Alternatively the features could be attributable to the presence of tetrahedrally coordinated $Ti(C,N)_4$ groups within the material. Ti_3N_4 has been predicted to form a spinel structure that would contain TiN_4 and TiN_6 groups[14].

The Fourier transformed Ti K-edge EXAFS data for all samples show two major peaks between 2 – 4 Å (see Figure 3.16). These distances correspond to the first and second shell distances in cubic TiN or TiC; analysis of the TiN standard revealed these distances to be 2.12 and 3.00Å respectively.

The first peak corresponds to the octahedral bonding of titanium to nitrogen (or carbon), the second peak corresponds to the Ti-Ti distance to the twelve edge centres of the face-centred cubic cell which are titanium atoms.

Additional oscillations were observed for samples prepared at high temperatures (800 – 1000 °C) (see Figure 3.16) which could be accurately modelled up to 5 shells of the cubic structure.

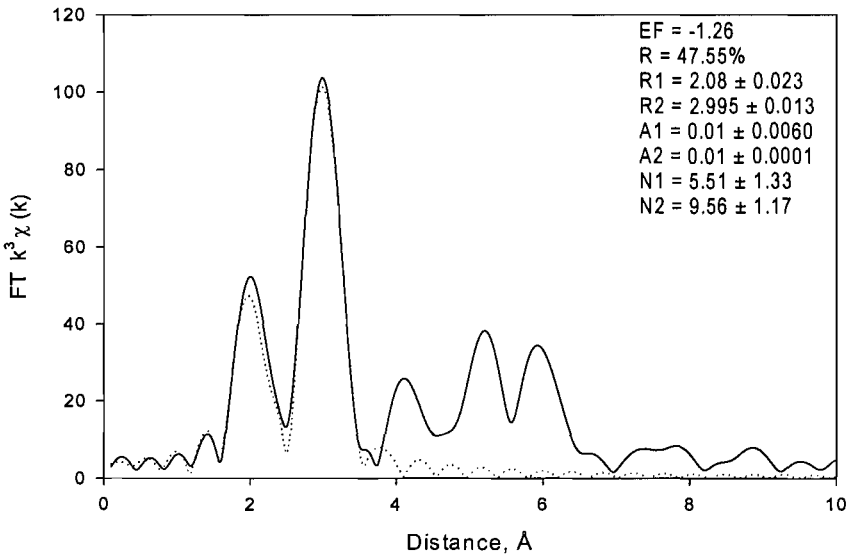

Figure 3.16: Fourier transformed Ti K-edge EXAFS of the material annealed at 900 °C in N_2 with dotted line indicating the modelled shells.

The oscillations of nanocrystalline (nc) Ti(C,N) closely resembled the TiN standard material however, the materials annealed at the lower temperatures of 400 – 700 °C

possessed only short range order and subsequently could only be modelled to the second shell (see Figure 3.17 and Figure 3.18) as accurate modelling of shells beyond the distance of 3 Å was not possible due to the unrealistic values for the Debye-Waller factors that were required to model the data.

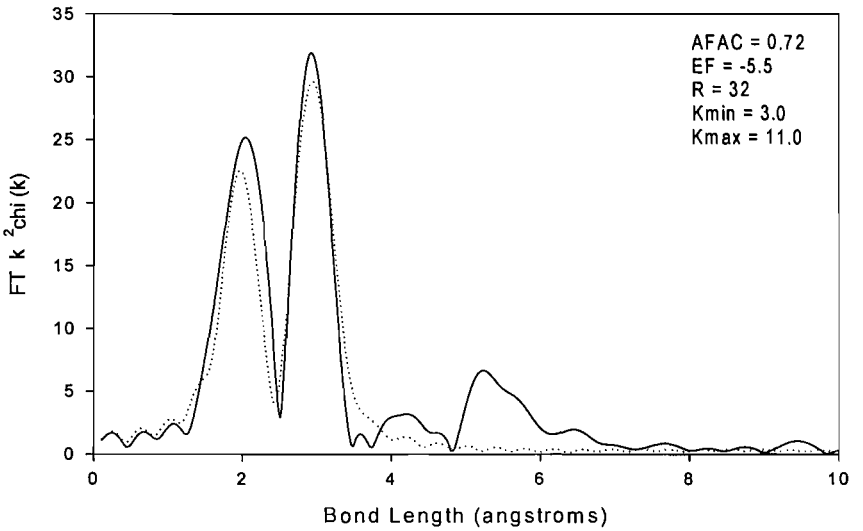

Figure 3.17: Fourier transform of TiN precursor annealed at 400°C in N_2 with dotted line indicating the modelled shells.

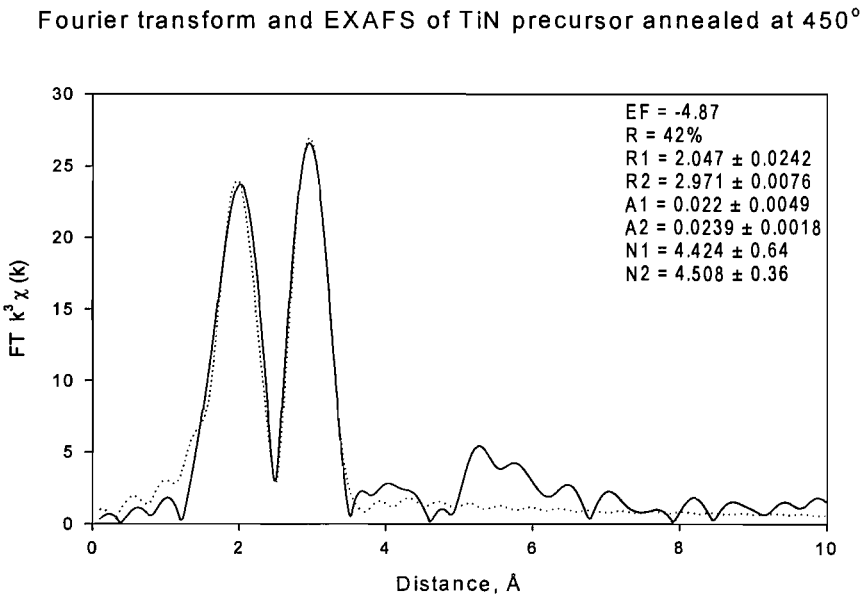

Figure 3.18: Fourier transformed Ti K-edge EXAFS of the material annealed at 450 °C in N_2 with dotted line indicating the modelled shells.

Had the low temperature annealed material been a spinel structure, the first shell (Ti-N bond) should have been recorded at a distance of 1.9Å as this corresponds to tetrahedrally coordinated TiN_4 or TiC_4 groups. Refinement of the EXAFS clearly show that this was not the case and that there was no significant broadening of the first-shell peak which could be interpreted as being an indication of the presence of tetrahedrally coordinated TiN_4 or TiC_4 groups.

The structure of the amorphous Ti-C-N sample most likely contained Ti-N/C sites which were octahedrally coordinated, as is found in the cubic rocksalt structured TiN or TiC.

The modelled bond-lengths of the first and second shells are detailed in a table below as a function of annealing temperature. (see Table 3)

	Ti – N Bond Data			Ti – Ti Bond Data			
Annealing Temperature (°C)	R_1 (Ti-N) (Å)	σ^2	Coord. no.	R_2 (Ti...Ti) (Å)	σ^2	Coord. no.	R (%)
400	2.032(9)	0.022(1)	4.87(32)	2.962(7)	0.021(2)	4.48(32)	32.68
450	2.047(24)	0.022(5)	4.42(64)	2.971(8)	0.024(2)	4.51(36)	42.00
500	2.029(12)	0.028(3)	4.62(56)	2.987(10)	0.026(2)	5.58(54)	42.56
600	2.036(12)	0.028(5)	4.53(53)	2.994(13)	0.028(3)	5.67(57)	43.29
700	2.080(2)	0.020(6)	4.50(50)	3.000(1)	0.020(2)	5.00(49)	42.80
800	2.082(20)	0.020(1)	4.959(91)	3.008(11)	0.022(1)	10.95(102)	47.67
900	2.080(23)	0.010(6)	5.51(133)	2.995(13)	0.010(1)	9.96(117)	47.55
1000	2.100(20)	0.010(2)	6.07(129)	3.000(10)	0.010(1)	12.00(115)	51.00

Table 3: Refined Ti K-edge EXAFS parameters obtained on samples annealed in N_2 (°C)

The first shell Ti-N/C bonding was modelled as being between 2.029 – 2.047Å for samples annealed from the temperatures of 400 – 600 °C. This increases to 2.08 – 2.1Å from 700 – 1000 °C whilst the second shell Ti-Ti distance increases gradually from 2.96Å at 400 °C to 3.00Å between 700 – 1000 °C.

These observations are consistent with the structural changes that would be observed within a rocksalt structured titanium nitride/carbide material as the structure crystallises and establishes order.

The second shell Ti-Ti distance remains consistent with that expected for the cubic rocksalt structure throughout the annealing series however, the coordination number is 5.5 below 700 °C which is much lower than the coordination number of 12 which should be expected for a rocksalt structure. This rises sharply when annealing temperatures exceed 700 °C (see Figure 3.19) to 12 as would be expected, indicating that the structure has densified and ordered itself removing vacancies to achieve an ideal coordination number.

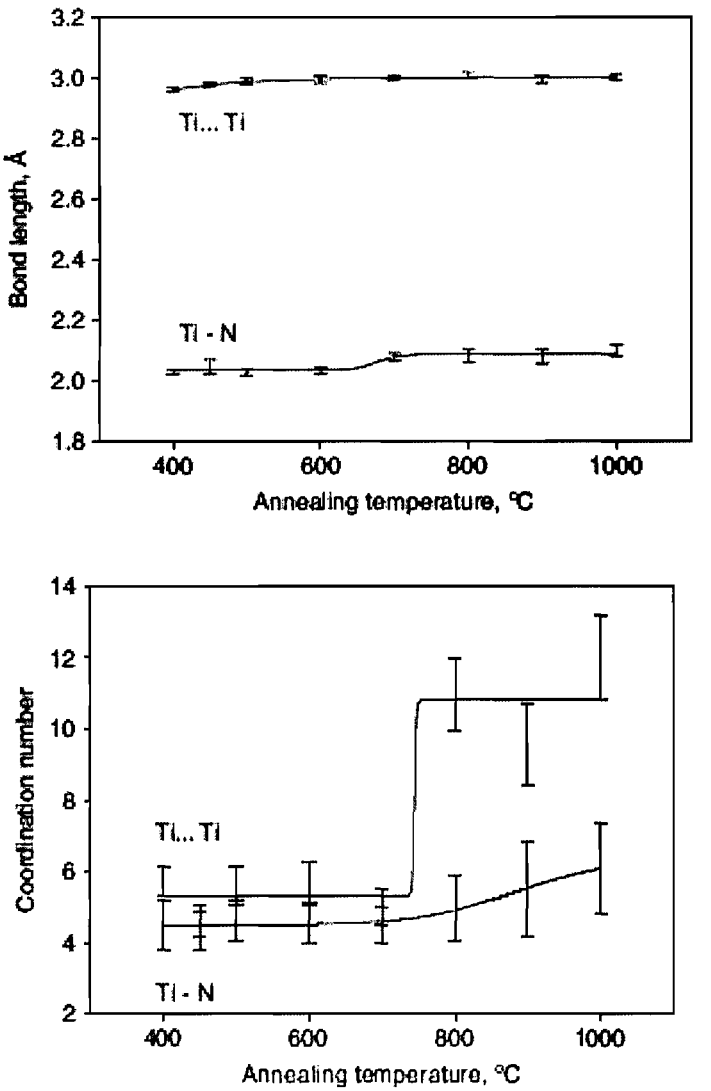

Figure 3.19: Variation with annealing temperature of refined bond lengths and shell occupations from Ti K-edge EXAFS data.

The Ti-N shell was determined to have a coordination number of 4.5 which indicates the presence of vacancies; the coordination number should, of course, be 6. However when annealing temperatures rose above 700 °C the coordination number gradually increased to the optimum coordination number. (see Figure 3.19)

The data accrued by all the previous analytical methods (XAS, TEM, IR, TGA) suggests that the structure of all the materials obtained from the ammonolysis of tetrakis(dimethylamino)titanium are based on the cubic rocksalt crystal structure of TiN/TiC. For the products annealed at temperatures below 700 °C the frequency of defects was much greater; 45% of Ti sites possessed vacancies. Anionic vacancies were lower with an average occupation of 75%, based on the first-shell occupation number determined from the EXAFS.

The anionic sites are occupied by either nitrogen or carbon atoms from the initial precipitation reaction to produce the precursor, hydrogen could also be present in small quantities.

The material produced at low temperature possesses a suggested stoichiometry of $Ti_3(C,N)_4$ and is X-ray amorphous by analysis using a Siemens D-5000 diffractometer with Cu-Kα_1 radiation and Bragg-Brentano geometry. However, some regions of the material did exhibit a degree of nanocrystallinity within the 'B1' structured motif that is detectable by electron diffraction (see Figure 3.20).

Figure 3.20: A diffuse electron diffraction pattern of the TiN precursor after annealing at 450 °C under N_2.

Whilst both nanocrystalline and amorphous areas are titanium nitride or titanium carbonitride, it is undetermined as to whether these areas possess the same stoichiometry. Upon annealing, condensation of the structure begins to occur. Gaseous carbon and nitrogen containing components are lost and the composition of the material gradually becomes the thermodynamically stable – and favoured – stoichiometric TiN or Ti(C,N) with the rate of C/N removal being proportional to the reductive nature of the atmosphere; greater amounts of carbon are removed in ammonia rich atmospheres.

The material produced from annealing at low temperatures is likely to be a highly defective, structurally disordered $Ti_x(C,N)_y$ whose basic arrangement of cations and anions is loosely associated with the cubic rocksalt-type crystal structure; 45% of the second shell Ti atoms are missing causing the density of the material to be less than 50% that of titanium nitride or carbide. However, the loss of density is not necessarily a disadvantage; if the material possesses the same or similar properties to their family group then it could find use as a low density alternative for current nitride applications.

The formation of 'laddered' $[TaN]_5$ units was illustrated during the ammonolysis of $(tBuCH_2)_3Ta(CHtBu)$ where additional ammonolysis, followed by thermolysis of the

product produced cubic TaN[59]. Flat laddered structures were suggested to be formed due to the steric bulk of the $^{t}BuCH_2$ groups.

In the case of titanium, octahedral symmetry can be maintained on the Ti irrespective of if the edge-linked Ti_2N_2 units are perpendicular to each other, due to fourth vertex of the cubic formation being able to be occupied by a bridging amine or amide ligand. (See Figure 3.21)

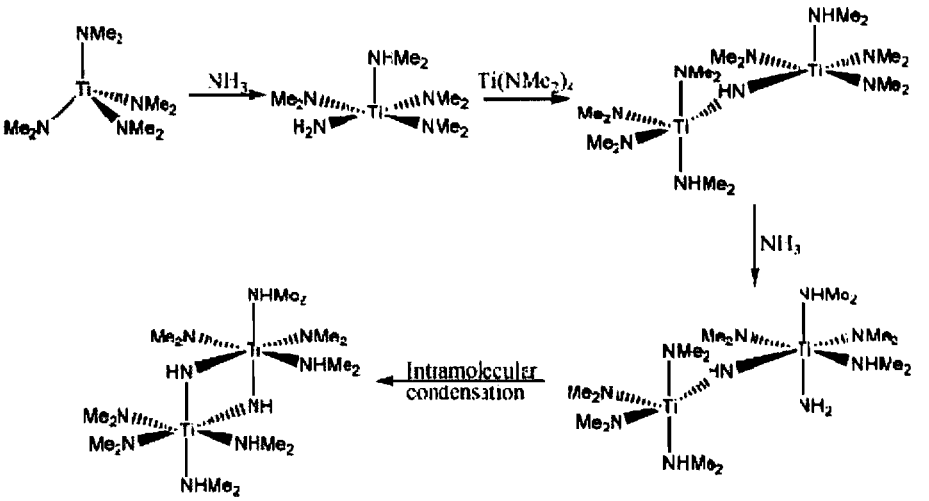

Figure 3.21: Formation of Ti_2N_2 rings with saturated Ti-coordination sphere by intramolecular condensation.

This leads to the resultant four-membered ring structure being more complex than the product observed in the ammonolysis of $(tBuCH_2)_3$-Ta(CHtBu). Large quantities of coordinated amine will still be present within the precursor material, resulting in a material rich in carbon, nitrogen and hydrogen ($TiC_{0.5}N_{1.1}H_{2.3}$). Thermolysis of the material to 400 °C resulted in the removal of amide and terminal dialkylamide groups in the form of amines and ammonia[13]. This would likely cause some relaxation of the titanium and anionic sub-lattices although the thermolysis temperature is not sufficient to facilitate widespread bond rearrangement within the material's lattice structure which occurs above 700 °C.

However, even at 'low' annealing temperatures, where diffusion is expected to be limited, the formation membered rings and consequently a rocksalt type crystal structure is still the thermodynamically favoured outcome.

The composition of precursor material approached Ti-C-N when thermolysed to 400 °C, with the titanium atoms placed on the cationic sites of the cubic lattice and holding an occupancy of 50%; carbon and nitrogen atoms inhabited the anionic sites and had an occupancy in the region of 50%, albeit slightly greater.

When considering the level of disorder that would occur from the collapse and recombination of 'cages' formed through such a process it is understandable as to why the final structure is so defective.

During the final heating stages of the precursor material, where the temperature of thermolysis is raised to 700 °C, significant levels of bond reformation and diffusion of volatilised species occur. The structure rearranges into cubic rocksalt TiN or Ti(C,N); thermodynamically stable in it's immediate environment and in equilibrium with the annealing atmosphere of nitrogen or ammonia.

3.4 Conclusions

The investigation of the solution phase reaction of tetrakis(dimethylamino)titanium with ammonia which precipitates $TiC_{0.5}N_{1.1}H_2$ established that it was a suitable method for preparing precursors useful for the synthesis of titanium nitride, or carbonitride, materials.

Decomposition of the material occurred in two stages, to yield a cubic rocksalt structured material when heated to 700 °C or above in an atmosphere of ammonia; when heated in nitrogen the composition was found to be $TiC_{0.2}N_{0.8}$ and nanoparticles in the region of 4-12 nm were formed from both reactive atmospheres.

Heating the material to 450 °C resulted in an X-ray amorphous compound with a composition of $Ti_3(C_{0.17}N_{0.78}H_{0.05})_{3.96}$, TEM analysis of this material indicated that nanocrystals in the region of 5 nm were embedded in an amorphous matrix. The local structure of the compound was related to cubic rocksalt Ti(C,N) but with a large proportion of titanium and nitrogen/carbon vacancies; first shell coordination numbers of the titanium being 4.5 and second shell 5.5, instead of 6 and 12 respectively.

The amorphous material was found to possess a density approximately 50% of what would be expected for Ti(C,N) and the structure is speculated to have resulted from the condensation of Ti_2N_4 species during the ammonolysis of tetrakis(dimethylamino)titanium.

A hardness rating of 100GPa has been claimed for nc-TiN/a-Si_3N_4 compared to 33 GPa for TiN and 92GPa for diamond, due to the inhibition of dislocation movement and growth within the material[41]. Potentially the same principle applies to the amorphous products produced from this methodology and gives rise to the potential for the material's use as a precursor for the synthesis of ultra-hard nanocomposites in the titanium nitride or carbonitride family.

4 FILMS FROM PRIMARY AMINES

4.1 Introduction

The aim of the work which is discussed in this chapter was to develop a sol-gel deposition method capable of depositing a thin film, using a methodology which enabled the films to self-condense and ideally, to be annealed under inert atmospheres removing the requirement of using ammonolytic species which would represent a beneficial step forward in the general processing of the material [60].

Titanium nitride films are commonly produced by physical or chemical vapour deposition for a variety of applications of which electronics is a major user utilising the films' quality as a low electrical resistance diffusion barrier. In engineering, the physical qualities of hardness with chemical and thermal stability are utilised[4,5,7].

Chemical vapour deposition is a method of forming dense coatings using the decomposition of relatively high vapour pressure gases. Gaseous compounds of the materials to be deposited are transported to a substrate surface where a thermal reaction/deposition occurs. Reaction by-products are then exhausted out of the system.

CVD[61] is a very versatile process used in the production of coatings, powders, fibres and monolithic parts. However, due to the nature of the precursor materials, by-products are almost always both highly volatile and toxic. For example, chlorides are used regularly for producing coatings of titanium nitride as is tantalum chloride, for the production of tantalum nitride. see Figure 4.1 below).

1. $TiCl_4 + NH_3 + ½\ H_2 = TiN + 4HCl$
2. $TaCl_5 + NH_3 + H_2 = TaN + 5HCl$

Figure 4.1: Examples of the use of chlorides to produce titanium and tantalum nitrides.

The process of depositing these films usually requires high temperatures, circa 1000 °C, although in CVD this can be reduced through the use of plasmas or by using molecular precursors with ammonia[62]. Whilst these techniques are highly developed and capable of

producing high quality films, there are factors which need to be considered before deposition can proceed by either method, such as deposition chamber size in relation to the target substrate. This has led to the consensus that the development of additional methods, such as sol-gel, can expand the range of conditions under which deposition can be successfully performed and only increase the accessibility of the material.

Sol-gel techniques can already access a variety of morphologies which would be of great interest if nitride materials could be manipulated in the same manner, for example, templating methods which can produce ordered mesoporous and macroporous arrays are of great interest for catalytic and filtration applications[63]. Many of these materials are silicon-based and the most common synthetic route to the production of silicon-based gels is *via* acid-catalysed ammonolysis. Examples of Si-based materials include the production of carbon free silicon nitride precursor xerogels from $Si(NMe_2)_3NH_2$[64]; the use of this precursor to deposit supported, porous Si_3N_4 membranes[65] and also the reaction of the precursor with boron chlorides, followed by additional ammonolysis, to produce Si-B-N precursor gels[21]. Halide or amine-templated porous SiN_x materials produced by the pyrolysis of such gels are promising solid base catalysts and subsequently Si-Al-N and Ga-N precursor gels have been produced with this specific purpose in mind[66,67].

With respect to *metal* nitrides, the area of sol-gel chemistry is much less developed; Jansen has published studies of mixed silicon/transition metal amide-derived gels from co-ammonolysis of $Si(NHMe)_4$ with $Ti(NMe_2)_4$, $Zr(NMe_2)_4$ or $Ta(NMe_2)_5$ from which pyrolysis yields amorphous ternary nitrides[23]; the same chemistry has been used to make binary transition metal and rare earth nitride powders by ammonolysis of metal amides followed by pyrolysis[6,13]. A major drawback of working with the ammonolysis of amides, whether they are main group elements or metals, is that the reaction often leads to uncontrollable precipitation; especially in the case of metal amides. This is due to the basic conditions under which the ammonolysis reactions are carried out. Base catalysis of the condensation process by which M-NH-M linkages are formed is well known, in oxidic sol-gel processes, to lead to particle growth[40].

Oxide films, typically, are produced under acid catalysed conditions, which favour chain growth and allow development of coating sols with high solubility. In systems where

control of the hydrolytic process is difficult, several alternative approaches have been developed, for example, doping of silica glasses with titanium is constricted by the difference in rates of hydrolysis exhibited by titanium and silicon alkoxides. This was overcome by the reaction of benzyl alcohol with chlorides in order to maintain stoichiometry in these materials[68]. These approaches are often termed 'non-hydrolytic' sol-gel methods; an analogy in the nitride system is the self-condensation of a primary amide according to the reaction below:-

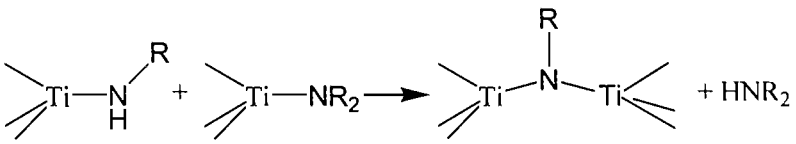

Figure 4.2: Diagram illustrating the self-condensation of a primary amide.

Bradley noted that the preparation of $Ti(NHR)_4$ by ligand exchange of $Ti(NMe_2)_4$ or $Ti(NEt_2)_4$ with excess primary amines often failed due to this process, which is facile with unsaturated metal centres and sterically unhindered amines[9]. Instead of molecular primary amides he obtained insoluble, polymeric materials. In this chapter this chemistry was developed to produce sols capable of coating glass and pyrolysed to produce titanium nitride or carbonitride films.

4.2 Experimental

All experimental procedures were carried out in a controlled inert atmosphere of nitrogen gas; using either a Schlenk-line for the synthesis, or a glove-box for the handling of reagents, products and storage.

Tetrakis(dimethylamino)titanium (3.0 ml, 0.0127 mol), provided by Epichem, was dissolved in sodium dried tetrahydrofuran and the amine dried using barium oxide.

As the sols were highly air sensitive the coating of the tiles could not be performed in a conventional manner as the sol would rapidly oxidise. A coating technique was devised, utilising a modified dropping funnel.

To emulate the immersion and submersion of a substrate in a coating sol, a substrate was suspended from a hooked glass rod inside the modified dropping funnel, the sol was pumped *via* reduced pressure from a separate Schlenk tube into the dropping funnel and the Teflon Young's tap was used to regulate the release of the coating sol from the dropping funnel back into its original containing vessel (see Figure 4.3); the release rate of the coating-sol was in the region of *ca.* 2 mm/s.

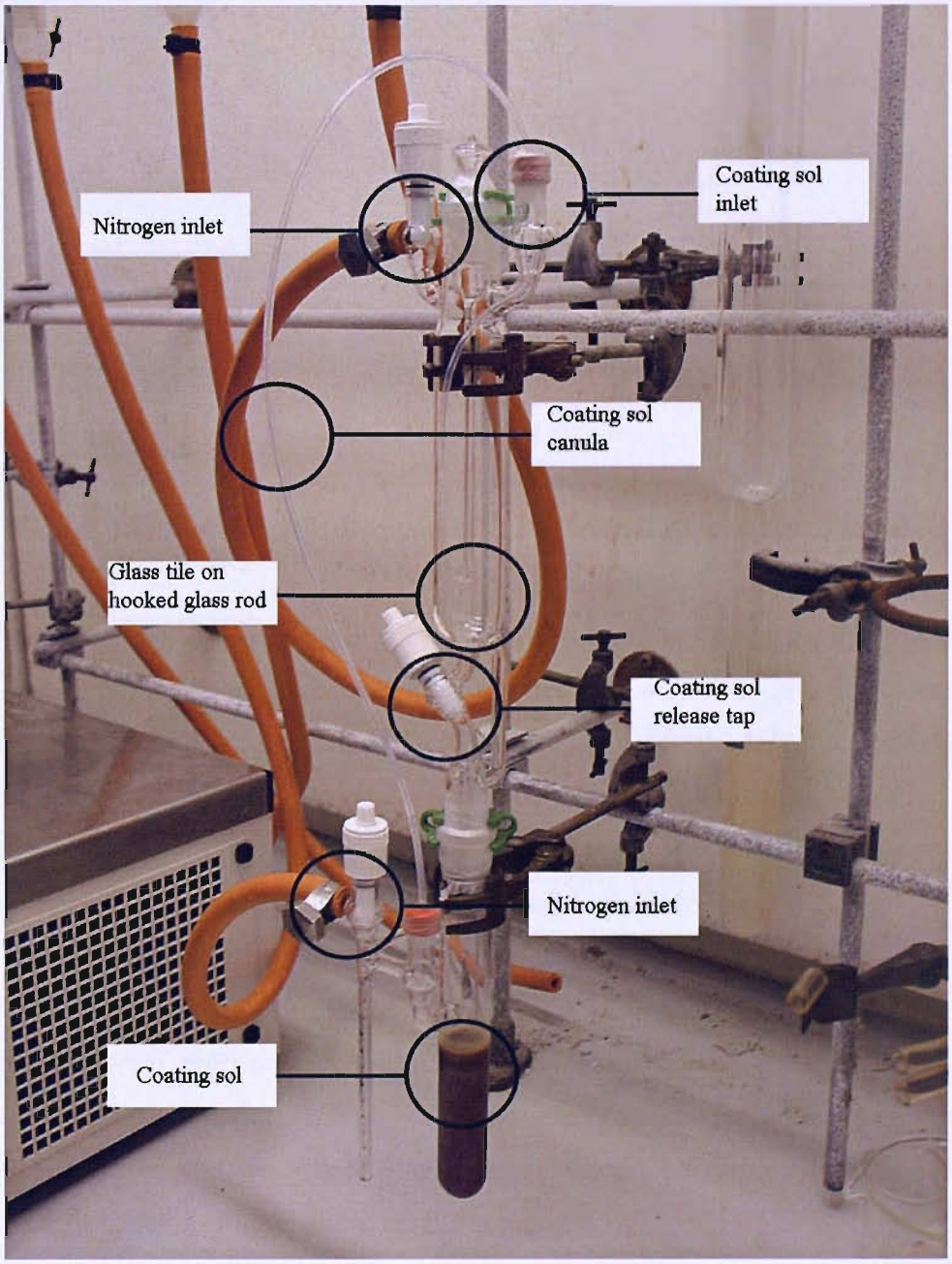

Figure 4.3: The modified dropping funnel, with highlighted areas of significance.

Once the sol had been drained from the dropping funnel, the tap was closed and the film was dried under a mild vacuum, as the viscosity of the coating-sol was low enough to run-off the substrate if the residual solvent was not removed. This was accomplished by the gradual evacuation of the dropping funnel.

The apparatus was transferred to a nitrogen-filled glovebox where the tile was loaded into a dry alumina boat. This was then loaded into a custom designed furnace tube; see Figure 4.4.

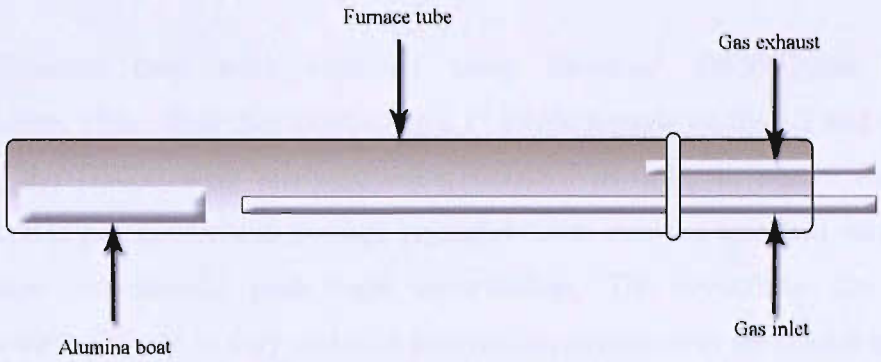

Figure 4.4: A schematic diagram of the custom designed furnace tube.

The apparatus was flushed with anhydrous ammonia or high purity nitrogen for approximately one hour and then heated to between 400 – 800 °C in order to anneal the tile. This temperature was increased at a rate of 2.5 °C/min to the target temperature, held for a duration of three hours and then allowed to cool back to room temperature.

Scanning electron microscopy was performed using Jeol JSM5910 and JSM6500F SEMs; Transmission electron microscopy was performed using a JEM3010 TEM.

SEM samples were prepared in a nitrogen-filled glovebox in order to minimise the potential for surface oxidation. The tiles were mounted on conductive stubs and usually did not require coating; the deposited film was, as should be expected for a nitride or carbonitride film, suitably conductive for the technique.

Analysis of the film thickness was achieved by the fracturing of the coated tile so a cross-section of the substrate could be viewed. This was then carbon coated to enable the uncoated 'core' of the substrate to be conductive. These tile fragments were then mounted in conductive putty 'edge-on' to the electron beam and detector.

TEM samples were again prepared inside a nitrogen-filled glovebox and coating fragments were shaved from the substrate surface by using a Stanley-knife blade. These 'shavings' were then ground in 1.0 ml deuterated benzene (C_6D_6) and a droplet of the solution was deposited onto a carbon/copper grid. The solvent was then allowed to evaporate leaving just the ground solid distributed across the grid.

X-ray diffraction data were collected using Siemens' D5000 and Bruker C2 diffractometers. Films were measured using a 1° incident angle on the C2 and the collected data using the D5000 were analysed using GSAS[69] in order to obtain the respective analytes' lattice parameters and average crystallite size. A silica standard was used to fix the Gaussian instrumental peak-shape contribution. The crystallite size and strain parameters were allowed to vary and then analysed as described in the GSAS manual[70].

X-ray photoelectron spectra were collected using a Thermo-Electron Theta-Probe with Al-K_α radiation. Depth profiles were collected with 50 × 20 s Ar^+ etching steps. Combustion microanalysis (C, H, N) was carried out by Medac Ltd and H^1 and C^{13} NMR spectra were collected using a Bruker 'Av300'. NMR samples were made up in the glovebox using C_6D_6 and allowed to develop for two hours before collection.

4.3 Results

The amines *n*-propylamine, *n*-octylamine and *t*-butylamine were used as the transaminating species and it was observed that when using the *n*-amines, a yellow translucent solution was initially formed which then darkened in approximately two minutes to a red translucent colour, which would then continue to darken over the period of one hour until an intense blood-red solution was obtained.

When using *t*-butylamine approximately 15 minutes passed before any visual darkening of the yellow solution commenced. After two hours the solution had achieved an orange-red colour, which was significantly less intense than what was seen for the *n*-amine reactions and, irrespective of the quantity of *t*-butylamine used, the solution never progressed beyond the visual stage of an orange-red solution. All sols produced were stable for a period of several days, after which point a fine precipitate began to form in the bottom of the reaction vessel. The precipitate was extremely fine and quantitatively there was very little, therefore upon attempting to separate the solution from the solid for analysis *via* vacuum filtration, the precipitate blocked a class four sinter and was unable to be physically removed as it had distributed itself throughout the pores of the sinter and not collected on the surface.

The viscosities of the sols were markedly different depending on which type of amine was used. A visual estimation of the viscosity was conducted by observing the solutions' flow characteristics and adhesion to the inside walls of the reaction vessel. *n*-propyl and *n*-octylamine products were relatively viscous and their viscosity increased proportionally with an increase in the concentration of reagents; the estimated viscosity being ~30 - 80 cP, the same as would be expected for milk. The *t*-butylamine solutions were near unchanged from the original viscosity of the THF/amide solution which would give an approximate viscosity of 0.48 cP. The coatings were prepared by stirring the aforementioned solution for two hours before use. Quartz silica tiles (14 × 25 × 1 mm) were prepared by immersion in 'Piranha etch' (1:3 H_2SO_4:H_2O_2) for 24 hours. This was performed in order to remove grease, dirt and other contaminants from the surface of the substrate; the presence of any foreign bodies would contribute towards poor adhesion on behalf of the coating-sol which would translate into cracking and flaking of the coating upon annealing at high temperature. The tiles were then removed from the piranha etch, rinsed in copious amounts of distilled water and then placed in a drying oven at a temperature of ≥100 °C for at least 24 hours. Acetone *was not* used to remove the potentially oxidative residue of distilled water as it was found to leave residues on the substrate surface itself.

A series of films were deposited onto silica substrates using sols produced from 11.2 mmols (3 ml) tetrakis(dimethylamino)titanium, 22.4 mmols of the amine $^{n}PrNH_2$, $^{n}OcNH_2$ or $^{t}BuNH_2$ and 5, 10 or 20 ml THF, of which each product/film was annealed at two

separate temperatures (400 and 800 °C), and under two different atmospheres (NH_3 and N_2). This gave an array of 36 coated substrates which individually varied in defects, colouration and adhesion. Generally they were found to be either grey or golden in colour. The golden films also exhibited iridescent qualities and all the films generally displayed good levels of adhesion to their respective substrates as judged by the use of the 'scotch-tape test'. This test involved pressure sensitive adhesive tape being applied to an area of the chosen film and then peeled off. The film was deemed to be sufficiently adhered to the substrate if, upon the removal of the tape, it remained intact.

SEM images of the coatings produced from $^{n}PrNH_2$, at all three of the levels of dilution and which were annealed under a nitrogen atmosphere at 800 °C are displayed in Figure 4.5.

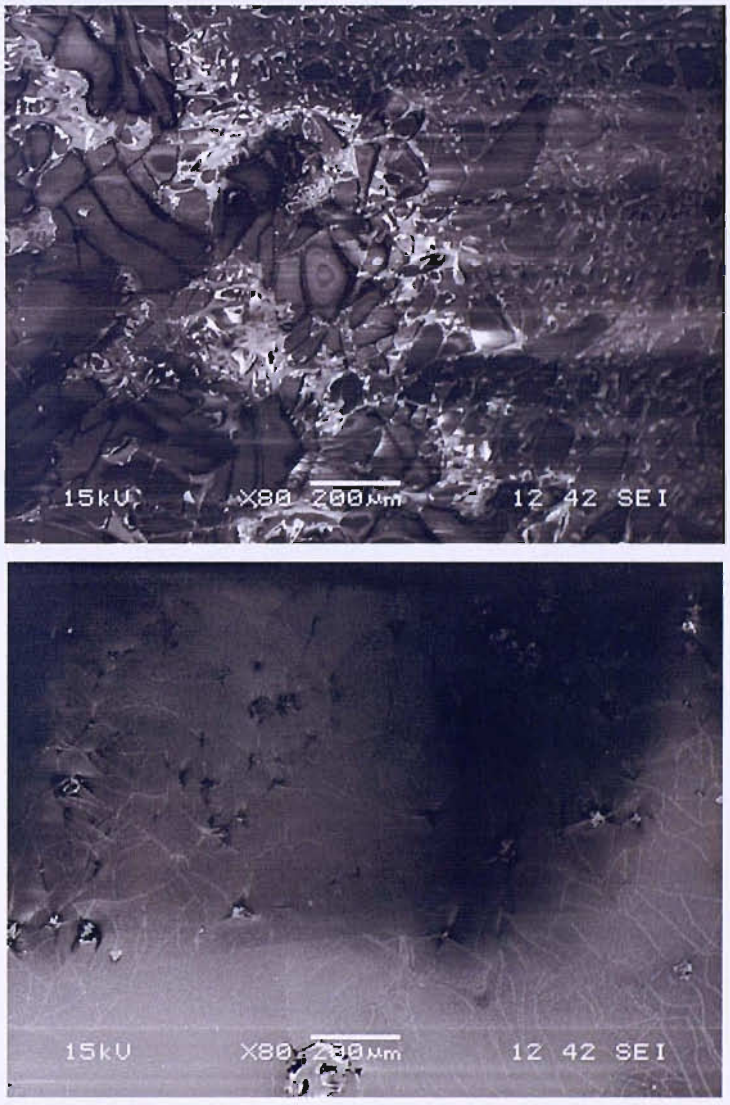

Figure 4.5: SEM images of films produced with $^{n}PrNH_2$ and $Ti(NMe_2)_4$ solutions, made with 20 cm^3 (Top), 10 cm^3 (Middle) or 5 cm^3 (Bottom) THF and then pyrolysed in N_2 at 800 °C.

The lowest concentration sol displayed poor coverage of the substrate and wide cracks are also present between which, the substrate was clearly visible. When the quantity of THF was reduced to 10 ml the coatings were much smoother and possessed narrow cracks and 'pinhole' defects around which some peeling of the film was also observed, (see bottom image Figure 4.5).

The highest concentration sol, using only 5 ml of THF possessed no cracks, although the presence of 'pinhole' defects was still observed. Similar trends were observed when heating films of the same concentrations to 400 °C under NH_3, (see Figure 4.6).

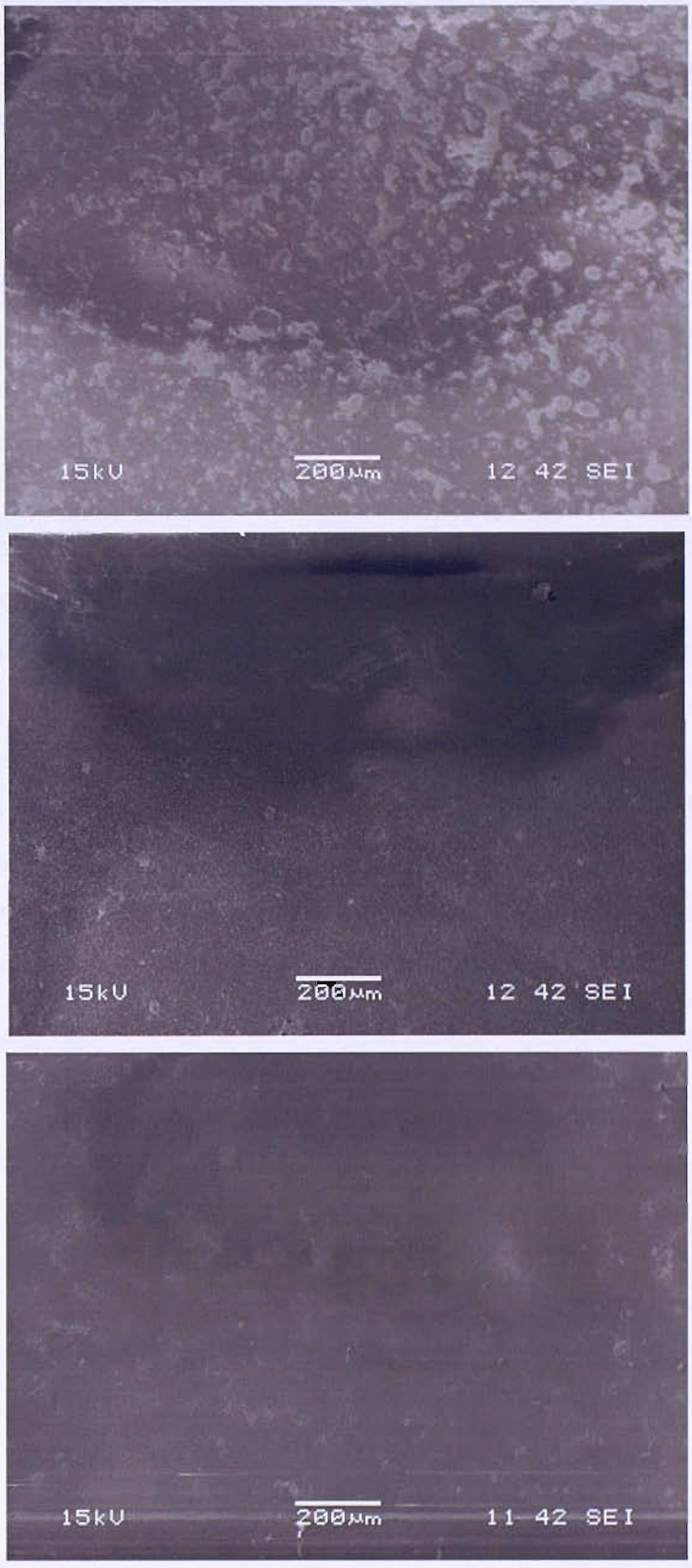

Figure 4.6: SEM images of films produced with $^{n}PrNH_2$ and $Ti(NMe_2)_4$ solutions made with 20 cm^3 (Top), 10 cm^3 (Middle) or 5 cm^3 (Bottom) THF and then pyrolysed in NH_3 at 400 °C.

It should be noted that the quality of the films is very good for such a basic 'single-dip' coating technique, indicating that automation and further refinement of the method of deposition should lead to further improvements in the quality of the deposited film.

As was stated earlier the coated tiles did not require a conductive carbon coating in order to dissipate electrons away from the beam. Some 'charging' (a phenomenon wherein white patches are observed which progressively increase in intensity and interfere with the overall image; caused by the absence of a conductive pathway for the electrons to be dissipated away from the beam), was observed which was concentrated around areas possessing defects where the silica substrate beneath the surface coating could be observed. Irrespective of the defective areas of the films, the substrates were still clearly conductive which was a good indication that the coating present was either titanium nitride or carbonitride as was intended, either of which are conductive.

Using $^{n}OcNH_2$ as the cross-linking agent resulted in a similar set of results, with the films exhibiting wide cracks and peeling when larger quantities of solvent were used, whilst smooth films with few pinhole defects and very few cracks were observed when the least amount of solvent was used (see Figure 4.7).

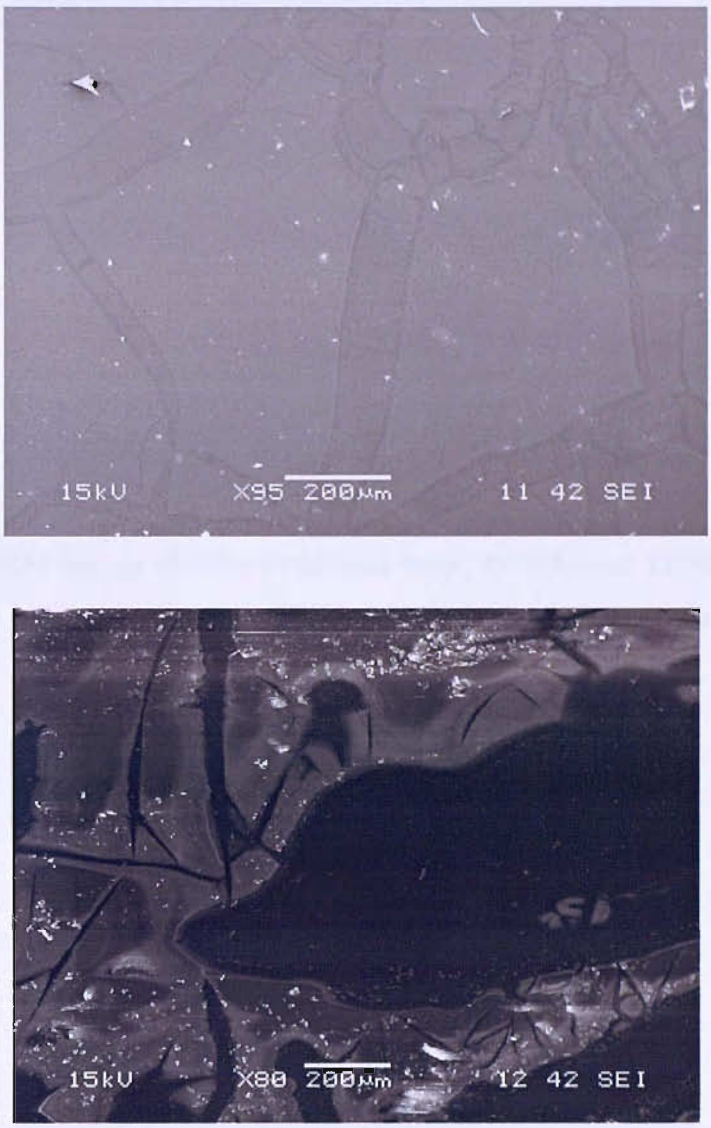

Figure 4.7:SEM images of films produced with $^{n}OcNH_2$ and $Ti(NMe_2)_4$ solutions made with 20 cm^3 (top) or 5 cm^3 (bottom) THF and then pyrolysed in NH_3 at 400 °C.

The quality of the films produced when using 10 ml THF was higher than when using $^{n}PrNH_2$, see Figure 4.8 and Figure 4.9, as whilst a network of cracks can be seen across the surface of the substrate, significantly, no peeling had occurred. Also, there is significantly less 'charging' occurring on the surface of the octyl-based film, denoting that there is a more comprehensive coating, with less defects present on the substrate. The films' thicknesses were established by measuring the depth of coating when imaging the cleaved substrates whilst mounted 'edge-on'.

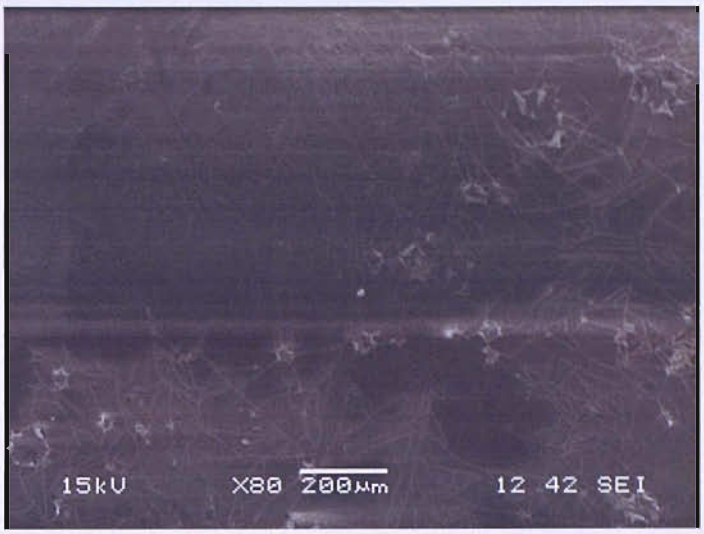

Figure 4.8: SEM Image of Film Produced with $^{n}PrNH_2$ and $Ti(NMe_2)_4$ from a Solution made with 10 cm^3 THF and then Pyrolysed in N_2 at 800 °C.

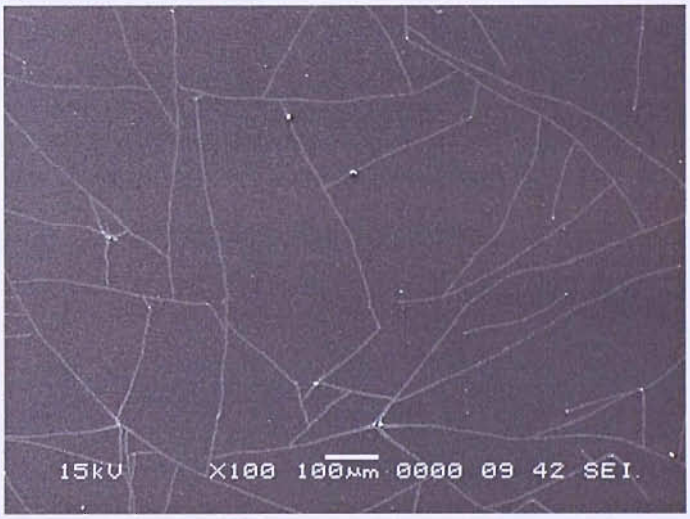

Figure 4.9: SEM Image of film produced with $^{n}OcNH_2$ and $Ti(NMe_2)_4$ from a solution made with 10 cm^3 THF and then pyrolysed in N_2 at 800 °C.

It was found that film thicknesses varied dependent on the concentration of the sol; thicker films tended to be provided from the higher concentration sols and it was found that the films produced using 10 ml quantities of THF gave films approximately 0.9µm thick, whilst sols formulated using 5 ml THF could deliver films over 2 µm thick, see Figure 4.10.

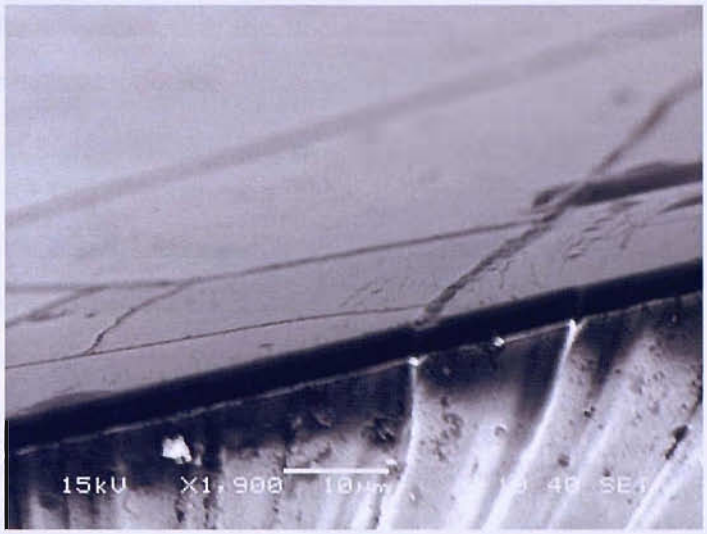

Figure 4.10: Edge-on SEM image of a film produced with $^{n}OctNH_2$ and 5 cm^3 THF, then pyrolysed in N_2 at 800 °C.

The films produced using $^{t}BuNH_2$ and pyrolysed under NH_3 were very thin with a large network of pinholes. The films produced using 10 ml THF which were pyrolysed at 800 °C possessed thicknesses in the region of 200 – 300 nm (see Figure 4.11).

Figure 4.11: SEM image of a film produced with $^{t}BuNH_2$ and 10 cm^3 THF, then pyrolysed in NH_3 at 800 °C.

The films annealed under N_2 were not homogeneous and were poorly adhered to the substrates and all these films exhibited the worst charging of all the samples analysed

which added to the evidence that the use of tertiary amines leads to very thin poorly conducting films possessing defects.

The likely reason for this phenomenon is due to the orientation of the methyl groups and the steric hindrance which occurs due to their arrangement. This would undoubtedly reduce the effectiveness of $^{t}BuNH_2$ as a transaminating species as the positioning of the methyl groups would physically block the two reactive species from getting close enough to react with each other. The likely result would be less substitution when reacted with tetrakis(dimethylamino)titanium which would give a lower viscosity sol which in turn would not be a effective at coating a substrate as a sol produced from straight-chain amines.

4.3.1 Characterisation of Films

Fragments of the deposited films were removed from the substrate by scratching, using a hardened-steel blade, for analysis by TEM. Figure 4.12 is illustrative of the material gained when heated under NH_3 to 800 °C.

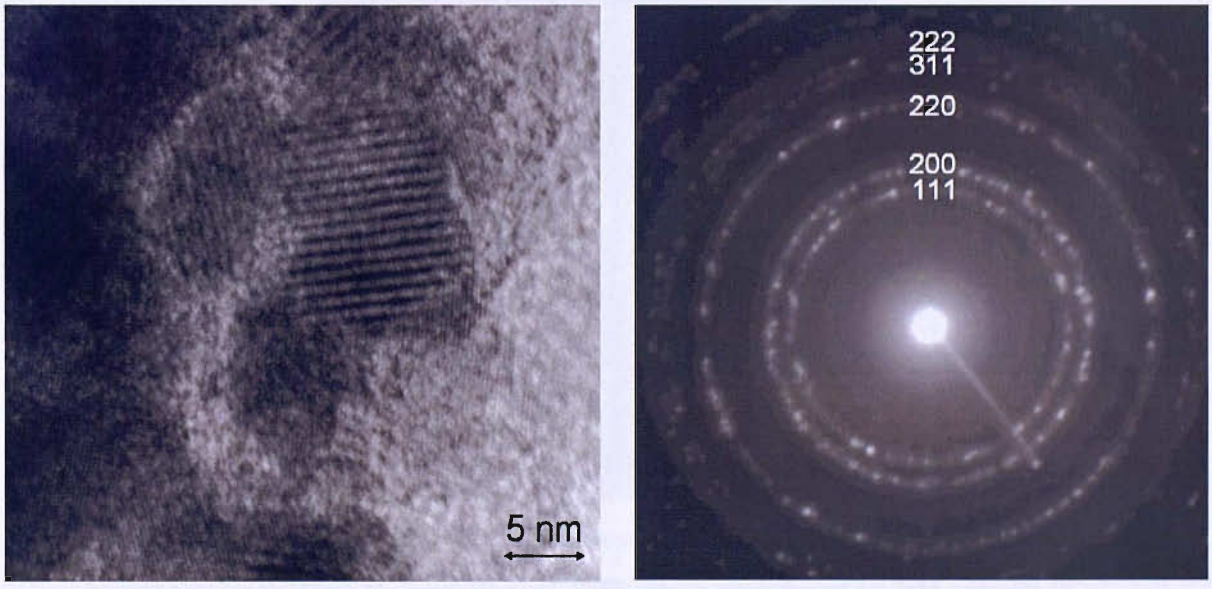

Figure 4.12: TEM image and selected area electron diffraction pattern of material excised from a film produced with $^{n}PrNH_2$ and 10 cm^3 THF, then pyrolysed in NH_3 at 800 °C.

The average crystallite size was measured to be less than 10 nm, even though after pyrolysis at 800 °C, when sintering can become possible that lead to larger particle sizes. Lattice fringes are clearly visible, demonstrating that the sample is crystalline, and the electron diffraction pattern for the material in various locations of the analyte, displayed five rings which could be indexed to the 111, 200, 220, 311 and 222 planes of a face-centred cubic cell with a = 4.22(3) Å. This compares favourably with reported unit cell values, which are between 4.235 – 4.270Å for $TiN_{\sim 1}$ and 4.243 – 4.297 for $Ti(N,C)_{\sim 1}$[71].

When the samples annealed at 400 °C were analysed it became apparent that the crystallite sizes were too small to characterise properly. Diffraction rings were faint and diffuse. However samples produced from $^{t}BuNH_2$ with 10 ml THF and heated to 400 °C under ammonia had features in the region of 1-2 nm and the ED pattern still clearly shows the first three rings of the pattern illustrated at the higher annealing temperatures, albeit more diffuse (see Figure 4.14). This result is markedly similar to previously observed patterns collected when titanium carbonitride powders were synthesised from tetrakis(dimethylamino)titanium with ammonia[72]

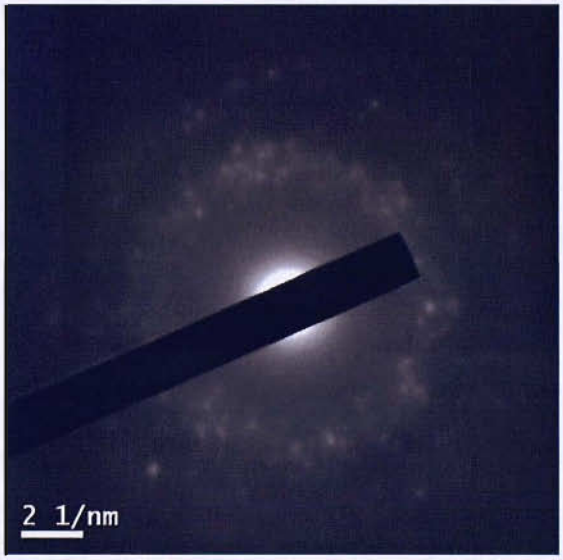

Figure 4.13: Selected area electron diffraction pattern of material excised from a film produced with $^{t}BuNH_2$ and 10 cm^3 THF, then pyrolysed in NH_3 at 400 °C.

This gives a strong indication that some crystalline material must exist, irrespective of the low annealing temperature, and will most likely exist as small nanocrystals in an amorphous media.

Powder X-ray diffraction was performed with a 1° incident angle using a Bruker 'C2 discover' diffractometer. It was found that even at such a low grazing incident, patterns were dominated by broad scattering features from the silica tiles. Bearing in mind that the films being analysed are in the region of 1 μm thick and nanocrystalline and it becomes understandable as to why the coatings diffract so poorly. This however, was not to say that the coatings did not offer any kind of diffraction pattern; peaks corresponding to a TiN-type phase were observed when the higher concentration films, annealed at 800 °C, were analysed using the same parameters. (Figure 4.14)

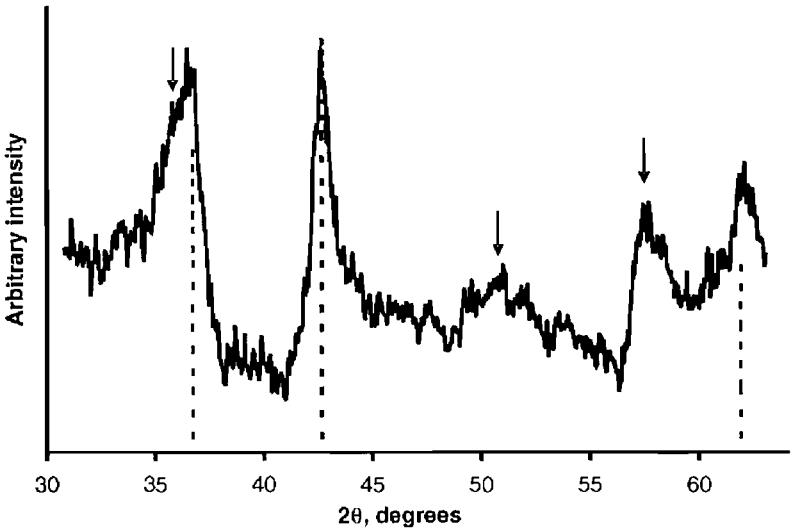

Figure 4.14: PXD pattern of a tin film produced with $^{n}OctNH_2$ and 5 cm^3 THF, then pyrolysed in NH_3 at 800 °C. Broken vertical lines show literature[20] peak positions, arrows represent positions of broad scattering features in an uncoated SiO_2 tile.

Energy dispersive X-ray analysis displayed a signal for titanium but did not display a signal for nitrogen, although it was thought that this was due to the insensitivity of the machine because of the detector probe possessing a boron nitride window. Silicon and oxygen were also observed however this was attributed to contributions from the silica substrate being excited due to the penetrating depth of the electron beam exceeding the depth of the deposited film.

However, using a FEG-SEM set at a low accelerating voltage or upon analysis using TEM, significant levels of nitrogen and low oxygen levels were observed despite the unavoidable exposure to air when loading the samples into the microscope. (see Figure 4.15)

(a)

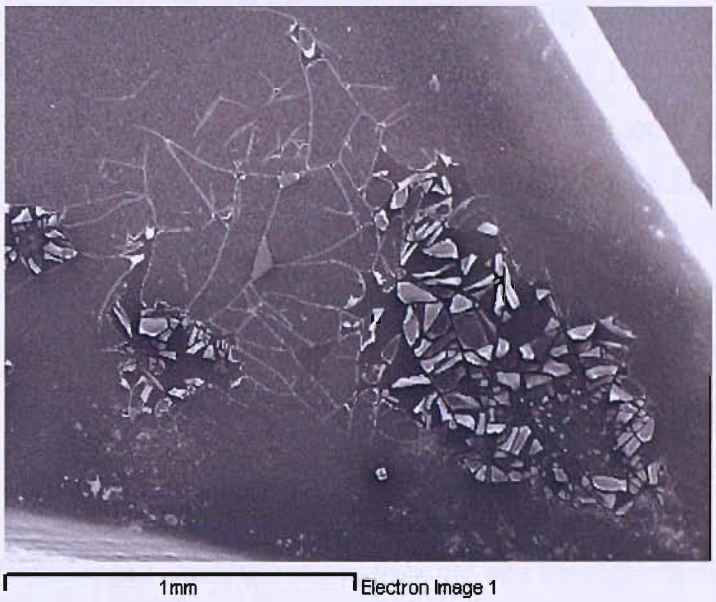

(b)

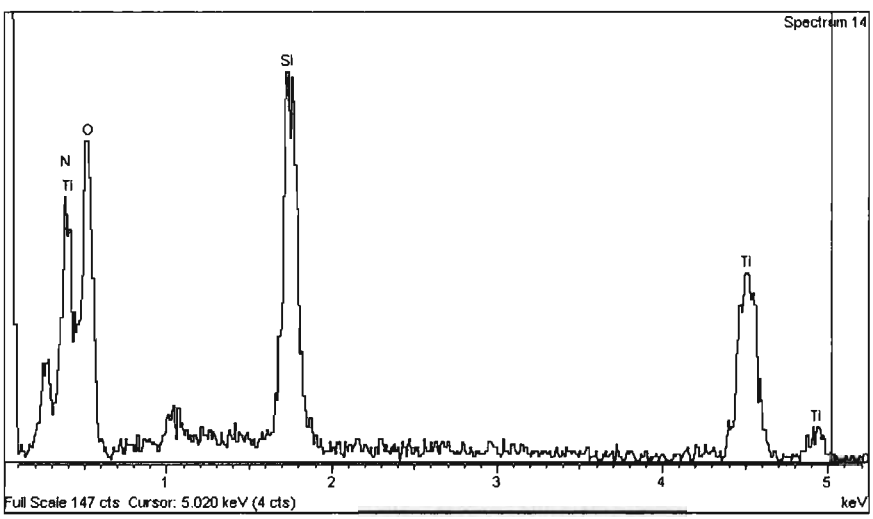

Figure 4.15: SEM image (a) & EDX spectrum (b) of a film produced from a $PrNH_2$-based sol with both titanium and nitrogen visible in the EDX spectrum.

An additional three samples were studied by XPS and in all cases strong signals at Si-2*p* (103 eV), O-1*s* (532 eV) and C-1*s* (285 eV) were observed at the surface. These peaks then rapidly dropped in intensity when argon etching was performed until, after approximately

60 seconds, the signal values were virtually nil. These peaks were attributed to small amounts of surface grease and hydrocarbons that would have inevitably been picked up during the handling of the samples.

The films produced from $^{n}OcNH_2$ and 10 cm^3 THF, which were pyrolysed under an atmosphere of ammonia at 800 °C, produced spectra possessing Ti-2*p* (458 eV), N-1*s* (397 eV) and O-1*s* (530 eV) signals which, over the first 100 seconds of argon etching, developed and then grew. A C-1*s* signal was observed once the initial fall was complete.

An area of note is the binding energy of the surface film compared to the 'bulk' material. These measurements were performed off-site, the films *were* handled in air for a prolonged period of time before any analysis was performed, therefore, it is unsurprising that there is a traceable oxygen content in the nanocrystalline samples. However, the strong nitrogen content (Ti : N = 1 : 0.77) and low carbon content (approximately 4%), which was recorded even after prolonged exposure to air, indicate that these films were close to a TiN composition.

An analogous sample pyrolysed under an atmosphere of nitrogen at 400 °C gave a final Ti : N ratio of 1 : 0.56 however, the carbon content was approximately 44% indicating that a carbonitride had formed.

Samples pyrolysed at 400 °C under nitrogen were analysed, and it was found that the tiles coated in sols prepared from $^{t}BuNH_2$ and 20 ml THF could only attribute 2% of their atomic weight to nitrogen.

The following two tables display a synopsis of all of the coating procedures performed:

Annealing performed under ammonia								
Amine			TDMAT		THF (ml)	Annealing Temperature (°C)	Visual Appearance	SEM Appearance
Type	ml	mmol	ml	mmol				
$PrNH_2$	1.84	22.4	3.0	11.2	20.0	400	Colourless & Iredescent	Defects & cracks visible
$PrNH_2$	1.84	22.4	3.0	11.2	10.0	400	Gold & Iredescent	Defects & cracks visible
$PrNH_2$	3.68	44.8	6.0	22.4	10.0	400	Gold & Iredescent	Minor cracks, good coverage
$PrNH_2$	1.84	22.4	3.0	11.2	20.0	800	n/a	n/a
$PrNH_2$	1.84	22.4	3.0	11.2	10.0	800	Grey/black	Defects & peeling, few cracks
$PrNH_2$	1.84	22.4	3.0	11.2	5.0	800	Dark grey	Small cracks, few defects
t-$BuNH_2$	2.22	22.4	3.0	11.2	20.0	400	Brown	Undeterminable
t-$BuNH_2$	2.22	22.4	3.0	11.2	10.0	400	Gold & Iredescent	Cracked with defects
t-$BuNH_2$	4.44	44.8	6.0	22.4	10.0	400	Brown	Badly cracked and peeling
t-$BuNH_2$	2.22	22.4	3.0	11.2	20.0	800	Grey	Lots of pinhole defects
t-$BuNH_2$	2.22	22.4	3.0	11.2	10.0	800	Dark Grey	Pinhole defects
t-$BuNH_2$	4.44	44.8	6.0	22.4	10.0	800	Dark Grey	Few pinhole defects
$OcNH_2$	3.71	22.4	3.0	11.2	20.0	400	Colourless	No defects or cracks
$OcNH_2$	3.71	22.4	3.0	11.2	10.0	400	Colourless & Iredescent	No cracks, few defects
$OcNH_2$	7.42	44.8	6.0	22.4	10.0	400	Colourless & Iredescent	Some defects and cracks
$OcNH_2$	3.71	22.4	3.0	11.2	20.0	800	Brown/Black	Broad cracks, pinhole defects
$OcNH_2$	3.71	22.4	3.0	11.2	10.0	800	Grey	Broad cracks, pinhole defects
$OcNH_2$	7.42	44.8	6.0	22.4	10.0	800	Dark Grey	Defects, no cracks

Table 4: A summary table of the coating results when annealed under ammonia.

As can be seen in table four, the typical outcome of the annealing of these coatings was to yield either a dark grey/black coloured coating or a golden coloured coating. These coatings tended to possess defects and cracks in the lower concentration (higher solvent volume) coating sols, and at the higher concentrations (lower solvent volume), these defects and cracks were much reduced. This was most likely due to the viscosity of the sol being high enough to be able to withstand any out-gassing from the film of excess solvent which was not evaporated during the initial room temperature curing phase.

Annealing performed under nitrogen								
Amine			TDMAT		THF (ml)	Annealing Temperature (°C)	Visual Appearance	SEM Appearance
Type	ml	mmol	ml	mmol				
$PrNH_2$	1.84	22.4	3.0	11.2	20.0	400	Colourless & Iredescent	n/a
$PrNH_2$	1.84	22.4	3.0	11.2	10.0	400	Colourless & Iredescent	Minor pinhole defects
$PrNH_2$	3.68	44.8	6.0	22.4	10.0	400	Gold & Iredescent	Major cracking
$PrNH_2$	1.84	22.4	3.0	11.2	20.0	800	Colourless & Iredescent	Multiple defects
$PrNH_2$	1.84	22.4	3.0	11.2	10.0	800	Colourless & Iredescent	Multiple defects & cracking
$PrNH_2$	1.84	22.4	3.0	11.2	5.0	800	Black	Pinhole defects, very minor cracking
t-$BuNH_2$	2.22	22.4	3.0	11.2	20.0	400	Colourless & Iredescent	Extreme number of pinhole defects
t-$BuNH_2$	2.22	22.4	3.0	11.2	10.0	400	Colourless	Few pinhole defects, no cracks
t-$BuNH_2$	4.44	44.8	6.0	22.4	10.0	400	Colourless	Very badly cracked, poor conductance
t-$BuNH_2$	2.22	22.4	3.0	11.2	20.0	800	Gold	Numerous small cracks
t-$BuNH_2$	2.22	22.4	3.0	11.2	10.0	800	Gold	Defects & surface charging
t-$BuNH_2$	4.44	44.8	6.0	22.4	10.0	800	Colourless	Surface charging, no apparent defects
$OcNH_2$	3.71	22.4	3.0	11.2	20.0	400	Colourless & Iredescent	Cracked coating & pinhole defects
$OcNH_2$	3.71	22.4	3.0	11.2	10.0	400	Brown	n/a
$OcNH_2$	7.42	44.8	6.0	22.4	10.0	400	Brown	Many cracks
$OcNH_2$	3.71	22.4	3.0	11.2	20.0	800	Colourless & Iredescent	Many cracks and defects
$OcNH_2$	3.71	22.4	3.0	11.2	10.0	800	Black	Few hairline cracks, no pinhole defects
$OcNH_2$	7.42	44.8	6.0	22.4	10.0	800	Black	Very few cracks, no pinhole defects

Table 5: A summary table of the coating results when annealed under nitrogen.

The results of using high purity nitrogen as an annealing gas rather than ammonia were found to give similar results. Overall via EA the nitrogen cured coatings were found to possess a greater quantity of carbon. Visually the coatings tended to display either a colourless appearance at the lower concentrations or a black appearance at higher concentrations. It was deemed that due to the milder, less reductive conditions, the removal of carbon from the system was not as efficient as when using ammonia and hence the concentration was greater – as was seen.

The characterisation of 'bulk' xerogels of the coatings were also analysed in an effort to further understand the nitride and carbonitride compositions produced. A coating sol was produced as described previously, except once the sol had reached a satisfactory level of completion the sol was dried under *vacuo* until a red xerogel was formed. It should be noted that as the solvent was removed from the system, the viscosity of the residue increased proportionally, until the viscosity of the solid could overcome the vapour pressure of the volatilised solvent and consequently trapped residual amounts in the material. The product was then pyrolysed under either ammonia or nitrogen at a range of temperatures from 400 to 1000 °C. Under all conditions a dramatic reduction in the volume of the material occurred, most likely due to the removal of solvent and the densification of the crystalline structure.

Under ammonolytic conditions a metallic golden-nugget of material was yielded. When pyrolysed under nitrogen, the product was black. Nitrogen fired materials all contained large quantities of carbon (24-26%) and subsequently were determined as being carbonitrides, albeit with high carbon contents. Annealing under an ammonolytic atmosphere led to lower carbon contents at all annealing temperatures: 4% at 400 °C; 3% at 800 °C and 0.5% at 1000 °C.

Powder X-ray diffraction of the propylamine-based xerogels, when pyrolysed in ammonia at 1000 °C, clearly showed crystalline titanium nitride with a lattice parameter of 4.234(2) Å and an average crystallite size *circa.* 60 nm, (see Figure 4.16)

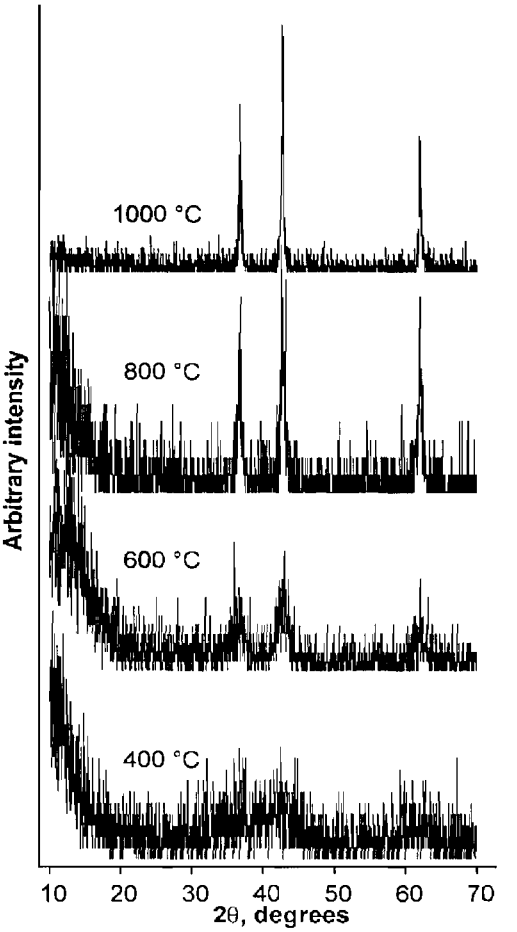

Figure 4.16: PXD pattern of materials produced from $^{n}PrNH_2$-derived xerogels pyrolysed in NH_3.

When pyrolysed at lower temperatures the samples were found to contain some amorphous material; crystallite sizes dropped to 30, 15 and 2 nm for the 800, 600 and 400 °C heating conditions respectively. Lattice parameters remained within expected tolerances except for samples annealed at 400 °C where *a* increased to 4.27(2) Å which could be an indication of a higher carbon content within the sample material.

The xerogel was relatively difficult to crystallise; samples were held at a maximum temperature for two hours which meant that only annealing at 1000 °C was enough to invoke crystallisation throughout the entire sample. However, Bragg peaks were visible for materials annealed even at the lowest temperature of 400 °C (Figure 4.16).

It could be concluded that the films annealed under an atmosphere of ammonia were likely to contain nanocrystalline and amorphous material as found in the 'bulk' material; although the crystallite sizes measured in the 'bulk' materials were marginally larger than

those observed by TEM in the films. The nitrogen annealed materials displayed similar distribution peaks when analysed and possessed broad peaks, at all temperatures, possibly due to the presence of graphitic carbon.

The carbon content of the octylamine-based xerogels were slightly higher than those produced for the propylamine system. This would make sense as there was approximately 2.6 times more carbon present in the reagent mixture than previously. The xerogel formed in a very similar manner to the propylamine-based system, if not slightly more viscous.

When annealed at 800 °C the compound contained approximately 30% more carbon when annealed under nitrogen and 4% more carbon when annealed under ammonia. Crystallite sizes were refined to 3 and 6 nm for nitrogen and ammonia respectively which were smaller than what was observed for the propylamine-based system under the same conditions.

When attempting to form a xerogel of the tertiary butylamine-based system a yellow/green solid material was instead yielded upon removal of the solvent from the system. Pyrolysis of this material at 800 °C under ammonia led to carbon free TiN and under nitrogen a material was produced which possessed only 9% nitrogen; 22.6% is required for stoichiometric TiN.

The nitrogen annealed material was amorphous however, the material annealed under ammonia gave a crystalline material with a crystallite size of 13 nm.

An NMR study was conducted on solutions of the coating sols made with the propyl- octyl- and butyl-amines in order to understand the differences between the coatings. Each respective coating sol was diluted in 1 ml of deuterated benzene (C_6D_6) in glovebox conditions. The sample vials were stoppered and then given an additional seal using 'parafilm' sealant tape in order to safeguard the contents from oxidation through an ingress of air for the duration of the analysis. These solutions were allowed to develop for two hours before collection. Both the propyl and octyl-based sols became red very quickly and possessed a darker red hue proportional to the amount of amine used. The $^tBuNH_2$-based

sol developed colour very slowly and was only a translucent shade of orange after several hours.

The ^{1}H NMR spectrum of the 1:1 mixture of $^{n}PrNH_2$ showed unreacted $Ti(NMe_2)_4$ (singlet at 3.2 ppm) and Me_2NH (doublet at 2.3 ppm, broad peak at 0.3 ppm with 6:1 intensity ratio). The methyl proton resonances from the two species were of equal intensity; no $^{n}PrNH_2$ resonances were observed. The C^{13} spectrum showed $Ti(NMe_2)_4$ at 33 ppm and Me_2NH at 39 ppm. With two equivalents of $^{n}PrNH_2$ the amide signal is very weak, consequently the Me_2NH dominates both the ^{1}H and ^{13}C spectra, even when two equivalents were added. No $^{n}PrNH_2$ was observed. The 1:1 ratio of TDMA to Me_2NH observed in the 1:1 mixture suggests that at this concentration not only transamination but also condensation with other Ti centres, forming Ti-N^{n}Pr-Ti links, must be virtually quantitative.

In the 1:2 reaction, transamination is also quantitative since no $^{n}PrNH_2$ is observed however the degree to which condensation proceeds is unclear. Broad, weak signals were observed in the ^{1}H spectra at 4.4, 3.4 and 2.4 ppm reminiscent of a propyl group. Analysis of the reaction with $^{t}BuNH_2$ indicated only small amounts of Me_2NH in the ^{1}H and ^{13}C spectra with the ratio of amide to amine methyl protons being 25:1 and 6:1 in the ^{1}H spectra for the 1:1 and 1:2 mixtures respectively. The butylamine resonance at 1.1 ppm (^{1}H) and 33 ppm (^{13}C) was strong in both ratios suggesting that the $^{t}BuNH_2$ was too bulky to successfully perform any significant transamination and consequently, it is unsurprising that the use of this amine results in poor coating sols.

The most likely explanation for the production of films when coating with $^{t}BuNH_2$ derived sols, is that reactions of residual amide with the ammonolytic atmosphere, occur and thus ammonia is the cross-linking agent in these cases.

4.4 Conclusions

The principle of this investigation was to use restricted amounts of primary amine, as the cross-linking agent, with the amide $Ti(NMe_2)_4$ to produce sols suitable for coating in which the condensed species remained soluble.

For the reaction to go to completion and ammonolytic species to crosslink to produce a sol, two moles of amine (H_2NR) per mole of amide would be required. This cross-linked polymer should be soluble, as is the material yielded when an excess of amine is used. However it is clear that the reaction goes to completion, certainly in the case of $^nPrNH_2$, as all propylamine is consumed during the reaction as illustrated by NMR. Therefore one explanation could be that using two equivalents of amine leads to soluble oligomers forming which are stable but still contain uncondensed $-NH^nPr$ and NMe_2 groups.

The weak propyl group resonances observed in the NMR spectra of the material could either be due to bridging N^nPr moieties or terminal $-NH^nPr$ groups, which would allow condensation to continue during the coating process and afterwards during solvent evaporation, which is precisely what is required to facilitate the formation of good quality, solid films.

In the case of the *n*-propyl and *n*-octyl based coating sols, the films produced were of similar morphology, albeit the octyl-based coatings were on average thicker and more carbonaceous. Due to their behaviour when concentration and number of dippings were adjusted, it should be possible to control the thickness and texture of the coating. It is also reasonable to assume that the incorporation of the use of an automated dip- or spin-coater would improve the quality of the coatings, reducing the number of pinholes and cracks.

The current coating method is basic and the films are imperfect, however, this does not remove the fact that the sol-gel deposition of a nitride film has been achieved. Pyrolysis of these films at 800 °C for two hours led to nanocrystalline TiN with a minor quantity of carbon. This achievement is underlined when it is considered that the conversion of TiO_2 to TiN, under ammonia, typically takes place at 1100 to 1200 °C[73,74]; a minimum of 300 °C higher. Additionally, a variable temperature study of TiO_2 illustrated that a minimum temperature of 1100 °C for a duration of five hours was required for the complete conversion of TiO_2 to its nitride analogue[75]. Therefore, it is clear that our route of synthesis for these coatings is much milder. It is highly unlikely that the conversion of oxide to nitride was occurring during pyrolysis, which is given credence by the fact that the nitridation of oxides doe not usually go to completion and leaves oxide residue in the lattice[76]; as this did not happen it illustrates the advantage of this process.

Pyrolysis at 400 °C under an atmosphere of ammonia gave materials possessing a higher carbon content and a lower level of crystallinity, although analysis of these materials clearly shows that there is still a degree of nanocrystallinity (see Figure 4.14) there are conductive titanium nitride/ carbonitride films, much like the materials synthesised from the reactions of metal amides with ammonia[72].

The major differences observed were that the films' appearance when produced from the octyl-based method were smoother in visual appearance (see Figure 4.8 and Figure 4.9) and possessed a marginally higher carbon content compared to the films created using the propylamine based route. It has previously been reported that, in the case of sol-gel derived silicon nitride, powders could be modified using different amines in the synthesis[77] so it may be that the $^{n}OcNH_2$ based films possess much wider pores, which in turn would allow the solvent to evaporate more readily, resulting in a smooth film.

When pyrolysis of the coatings was carried out under nitrogen the carbon content was high, as was the quantity of amorphous material. Therefore it should be concluded that these coatings are carbonitrides which is advantageous for many applications requiring hard coatings, as it is proven that the incorporation of carbon into the material markedly increases the hardness rating[55].

The coating of silica tiles with titanium nitride and carbonitride has been achieved via a non-oxidic sol-gel process. Straight chain primary amines, which possess very little steric hindrance, provide a good alternative to gaseous ammonia when used for transamination of amides and self-condensation of the hybridised species. The coatings were nanocrystalline and did require further annealing under ammonia to reduce the carbon content in the film. However, this represents an important step forward in the development of sol-gel coating technologies that can allow the deposition of a nitride thin film from a solution, paving the way for the synthesis of novel morphologies of nitride materials.

5 AMMONOLYTIC SOL-GEL ROUTE FOR FILMS

5.1 Introduction

The principle behind the development of an ammonia-based sol-gel film technique was to devise a method which enabled production of titanium nitride coatings from single-source precursor sol rather than requiring NH_3 annealing. The benefit of sol-gel is its versatility with respect to the variety of end-products it can produce; it is possible to fabricate ceramic or glass materials in a wide variety of forms including ultra-fine powders, thin film coatings, ceramic fibres, micro porous inorganic membranes, monolithic ceramics and glasses, or extremely porous aerogel materials.

The primary aim of this chapter was to investigate and develop the possibility of producing carbon-free TiN films. Integral to achieving this result is developing a method utilising ammonia instead of primary amines which could yield ceramic coatings of titanium nitride on a substrate. Films should possess good physical properties such as: adhesion, coverage and durability. This would provide a platform for further development of sol-gel methods with additional transition metal precursors, which would eventually give a single 'core' methodology and be a stepping-stone to sol-gel chemistry with metal nitrides generally, but also allowing for a plethora of elementally different materials to be produced.

Alkoxide based sol-gel techniques can already produce a wide variety of products, the following types of materials should however, also be accessible by amide based chemistry as the amide based methodology is an analogous process. Thin films can be produced on a piece of substrate by spin-coating or dip-coating. When the sol is cast into a mould, a wet gel will form. With further drying and heat-treatment, the gel is converted into dense ceramic or glass. If the liquid in a wet gel is removed under a supercritical condition, a highly porous aerogel can be obtained or as the viscosity of the sol is adjusted into a proper viscosity range, ceramic fibres can be produced. Ultra-fine and uniform ceramic powders can also be formed by precipitation, spray pyrolysis, or emulsion techniques.

As a consequence of developing such a method, the market for potential applications would be expanded, as nitrides are highly desirable as coatings due to their physical qualities such as, high temperature stability, hardness, chemical stability and good

conductivity[5,7,47]. It would also present an important step toward general sol-gel processing of nitride materials.

The ammono based analogue of the well established alkoxy route to sol-gels is inherently difficult to control[13](see Figure 5.1). The basicity of the system and the overwhelming tendency of the starting materials to favour particle growth which means a precipitate rather than a stable emulsion is produced, unless both environment and synthetic pathway are carefully controlled.

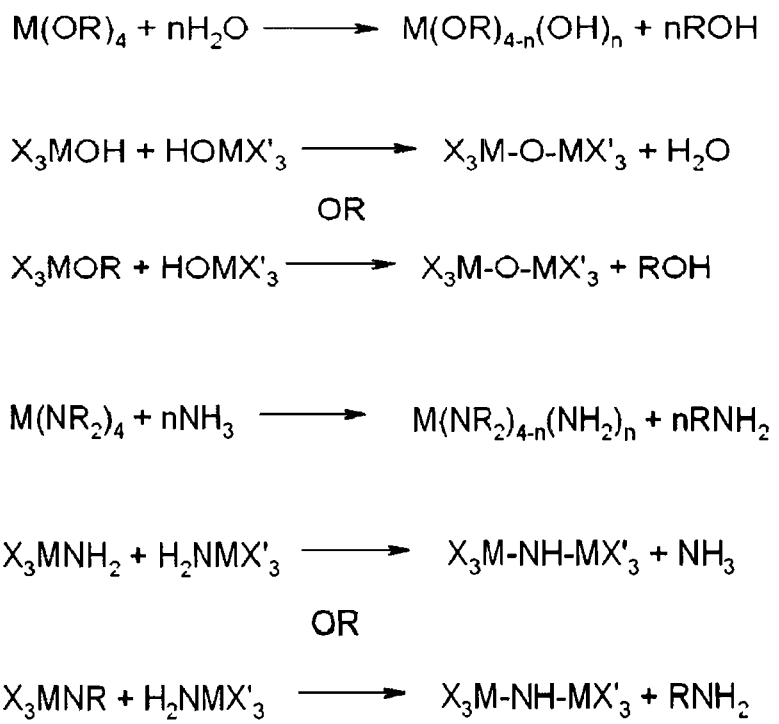

Figure 5.1: The hydrolytic condensation route (top) and the ammonolytic condensation route (bottom).

Therefore current publications of sol-gel route nitrides describe production of powders as opposed to films, gels, or monoliths[12,13].

Investigation of the published ammonolytic routes revealed, surprisingly, that the quantities of ammonia involved were always in a large excess and that there were no concerted efforts to regulate the quantity of ammonia being administered into the reactions in an effort to establish control of the reaction kinetics of the overall mechanism.

Repetition of the published techniques (see chapter three) resulted in precipitation of solid materials from solution, as has been previously described[9,13].

The formation of the solid precursor material from solution was observed after approximately five seconds of ammonolysis (see bottom of Figure 5.1). Simple control of reagent concentrations, in the form of stoichiometric amounts of amide being used and controlled exposure of the amide solution to the gaseous ammonia, did not yield sufficient control of the reaction in order to gain any kind of sol; the restriction of ammonia only limited the amount of precipitate formed as any ammonia gas added to the solution containing the amide would be consumed by the amide at the point of contact with the ammonia (i.e. the surface of the solution). Consequently an alternative method was sought.

5.1.1 Acid Catalysis

The concept of using acid catalysis was introduced to see if the ammonolytic route would behave in a similar manner to the analogous alkoxy based system when catalytic amounts of Trifluoromethane sulfonic (triflic) acid were added to the reaction mixture.

Successful use of catalytic amounts of triflic acid had been cited in similar reactions using the amide silicon tris(disilylamide) (TDSA), sodium dried THF and anhydrous ammonia solution[3]. In these cited reactions the products obtained were always opaque rigid gels which self condensed after several ammonolytic steps, involving the addition of uncontrolled amounts of ammonia gas.

Reactions mimicking the conditions used in the TDSA-based methods were attempted using TDMAT. What was observed was almost identical to the straight addition of ammonia to solution without any super-acid, except that the formation of precipitate occurred in clumps rather than as dispersed particles. This clearly indicated that the method was unsuitable for the required purpose as a stable emulsion could not be achieved.

The result was possibly due to the electronic properties of the titanium centre and the polarisation of the molecule. With TDSA the silicon central atom has an electronegativity of 1.9 on the Pauling scale[78], the Titanium metal centre in TDMAT however, possesses an

electronegativity of 1.54 on the Pauling scale[78], 19% weaker than that of silicon. The silicon-based amide can enable transamination to proceed at a tempered rate due to the electronegativity of the central metal making transamination more difficult for the incoming NH_3 groups. Due to the lower electronegativity of TDMAT, transamination is facile and becomes increasingly so as more substitution occurs due to the increases in polarisation of the molecule. Thus control over the ammonolysis and condensation processes is very difficult to achieve.

5.1.2 Base Catalysis

However, due to the overwhelming basicity of the reaction system (ammonia possesses a pKa ~41, THF a pKa of ~36) and the basic properties of the starting material tetrakis(dimethylamino)titanium, it was impossible to maintain a neutral or slightly acidic environment within the reaction solutions. Base catalysis possesses a unique set of difficulties to overcome. The dimethylamine groups on TDMAT are good leaving groups, sterically bulky and more electron donating than the incoming NH_3 groups. Therefore the negatively charged transition state of TDMAT in base catalysis will naturally favour substitution with NH_3. Upon substitution the stability of the transition state increases and subsequently the rate of transamination increases.

The reaction temperature was held low as this can suppress the rate of transamination by simply reducing the reaction's kinetic energy and therefore increasing the chance of nucleation. When suppressing the environmental temperature to -20 °C or less, particle growth was simply delayed, whilst apparent condensation reactions were taking place within the solution, upon returning the reaction mixture to room temperature particles would soon agglomerate and settle in the bottom of the Schlenk tube.

The biggest development came with the introduction of 2-2' bipyridyl, the intention was for it to act as a reaction moderator to control the addition of NH_3 to the amide species and promote a stable sol, with the introduction of 2-2' bipyridyl prior to the ammonolysis of the reaction mixture it was hoped that the bidentate ligand would chelate with the two vacancies on the central titanium atom of TDMAT, thus preventing ammonia from undergoing addition and instead having to undergo transamination. This would, in theory,

prevent the individual molecules from growing from 4 to 6 co-ordinate which would result in their densities increasing to the point at which the individual clusters could precipitate from the solution. However, using NMR to ascertain the presence of an intermediate adduct, revealed that there was no change in chemical shift observed when comparing the spectra of the metal amide to that of the mixture of 2-2' bipyridyl and TDMAT (see Figure 5.9). This asks an interesting question of what role 2-2' bipyridyl has within the system as it is apparent that without it, the successful production of a coating sol could not be possible within this set of parameters.

5.2 Experimental

5.2.1 Diethyl-, Dipropyl- and Dibutylamide Preparation.

A literature[79] preparative technique was used, however the quantities and process were slightly modified.
The TDMAT used for all transamination reactions was kindly donated by Epichem; purity was verified by NMR.

Tetrakis(diethylamino)titanium:

TDMAT (25.0 ml, 23.67 g, 93.2 mmol) and Diethylamine (200 ml, 141.48 g, 1.93 mol) were mixed together and stirred at 52 °C for 72 hours, over which period the colour changed from a clear orange solution to a dark red/brown solution which transmitted very little light. The excess Diethylamine was then removed from the mixture *via* reduced pressure at room temperature. The desired amide was then distilled from the crude product at 100 °C. The residual product was then attached to a collection flask *via* a sublimation tube and heated to 100 °C. The distilled product was a vivid, clear yellow liquid. The product was characterised by NMR and stored in the glovebox for future use.

Tetrakis(dipropylamino)titanium:

TDMAT (20.0 ml, 18.94 g, 74.6 mmol) and Dipropylamine (175.00 ml, 129.50 g, 1.279 mol) were added together and stirred at 80 °C for 72 hours. The solution progressively

darkened from an orange to a dark brown/red colour solution. The excess Dipropylamine was then removed via reduced pressure at room temperature, followed by reduced pressure and mild heating. The residual product was then attached to a collection flask *via* a sublimation tube and heated to 150 °C. The distillate was a vivid, clear yellow liquid which crystallised on the walls of the collection flask after cooling. The product was characterised by NMR and stored in the glovebox for future use.

Tetrakis(dibutylamino)titanium:

This involved the mixing of TDMAT (25.0 ml, 23.67 g, 93.2 mmol) with dibutylamine (185 ml, 140.6 g, 1.088 mol) at 100 °C for 72 hour,.during which time the solution changed from a clear, yellow solution to a dark brown solution which would not transmit light. Excess dibutylamine was removed at 55 °C and 0.1 mm/Hg, however the residue was completely solid and sublimation/distillation was not possible in order to collect any refined amide. Subsequently use of this amide as a reagent was abandoned.

5.2.2 Reaction Methodology

Acid-catalysed Method

1.0 ml tetrakis(dimethylamino)titanium (TDMAT) was pipetted into a Schlenk tube in a nitrogen filled glovebox, the tube was then sealed and transported to a fume hood where it was connected to a Schlenk line. 30 ml of dry solvent was then added and the mixture stirred for 30 minutes. Approximately 0.3 ml of $NH_3(l)$ was then separately condensed and added to the solution. The solution was then left overnight for approximately 18 hours. Ammonia was then bubbled through the solution at a steady rate for approximately 5 seconds. The mixture was again left overnight for approximately 18 hours.

When acidifying the reaction mixture, 1.0 ml TDMAT was pipetted into a modified Schlenk tube possessing a graduated sidearm in a nitrogen filled glovebox. The tube was then sealed and transported to a fumehood where it was connected to a Schlenk line. Dry solvent was then added followed by 25 µl (0.0424 g, 0.282 mmol) of triflic acid and the mixture was stirred for 30 minutes. 0.1, 0.2, 0.3 or 0.4 ml of $NH_3(l)$ were condensed into

the sidearm of the modified Schlenk and then released into the main body of the reaction vessel gradually, in an attempt to reduce the amount of saturation occurring at the surface which would result in precipitation. The solution was then left overnight.

2-2' Bipyridyl Method

1.0 ml (0.947 g, 3.73 mmols) of TDMAT was placed into a modified Schlenk tube inside a nitrogen filled glovebox. 2 molar equivalents (0.64 g, 7.46 mmols) of 2-2' bipyridyl were then added. The tube was then sealed and transported to a Schlenk line. The reaction mixture was solvated in 40 ml of dry THF and then cooled to approximately -78 °C. An aliquot of NH_3 (between 1 and 5 equivalents) was condensed into the sidearm of the Schlenk tube, and then gradually allowed to react with the reaction mixture. Once the transfer of the required amount of NH_3 was complete, the Schlenk tube was immediately placed into a cool-bath maintained at a temperature of -20 °C. The reaction mixture was then left overnight for approximately 18 hours.

Upon removing the mixture from the cool-bath a brown opaque emulsion was found, and the subsequent stability of the emulsion directly related to the amount of ammonia used in the ammonolysis stage.

The optimum quantity of NH_3 required to achieve a stable sol was found to be 3 molar equivalents this equates to 0.048 ml of NH_3*(l)* per 1.0 ml of TDMAT. Above that quantity and particle growth was sustained causing precipitation.

5.2.3 Ammonolytic coating-sol generation

Using Tetrakis(diethylamino)titanium

TDEAT :- 1.0 ml, 0.931 g, 2.76 mmol
THF :- 30.0 ml
NH_3 *(l)* :- 0.13 ml, 0.0962 g, 5.64 mmol

The TDEAT was mixed with THF which was then combined with the NH_3 at -78 °C, in order to reduce the kinetic activity of the reagents in an effort to reduce localised

condensation and promote a homogenous mixture. The mixture was then transferred to a cool bath set at -20 °C for approximately 17 hours, and was then allowed to warm slowly to room temperature, *circa.* 20 °C.

Using Tetrakis(dipropylamino)titanium

TDPAT :- 0.1 ml, 0.05 g, 0.111 mmol
THF :- 2.0 ml
NH_3 *(l)* :- 3.796 mmol, 0.0646 g, 0.087 ml

The mixture turned a pale yellow colour upon addition of THF and upon immersing in dry ice it solidified; the mixture was left for ~20hrs at dry ice temperature in a slush bath. It was noted that upon exposing the sol to temperatures closer to ambient conditions particle growth occurred over a relatively short period of time, approximately 30mins to 1 hour.

This could be controlled by keeping the sol at a temperature of approximately 5 °C. The sol did not precipitate until its local temperature was raised at which point the sol had a semi-opaque, yellowish appearance.

5.2.4 The dip-coating Procedure

Coating Substrates

Initially the substrate used for coating was pre-cut alumina (14 × 25 × 1 mm). Due to adhesion problems (see section 5.3.2) these were replaced by quartz-silica tiles (14 × 25 × 1 mm) which were found to accept the coating sols far more readily and give a much better quality coating. The preparation for either type of substrate involved the tiles being immersed in piranha etch (1:3 H_2SO_4 to H_2O_2) for approximately 24 hours, in order to remove all organic residues and other contaminants that could potentially have been present on their surface, due to handling during the manufacturing and cutting process. These were then rinsed and sonicated with copious amounts of distilled H_2O and placed in a drying oven at approximately 100 °C for at least 12 hours before use.

Apparatus

Coating was performed using the same apparatus setup as previously used for coating using primary amines (see Figure 4.3)

The Coating Method

The coating method involved attaching the Schlenk tube containing the coating-sol to a modified dropping funnel containing a tile hanging from a hook attached via a glass rod to the glass stopper on top of the funnel.

The sol was transferred via a canula into the dropping funnel, filling the vessel and partially immersing the hanging tile. The sol transfer was halted, and then was released from the dropping funnel through the Young's tap assembly, simulating a dip coating procedure, at a rate of approximately 2 mm s^{-1}.

The coated tiles were then cured under a light vacuum until the tile appeared to be visually dry. It was then transferred to the glovebox and loaded into a dry, clean alumina boat in a silica tube and then annealed under either $NH_3(g)$ or $N_2(g)$.

5.2.5 Coating with the Tetrakis(dipropylamino)titanium Derived Sol

Coating took place inside a N_2 filled glovebox using quartz silica tiles as substrates pre-treated via the previously described method in section 4.2.

The coating sol was transferred into the glovebox and a simple dipping process was used using a ~7" long piece of copper wire with a hook fashioned on it's tip. 6 tiles were coated and suspended within the glovebox to cure for 30mins before re-applying the coating sol using the same technique.

The 6 tiles were coated with increasing amounts of the sol. (i.e. tile 1 = 1 dip, tile 6 = 6 dips).

5.2.6 Annealing

A tube furnace was used to anneal all the coated tiles produced under an atmosphere of either ammonia (Air Products, anhydrous grade) or nitrogen (Air Products BiP grade). Samples were loaded into a custom made silica furnace tube which enabled reactive gases to be flushed through part of the apparatus without disturbing the sample in an effort to purge the system of water and oxygen (see chapter 4, Figure 4.4).

Once the purge cycle had been completed, typically after 30 minutes, the apparatus was opened to the reactive gas and the pre-programmed heating conditions were started. The method involved a 'mild' 2 to 5 °C min^{-1} heating ramp, to allow the coatings to cure further if necessary and to minimise cracking, either due to substrate expansion or rapid shrinkage of the coating. The maximum temperature was programmed to be 850 °C. Once the annealing had been completed the samples were stored in a nitrogen filled glovebox prior to analysis.

5.3 Results

5.3.1 General Film Morphology

Scanning Electron Microscopy was used for surface characterisation of the deposited films. EDX and surface mapping was performed to ascertain the elements present in the film composition.

The EDX detector used on the SEM used was insensitive to the presence of nitrogen due to the detector probe possessing a boron nitride window. This meant that in general, nitrogen could not be detected in the films. However, in isolated cases when a field emission gun electron microscope was used, nitrogen *could* be detected. This was not always the case, and in an effort to combat the shortcomings of SEM, it was combined with other techniques such as diffraction. This enabled crystallographic data to be collected which

could identify the crystal structure of the coating and assist in the identification of the film's composition.

5.3.2 Coating onto Alumina Substrates

The initial coatings were deposited onto alumina substrates. Annealed coatings were a grey colour upon visual inspection and reasonably well adhered to the substrate (scotch tape test).

Alumina was not an ideal substrate, as it did not possess a flat topography (see Figure 5.2) and also because of the poor wettability of the alumina's surface.

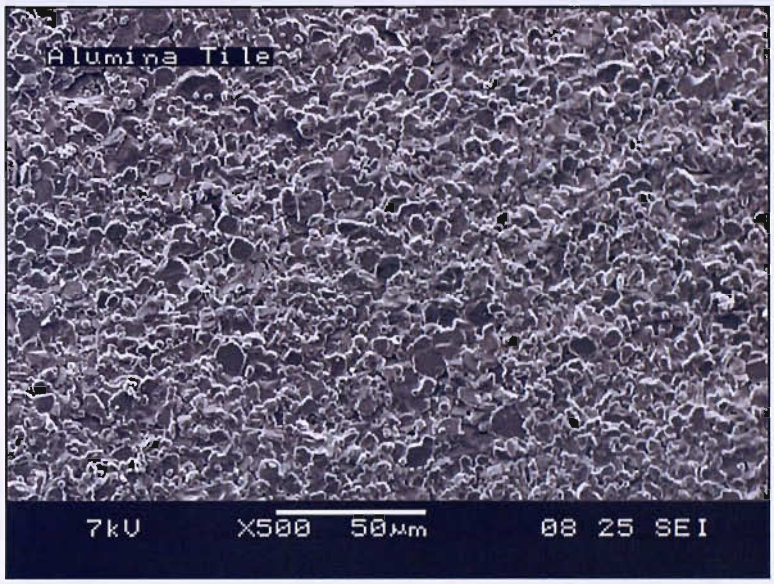

Figure 5.2: A blank alumina tile illustrating the substrate's uneven topography.

Therefore it is a testament to the adhesive qualities of the coating sol that it was able to coat the substrate although, in some cases, it was not able to adhere to the random topography of the alumina and retain a continuous, unbroken film (see Figure 5.3).

The sol had a tendency to collect in the 'wells' of the substrate leading to areas of the tile being insufficiently coated with the sol and upon annealing this caused the film to be patchy in areas. This was due to the relatively level areas of the substrate creating a bridged network of coating, whilst the raised or pitted areas where the sol was unable to sit

had either been totally pyrolysed or not had sufficient coverage to maintain the continuity of the coating.

It was found that with coatings with four molar equivalents of ammonia, coverage was very poor; substrate coatings lacked homogeneity and there was indication that there was poor adhesion to the substrate in some areas, due to large cracks forming and, in isolated cases, areas where the film *was* adhered to the substrate, some peeling of the coatings could be seen (see Figure 5.3).

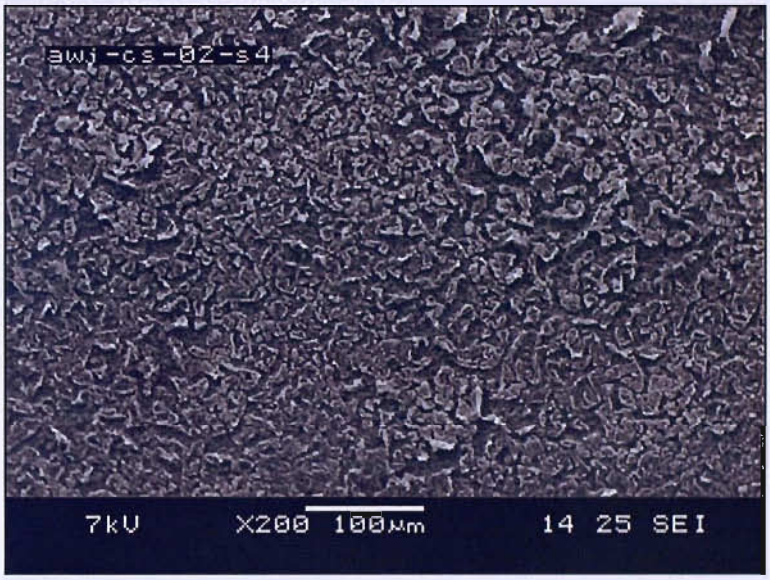

Figure 5.3: Low magnification image of poor coverage and peeling attributed to the unsuitability of alumina as a coating substrate.

Coverage was markedly improved with the use of the coating sol with two molar equivalents of ammonia; it can be seen that, whilst the coating did possess defects (see Figure 5.4), across an extended area it clearly is adhered and, on the whole, continuous (see Figure 5.5).

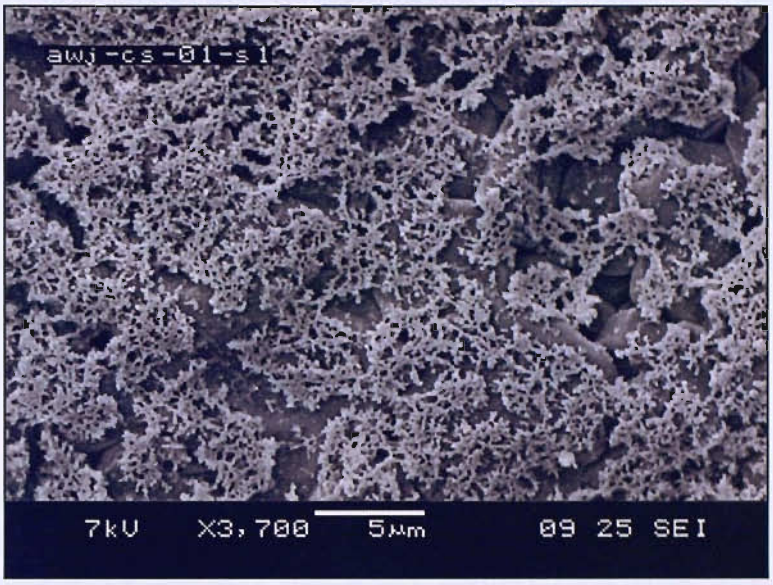

Figure 5.4: Coated alumina at x 3,700 magnification.

Figure 5.5: Coated alumina at x500 magnification.

EDX of the coatings gave signatures of titanium, aluminium and oxygen; this was due to the penetrating depth of the electron beam exceeding the film thickness *and* the exposed areas of the alumina substrate giving additional contributions to the EDX analysis.

5.3.3 Coating onto Silica Substrates

Quartz silica was chosen as a suitable replacement material for the alumina tiles, primarily due to the flat topography of the material. The quality of the silica also allowed for more accurate analysis via EDX as the elemental composition of the tiles were constrained to silicon and oxygen. The flat nature of the tiles also allowed low-angle diffraction experiments to be attempted on the samples.

It was immediately apparent upon coating the silica tiles that coverage with the same sols was dramatically improved. The coatings were continuous and possessed very few defects, although precipitous material in the sol was still a problem, as solid bodies could be observed when analysing the quality of the coating via SEM (see Figure 5.6). Those areas which did possess cracks in the coating served as confirmation that coatings were indeed present on the surface of the silica substrate (see Figure 5.7). EDX analysis indicated the presence of titanium, silicon and oxygen, although the presence of the latter two elements was attributed to the penetration depth of the electron microscope.

Figure 5.6: Ammonolytic coating, on silica, with no cracks but some solid fragments.

Figure 5.7: SEM image confirming the coating of the substrate via the presence of imperfections in the film (see centre of image).

5.3.4 Coating with TDMAT and 2-2' Bipyridyl Derived Sol

Reaction of $Ti(NMe_2)_4$ with THF and stoichiometric amounts of NH_3 at low temperatures (*circa. -20 °C*) resulted in opaque brick red/ brown suspensions. However, when the suspension was warmed to room temperature (approximately 20 °C) precipitation of dark brown solid material was observed within the reaction mixture, which would continue until phase separation of solid and solution occurred. It was decided that modification of the reaction using 2-2' bipyridyl (bipy) would be investigated in an attempt to assuage the facile nature of the precipitation.

It was thought that by using the bidentate chelate-ligand 2-2' bipyridyl, as a reaction moderator, the two vacant sites present on the Ti^{4+} central metal of tetrakis(dimethylamino)titanium would be occupied, forcing ammonolytic species subsequently added to undergo transamination with the existing dimethylamine groups, rather than undergoing addition-reactions with the central metal, which were thought to be the major contributor towards the precipitation of solid.

Addition of the reaction moderator into the original method resulted in immediate stabilisation of the emulsion (see comparison in Figure 5.8); it was assumed that the 'bipy' was functioning in the manner that was intended.

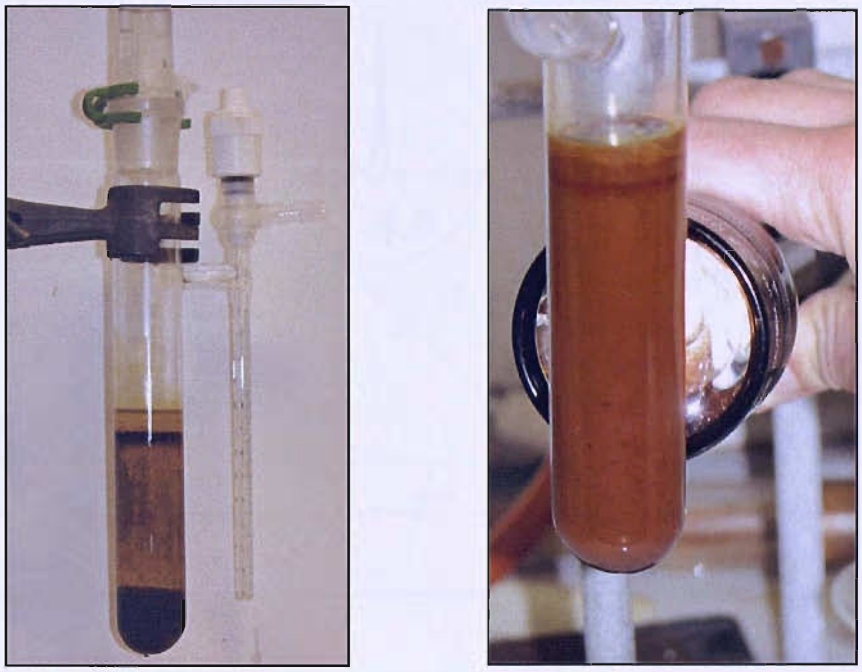

Figure 5.8: Comparison of attempted coating sol generation without bipy (left), and with bipy (right), after being stood for several hours at room temperature, post reaction.

When NMR studies were utilised to ascertain the chemistry between the two compounds, it could be seen that some form of chemical shift had occurred within the carbon environment of the amide. This suggested that an intermediary adduct had indeed formed from the combination of the two reagents. Even though the chemical shift was very small (3.0828 before addition and 3.0676 after addition), it could still be seen that the amide was altered by the presence of the bipy and the amide's environment was changed (see Figure 5.9).

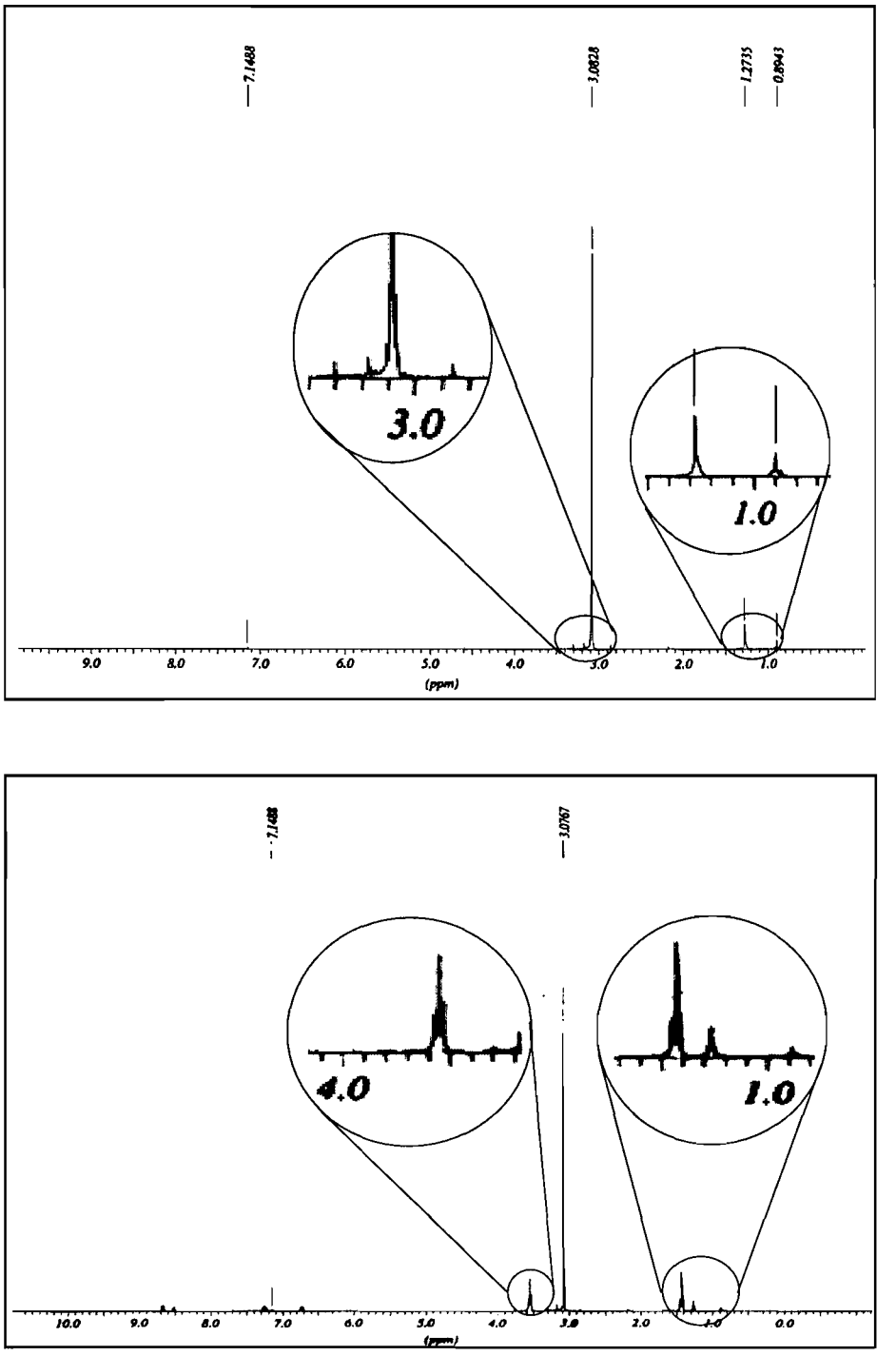

Figure 5.9: C^{13} NMR spectra of $Ti(NMe_2)_4$ (top) and a mixture of 2-2' bipy and $Ti(NMe_2)_4$ (bottom) with a minor shift, in the peak value, of $Ti(NMe_2)_4$ (~3.0ppm).

Therefore, it is assumed that the 2-2' bipy acts as a reaction moderator; for a stable coating sol to be produced there is a dependency on the presence of the bipy. Subsequent dip-coating of silica yielded slides coated with the precursor sol, which upon annealing under ammonia at 800 °C formed good quality coatings with very few defects (see Figure 5.10

and Figure 5.11). EDX was used to characterise the annealed films (Figure 5.12 and Figure 5.13), indicating the presence of titanium, which manifested itself as lighter areas of the titanium mapping and darker areas of the oxygen mapping.

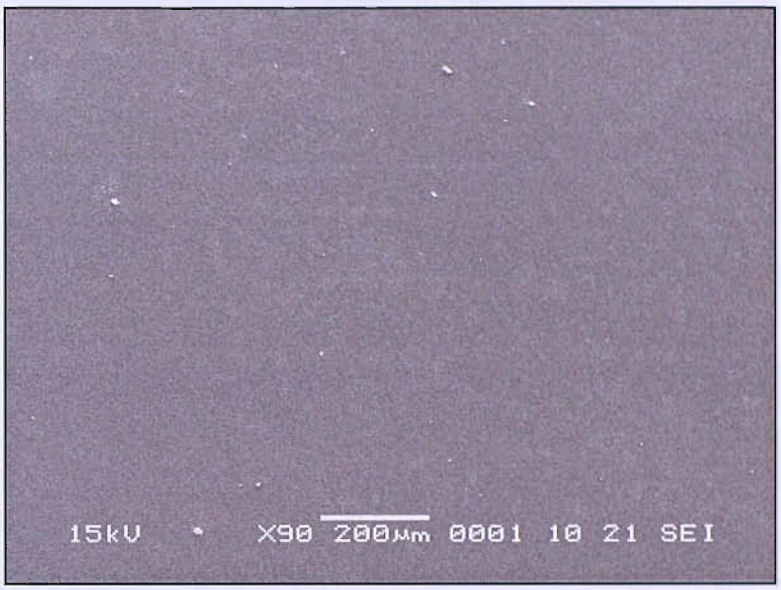

Figure 5.10: Higher quality films were possible with less precipitous materials present on the surface of the substrate.

Figure 5.11:The occasional presence of imperfection confirmed that a coating was present.

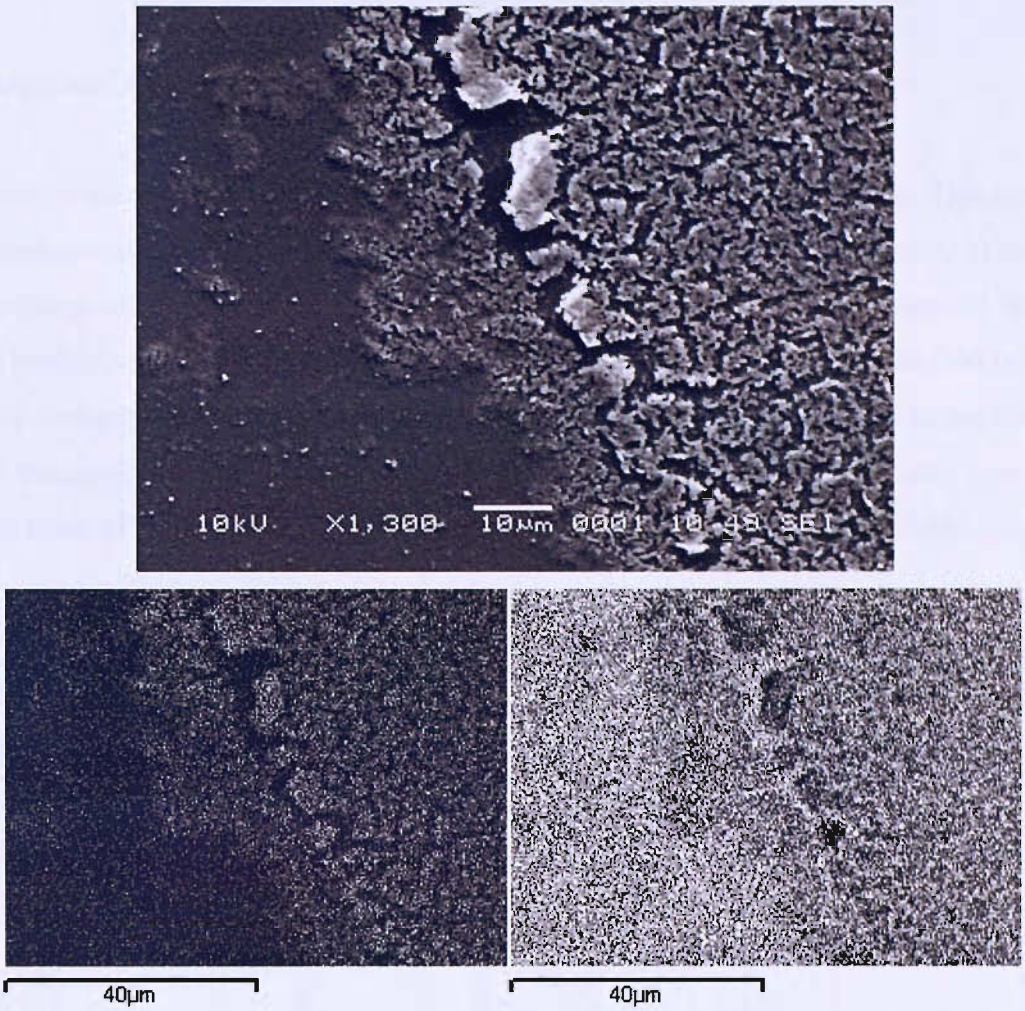

Figure 5.12: Image of area mapped (top) with EDX mapping of titanium (bottom left) and silicon (bottom right).

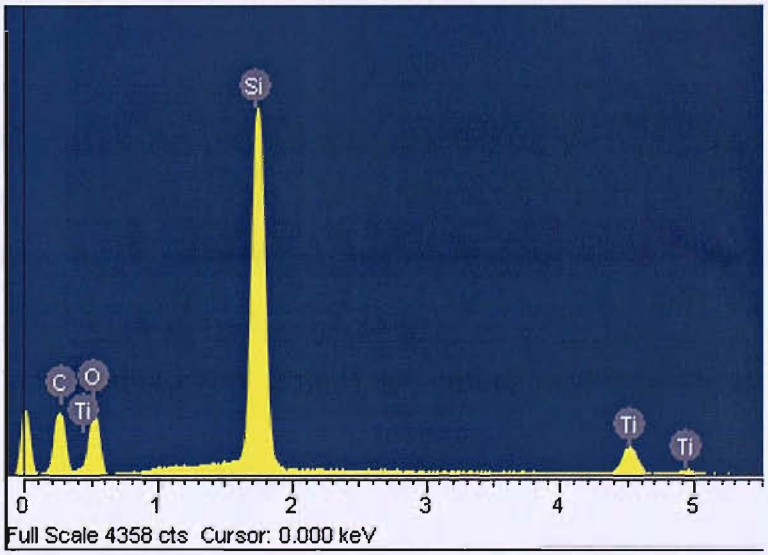

Figure 5.13: Qualitative analysis of the coatings confirmed the strong presence of titanium.

Compositional Analysis of the Coatings

Analysis of the 'bulk' material was performed via powder X-ray diffraction. This material was produced using the same reagents in an excess – in order to induce precipitation and the resulting solid was heated in NH_3 at 800 °C, as for the films. PXD showed that the 'bulk' product could be indexed to a face centred cubic type crystal structure (*Fm3m*) with a lattice parameter of 4.228 Å (see Figure 5.15). This compared favourably to the titanium nitride standard, purchased from Aldrich chemicals, which was indexed as also being face centred cubic (*Fm3m)* and possessed a lattice parameter of 4.238 Å (Figure 5.14).

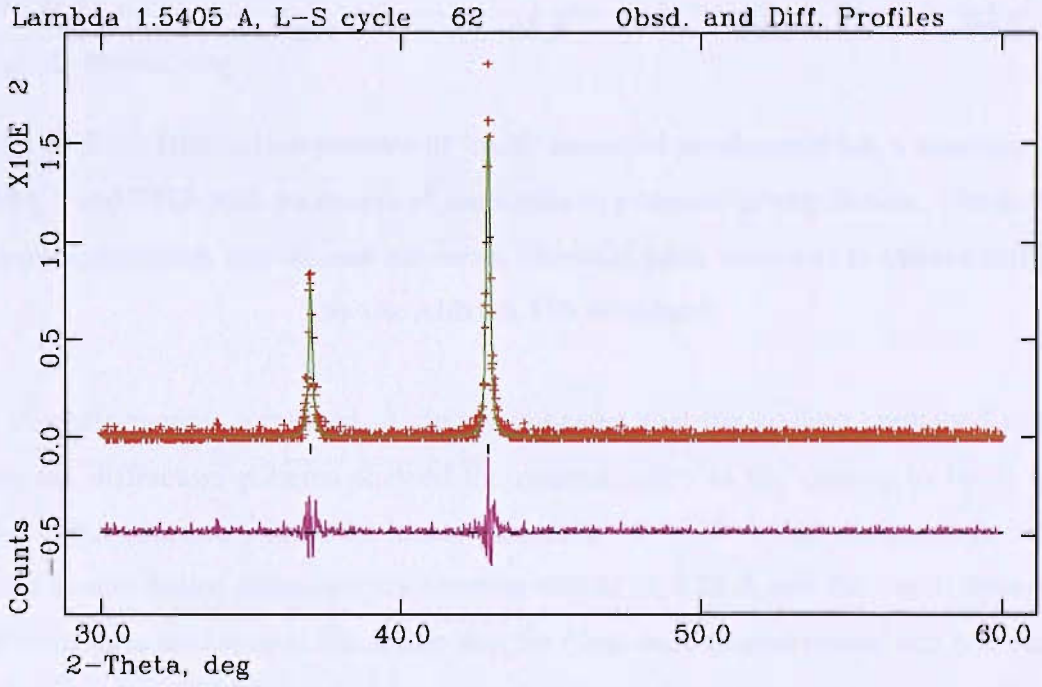

Figure 5.14:Refined diffraction pattern of Aldrich TiN displaying peaks at 34.5 and 42.8 degrees respectively, corresponding to the (JCPDS) standard.

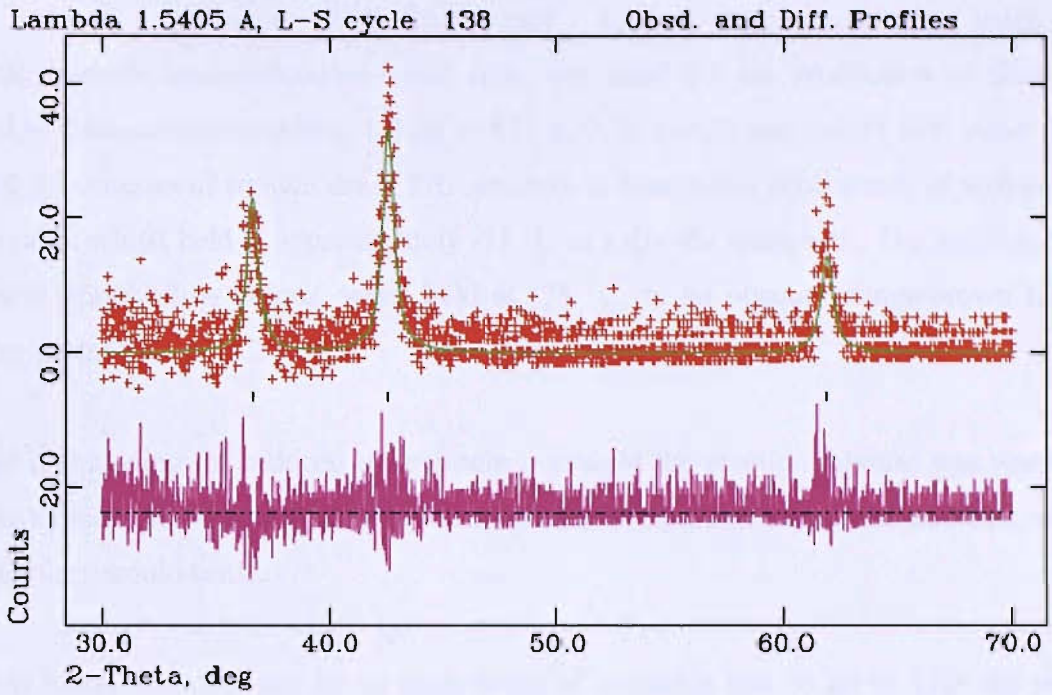

Figure 5.15: Diffraction pattern of 'bulk' material produced from a solution of TDMAT and THF with an excess of ammonia to promote precipitation. The pattern indexes as titanium nitride and possesses identical peak positions to those exhibited by the Aldrich TiN standard.

With this information combined, it clearly indicated that the coating contained titanium nitride; the diffraction patterns showed the material used as the coating to be of a face centred cubic structure with a the lattice parameter of 4.228 Å that compares favourably with the known lattice parameter for titanium nitride of 4.24 Å and the visual appearance of the films gave credence to the notion that the films were indeed nitride and not oxide as the films were not white in colouration but rather brown/black or grey.

5.3.5 Coating with the Tetrakis(diethylamido)titanium Derived Sol

Tetrakis(diethylamido)titanium was used in an attempt to increase the solubility of the amide polymers, where partial condensation had occurred, giving dimers and trimers etc, in solution and to increase the propensity of cross-linking during condensation reactions through the longer alkyl chain length.

A method, analogue to that used to produce coatings using the tetrakis(dimethylamino)titanium-based sols, was used for the production of films with tetrakis(diethylamino)titanium; 1.0 ml (0.931 g, 2.76 mmol) was mixed with either 10, 20 or 30 ml volumes of sodium dried THF and two to four molar equivalents of sodium dried ammonia; whilst held at approximately -78 °C in a dry ice slush bath. The solution turned from a straw/yellow colour, when held at -78 °C, to an opaque orange/brown solution when warmed to -20 °C.

After maintaining the reduced temperature overnight the reaction mixture was warmed to room temperature. The mixture was then left for 24 hours to ensure the contents, if solid containing, would settle.

It was found that with two molar equivalents of ammonia and 30 ml of THF the product was an opaque brown solution, however upon agitation of the containing vessel it became apparent that the consistency was far more akin to a weakly bound gel with large gelatinous sections possessing shear faces and showing some signs of elasticity when agitated.

The reaction was repeated several times using the same conditions, in order to ascertain if the results were erroneous, however, the results were very similar to the first attempt. Upon reducing the amount of solvent in the reaction mixture, the product yielded seemed to be more susceptible to phase-separation although the solid material produced still closely resembled a weakly bound gel.

Further parameters were adapted within this reaction scheme which lead to the development of a reliable method of producing monolithic gels, which shall be discussed in the next chapter. However, for the goal of achieving a suitable coating sol, using the precursor TDEAT was unsuitable as the variation in parameters did not enable the production of a coating-sol, hence, further modification of the amide reagent was sought.

5.3.6 Coating with the Tetrakis(dipropylamino)Titanium Derived Sol

The alkyl groups of the metal amide were further extended to propyl in an effort to increase solubility.

Upon addition of the amide to the THF, a clear solution with a pale yellow hue was observed. When combined with the ammonia and chilled to -78 °C the solution solidified and only became liquid again once the card-ice slush bath had partially evaporated after 6 – 8 hours. The localised temperature remained suppressed for a further 8 – 10 hours.

Once removed from the cool bath, the solution was semi translucent with no sign of precipitation and this remained stable for several hours. The solution was transported to a nitrogen filled glovebox where the coating took place.

Coatings were performed in a sequential manner with the first slide receiving 1 coating and the sixth slide, six. This was performed in order to build-up the coating thicknesses to produce films that could be analysed via SEM and TEM/ED.

Complications were encountered during the coating process as the ambient temperature in the glove box and glove box room was elevated by approximately 5 – 10 degrees celcius relative to ambient temperatures of 20 °C. Precipitation began to occur within the coating sol at an accelerated rate. This resulted in solid species being deposited onto the surface of the coating as is illustrated with the SEM acquired (see Figure 5.16) which clearly shows that the instances of solid deposits upon the surface of the tiles coating increase with the number of coatings applied.

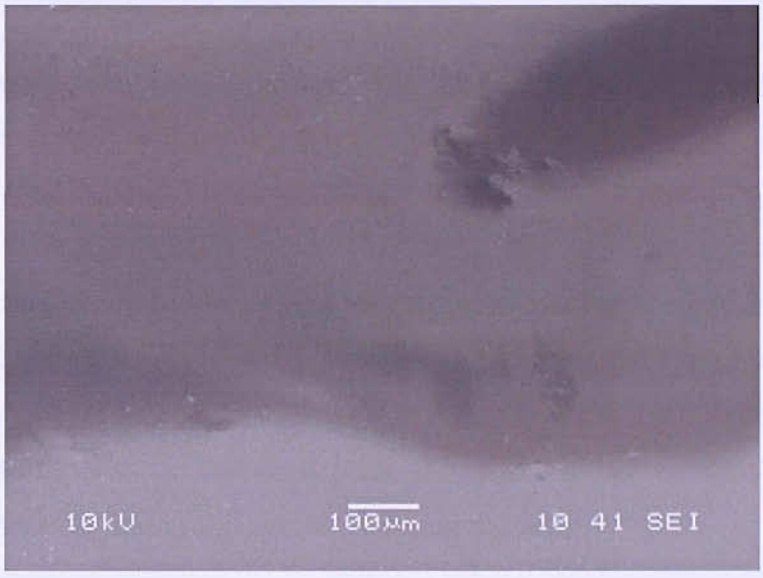

Figure 5.16: A five dip propylamide-based coating after annealing, exhibiting solids on the surface of the film.

The SEM images clearly show the presence of a coating on the slides, as can be seen in Figure 5.17.

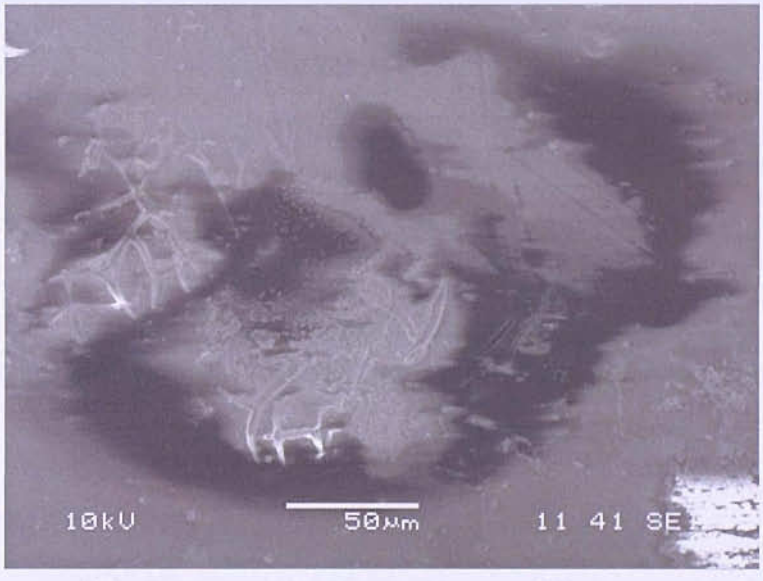

Figure 5.17: A propylamide-based six dip coating with fractures in the film surface, illustrating the presence of a film beneath the precipitous materials on the film's surface.

EDX was also performed on the coated tiles; whilst the same issues were present with this technique as had been experienced before, the EDX scans displayed, as had been previously observed, signatures for titanium. (see Figure 5.18).

In the thicker coatings it can also be seen that the coating surface is cracked in several places further reinforcing that a coating is present on the tile rather than the results being collected due to solid deposits on the substrate surface due to the wanted self-condensation.

This method showed the most promising potential for producing good quality films. Due to the increased ambient temperatures that were incurred during the deposition stages future work carried out should be sought to be performed at lower ambient temperatures which would enable the films to be deposited prior to any significant condensation occurring, which would otherwise cause solid species to for on the films.

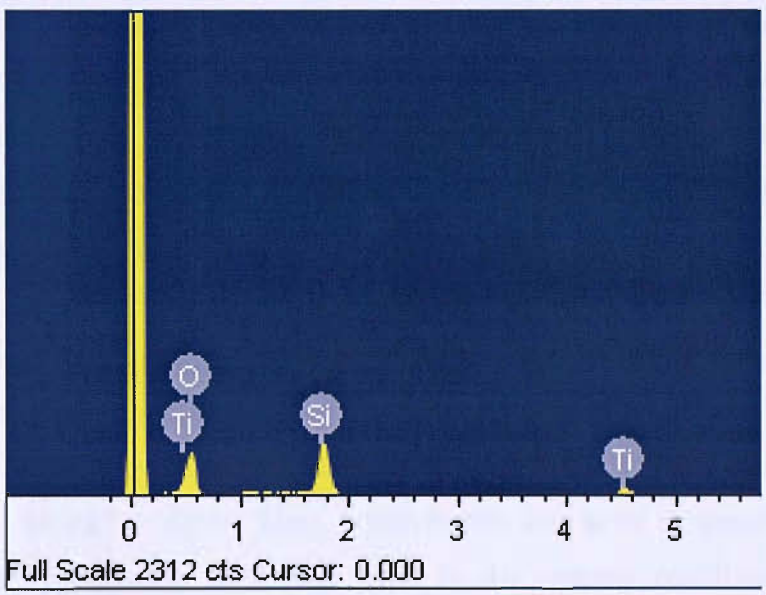

Figure 5.18: Qualitative analysis of the propylamide-based coatings confirmed the presence of titanium.

5.4 Conclusions

The addition of stoichiometric amounts of NH_3 to tetrakis(dimethylamino)titanium resulted in precipitation and it was only the addition of the reaction modifier 2-2' bipyridyl which enabled a coating sol to be produced. Not only did the diethylamide not require a reaction modifier to sustain a suspension within solution, but it was also able to crosslink and form a weakly bound solid over time, as opposed to a precipitate, which would have subsequently settled. The reasoning behind this could be attributed to the extended alkyl chain length which, whilst not long enough to improve the solubility of the amide to the

point at which it could remain in solution after ammonolysis, was able to sterically hinder the attack of the central metal by the ammonia groups and thus enable the creation of 'activated' alkyl branches which could then go on to create imide bridges with similar alkyl groups on other molecules and thus create a network which was observed.

Coating of both alumina and silica tiles with a stable ammonolytic sol has been achieved using a variety of different methods. The most successful of these has been in conjunction with the longer chain alkyl amide, tetrakis(dipropylamino)titanium on silica substrates. SEM and EDX confirm that the deposition has been successful as a conductive, titanium containing coating is present.

Visual inspection of the tiles confirmed the material on the thicker coated tiles to be grey/black, as were the shavings that were removed from the coatings prior to TEM inspection. The attempted use of tetrakis(diethylamido)titanium has lead to an interesting series of developments, which will be discussed in the following chapter, however for the purpose of this area of the research, has proved to be unsuitable.

With the further extension of the alkyl group the desired effect of retaining a solution which was saturated with an ammonolysed amide was achieved and with this, deposition of a continuous film with relatively few defects became possible. The coatings did contain solid species on the surface of the films, however this was to be expected as the sol was progressively self-condensing over time. Due to the coating conditions being above ambient temperatures, this phenomenon was accelerated. The SEM images indicate that a coating is present below the solid deposits.

6 MONOLITHIC NITRIDES VIA SOL-GEL

6.1 Introduction

Metal nitrides have attracted a great deal of interest due to the physical and chemical properties that have been discussed previously in chapter 3 with respect to their hardness, chemical and thermal stability. However there has been a growing interest in the development of their catalytic properties, with respect to their use as selective gas membranes, their applications in heterogeneous and base catalysis[80].

Silicon-based nitrides have been found to be useful as selective gas filters for example, in the case of silicon nitride membranes templated by Al_2O_3, where CO_2, H_2 and propane were able to diffuse through the membrane whilst NO_2 was completely retarded[81]. They are also of interest as potential heterogeneous catalysis material, as solid base catalysts in knoevenagel reactions, such as the condensation of benzaldehyde with malonitrile and, after impregnation with potassium, as efficient 'superbase' catalysts.

By preforming the nitride in precursor format, via gelation of amides with stoichiometric amounts of ammonia, the pore structure can be retained and the dimensions of the resultant monolith can be tailored to the desired shape required for the application. Additionally as the method of formation does not require sintering, solvent can be removed via supercritical extraction to protect the pore structure from any potential damage which may occur as a result of solvent extraction.

With the material free of solvent, the monolith can be annealed under nitrogen or ammonia to produce nitrides or carbonitrides, keeping the temperature low enough to avoid sintering In the ammonolysis of oxide precursors, the conditions of low temperature ramp and high NH_3 space velocity were required as to minimise the partial pressure of the H_2O created, which was thought to reduce the surface area of the product due to hydrothermal sintering[82]. Generally avoiding high temperature processes such as oxide ammonolysis should maximise surface area.

By pre-forming the material in precursor form, supercritically extracting the solvent in order to retain the pore structure and carefully heating the sample, these aforementioned problems can potentially be overcome. This chapter presents a highly promising set of results which give the strong indication that this process is possible with just metal amide precursors and stoichiometric quantities of ammonia and could be the vanguard of an important step in the processing and formation of such materials, potentially expanding the range of applications in which they are currently used.

6.2 Experimental Procedure

6.2.1 Amide Preparation

The TDMAT used for all transamination reactions was kindly donated by Epichem; purity was verified by NMR. Electronic grade (99.99%) tetrakis(diethylamino)hafnium and tetrakis(diethylamino)zirconium were purchased from Aldrich chemicals. Upon the consumption of the distilled tetrakis(diethylamino)titanium, an industrial grade (98%) replacement was purchased from Fluka.

Tetrakis(diethylamido)titanium Preparation

Tetrakis(diethylamino)titanium was used in an attempt to increase the solubility of the amide in solution and to increase the propensity of cross-linking during condensation reactions through the longer alkyl chain length. The preparation of the amide was exactly as previously detailed in chapter 5.

6.2.2 Gel Synthesis

Using Tetrakis(diethylamino)titanium

TDEAT :- 1.0 ml, 0.931 g, 2.76 mmol
THF :- 30.0 ml
NH_3 *(l)* :- 0.13 ml, 0.0962 g, 5.64 mmol

The TDEAT was mixed with THF which was then combined with the NH_3 at -78 °C, in order to reduce the kinetic activity of the reagents in an effort to reduce localised condensation and promote a homogenous mixture. The mixture was then transferred to a cool bath set at -20 °C for approximately 17 hours and then allowed to warm slowly to room temperature.

N.B.

Replacement TDEAT was purchased from Fluka in the form of "industrial grade" 98% pure TDEAT, when the initial stock of amide was consumed. It was found that this amide behaved in a completely different manner to the previously used reagent and could not be made to gel at all.

Using Tetrakis(diethylamino)hafnium

TDEAH :- 0.50 ml, 0.6245 g, 1.33 mmol
THF :- 10.0 ml
NH_3 *(l)*:- 0.062 ml, 0.0456 g, 2.66 mmol

The TDEAH was dissolved in THF and then mixed with the NH_3 at -78 °C, in order to reduce the kinetic activity of the reagents in an effort to reduce localised condensation and promote a homogenous mixture. The mixture was left in a dry-ice coolbath to warm to room temperature, which took approximately 20 hours by which time a dense gel monolith, with some cracks, had formed (see Figure 6.4).

Using Tetrakis(diethylamino)zirconium

TDEAZ :- 0.50 ml, 0.513 g, 1.351 mmol
THF :- 10.0 ml
NH_3 *(l)*:- 0.0622 ml, 0.046 g, 2.702 mmol

The reaction of TDEAZ with ammonia in THF proceeded in exactly the same manner as the titanium and hafnium containing analogues, however the densification of the gel occurred rapidly, resulting in a densified and deformed gel with large cracks, which upon the removal of solvent fell into small fragments.

6.2.3 Bomb Preparation

A Parr 7470 autoclave was used with the silica-tube lining. Both were rigorously dried before use by heating at 100 °C under vacuum in an oil bath for 24 hours. The bomb was then backfilled with nitrogen via the Schlenk-line, sealed and transferred to a nitrogen-filled glovebox.

The silica liner was removed from the bomb and the reagents were placed inside in the required amounts. This was then placed back inside the main body of the bomb and the apparatus was reconstructed.

The head unit of the bomb was screwed hand-tight onto the main body and all valves were shut. The apparatus was then removed from the glovebox and, using a torque-wrench, the head-bolts on the head-unit were tightened.

6.2.4 Supercritical Extraction of THF

The bomb was cooled to -78 °C; this was done in order to distil NH_3 to the bomb and to sufficiently cool the reagents, so they would be less likely to react immediately when coming into contact with ammonia.

Ammonia was condensed into a separate Schlenk tube and then transferred into the bomb via evaporation, involving canulation of the ammonia, in gaseous form, through a resealable diaphragm in the valve assembly of the bomb head-unit, into the main body of the bomb which was re-cooled to -78 °C and thus condensed back to a liquid.

Once all the ammonia had evaporated from the separate Schlenk tube, the canula was removed from the bomb and the unit was sealed. The bomb was then left to gradually warm to room temperature and then stand for approximately 24 hours.

The residual gaseous ammonia was removed via the cooling of the bomb to -78 °C followed by the gradual opening of the bomb inlet/outlet valve and then gradual warming back to room temperature, allowing the excess pressure to be released and any ammonia to evaporate.

Once this was completed the bomb was re-sealed, heated to 430 °C and then opened again, in order to supercritically extract the residual THF without, in principle, damaging the monolithic species created by the preceding reaction.

Once this process was completed the bomb was allowed to cool, backfilled with nitrogen, sealed and transported to a nitrogen-filled glovebox where the product was unloaded and appropriately stored in preparation for analysis.

6.3 Results and Discussion

6.3.1 Initial Observations

It was found that with two molar equivalents of ammonia and 30 ml of THF the titanium-based product resembled an opaque brown solution however, upon agitation of the containing vessel it became apparent that this was in fact a fragile gel as the product began to split into large gelatinous sections possessing shear faces which displayed signs of elasticity when agitated. This led to the reaction being repeated several times using the same conditions, in order to ascertain if the results were erroneous. Encouragingly, the results were very similar to the first attempt.

Upon reducing the amount of solvent in the reaction mixture, the product yielded seemed to be more susceptible to phase-separation although the solid material produced was still a fragile gel.

6.3.2 Titanium-based Gels

Gelation Results

It was realised that the weak gelation that was being observed could potentially be due to the gel being in the early stages of syneresis and that by agitating the vessel the weak cross-links of the gel were being easily overcome. Therefore, upon repeating the experiment it was decided that the product should be left in isolation for at least two days. Upon inspecting the brown product after 48 hours it became clear that the product was an elastic gel as it could withstand agitation and only after repeated movement did the gel begin to display signs of fatigue and begin to split.

Upon repeating the same reaction conditions for a third time and leaving the gel for *three* days whilst monitoring the progress of syneresis, physical shrinkage of the gel was observed; the initial stages of gelation occurred upon warming to room temperature with a brown semi-rigid opaque gel initially forming after approximately 24 hours, this then established structural integrity over the course of the next 24 hours although no physical change in the shape of the gel was observed (see Figure 6.1, left). After a period of 72 hours the gel had begun to densify and expel the THF solvent from its pore structure (see Figure 6.1, right).

It was noticed at this point that the surface of the gel, to a depth of approximately 1 mm, was gradually changing colour and becoming a lighter shade of brown. It was unknown what the cause was of this colour change was although it was speculated that it could be a result of faster ageing occurring on the sample surface due to its close proximity to the region of the solution where evaporation was most prominent. Similar to the phenomenon of "phase transformation".

After a further 24 hours the compacted gel began to show signs of cracking and was now of overtly smaller dimensions than had previously been seen and the area on the surface of the gel had also turned a very pale brown/beige colour.

Upon removal of the excess solvent it was found that the dimensions of the gel were a lot smaller than had been previously anticipated (see Figure 6.2). This was due to the optical effect of the gel being immersed in THF which masked the gradual shrinkage of the gel's diameter, whilst the shrinkage in height was clearly observed (see Figure 6.1, right). Upon further removal of solvent, via reduced pressure at -78 °C, the monolith shrank further still until it was 5 mm in diameter and 10 to 15 mm in length. This was annealed under ammonia to 800 °C and then analysed via PXD.

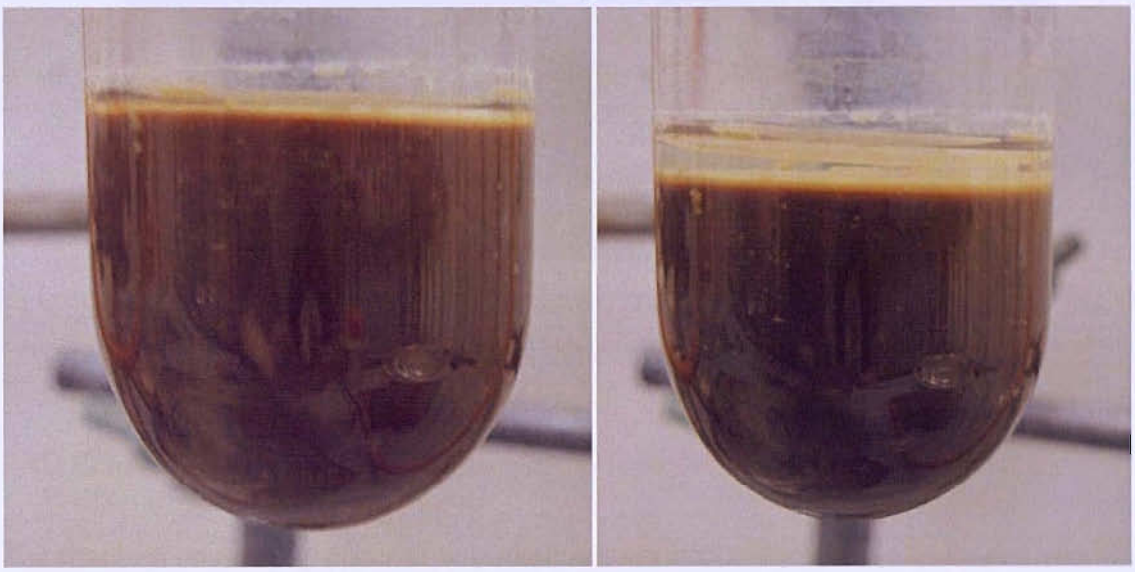

Figure 6.1: Images displaying the process of syneresis in the tin precursor gel after 24 hours (left) and 48 hours (right).

Figure 6.2: Image of TiN precursor gel after solvent removal, clearly displaying the same shape as the containing vessel.

PXD Results

The titanium containing material was analysed via PXD. The pattern collected was found to be a face centred cubic species with the space group *Fm*3*m* and a lattice parameter of 4.195(8)Å, all of which give the strong indication of the presence of titanium nitride especially as the lattice parameter compared favourably to that of the literature value for TiN (4.24Å)[56].

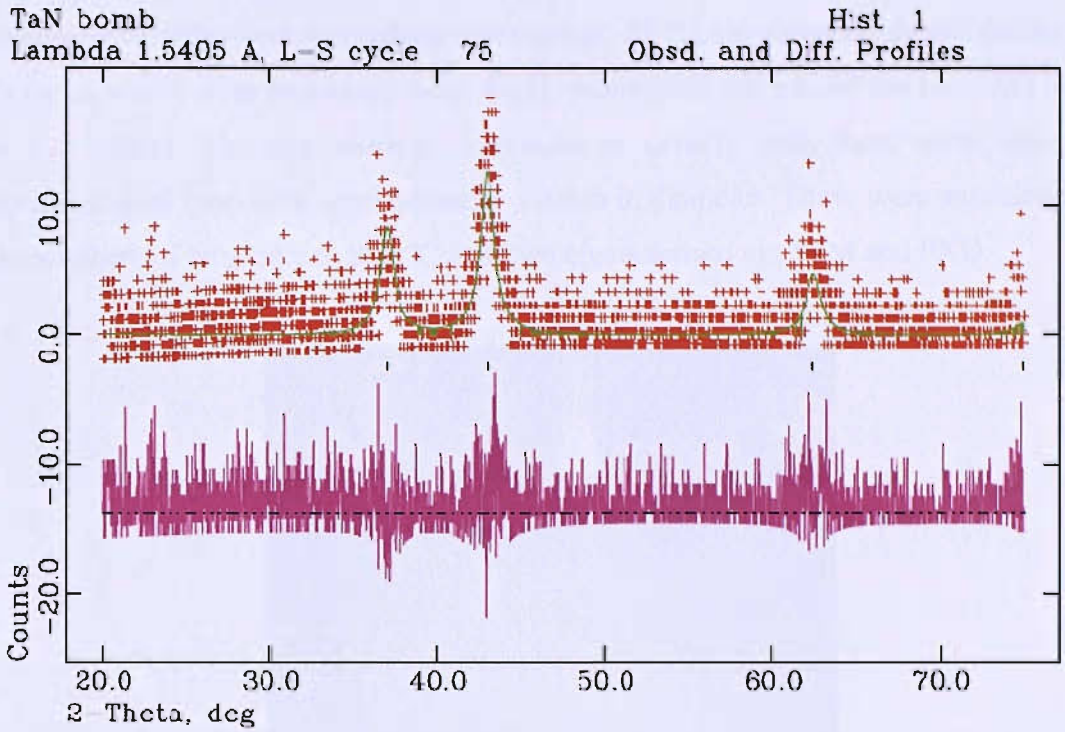

Figure 6.3 PXD profile of the monolithic titanium precursor, annealed at 800°C under ammonia, which matches a rocksalt-type TiN template.

6.3.3 Hafnium-based Results

Gelation Results

The formation of a gel took place over a period of two days. The initial stages of gelation occurred within 24 hours of warming to room temperature in the same manner as was observed for the titanium-based gel except over a much shorter timescale. A white/ivory rigid, opaque gel, initially formed which closely resembled the contours of its containing vessel. After a further 24 hours the gel had densified much further (see Figure 6.4) and began to resemble a spherical monolith.

After an additional 24 hours the compacted gel began to show signs of cracking and deformation, possibly due to the repeated agitation of the vessel when being observed.

Upon removal of the excess solvent a cylindrical monolith was produced, however, upon further removal of solvent, via reduced pressure at -78 °C, the monolith shrank further until the cracks, which were previously only slight, propagated and caused the monolith to split into two pieces. The two sections continued to densify until there were two small spherical-shaped monoliths approximately 10 mm in diameter. These were annealed under an atmosphere of ammonia to 800 °C and then characterised via SEM and PXD.

Figure 6.4: Image of hafnium precursor gel after18 hours.

Figure 6.5: Hafnium precursor gel after solvent removal.

SEM Results

The annealed hafnium product was analysed via EDX and it was found that the core of the monoliths were oxygen free (see Figure 6.7). The monoliths produced were highly compacted (see Figure 6.6) with a relatively low surface area of 31.86 m^2/g and physically, they were very hard to mechanically manipulate, as would be expected for a nitride material.

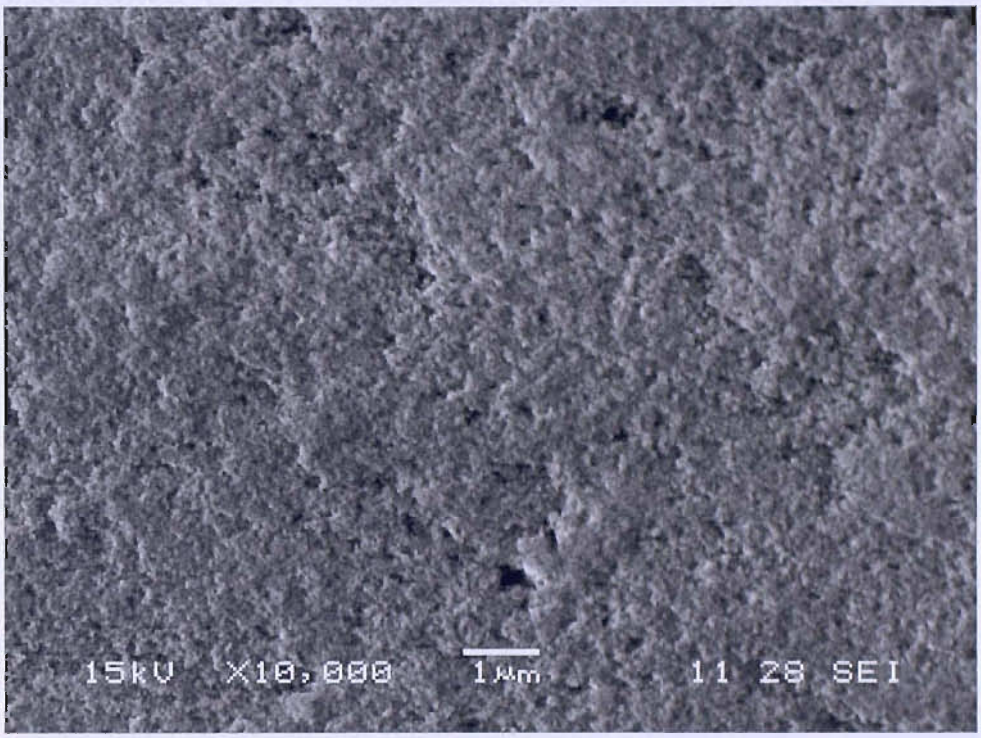

Figure 6.6: x10,000 magnification image of Hf product illustrating the compacted and amorphous structure of the monolith.

Photographic analysis via SEM revealed that there was a highly compacted amorphous structure, as would be expected for a sol-gel derived solid (see Figure 6.6 and Figure 6.7).

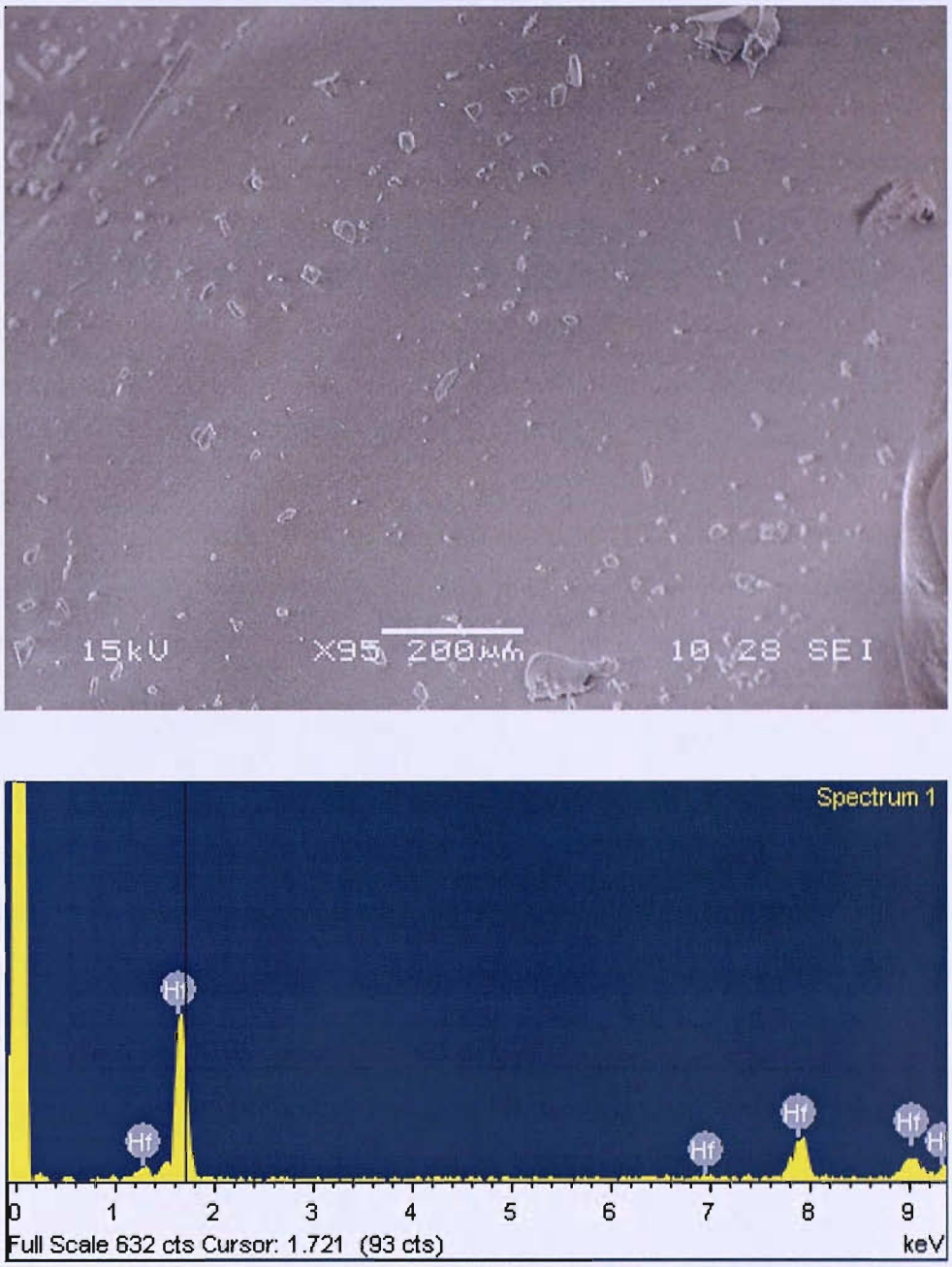

Figure 6.7: Low magnification image of Hf product (top) and the respective EDX area analysis displaying no trace of oxygen (bottom).

EDX showed the presence of hafnium whilst, critically, no oxygen was detected in the sample (see Figure 6.7). Nitrogen was undetected due to the SiLi detector possessing a BN window which effectively made the presence of the element 'invisible'.

PXD Results

The hafnium containing material was analysed via PXD but due to the quantity of the sample used for analysis, the peaks were found to be too wide to be definitively refined and characterised. A dummy histogram of Hf_3N_4 was constructed to compare the profile of the diffraction pattern gained. The collected pattern was found to resemble the histogram which represented a distorted rocksalt structure, similar to those previously reported by Riedel *et al.* for Hf_3N_4[17]. Using this method the space group was determined to be rhombohedral *R* -3*m* and possessed a lattice parameter of 4.49Å.

There was also the possibility that the material could be HfO_2. This did seem to be visually likely as the materials synthesised tended to possess a pale crust on their surface after annealing under ammonia, indicating that an additional reaction was occurring on the surface of the material.

Considering the influence of the f-block on the characteristics of hafnium, which results in its oxophilicity disproportionately increasing in relation to its periodicity. It seems most likely that oxidation was occurring during the annealing phase due to suspected trace amounts of oxygen in the ammonia gas. It is thought that during the annealing of the titanium-based precursors, due to the much lower oxophilicity of the system, the trace amounts of oxygen were so low as to not cause any detectable oxidation. It is thought that this is why oxidation had not been observed until the annealing of the more oxophilic compounds had been performed.

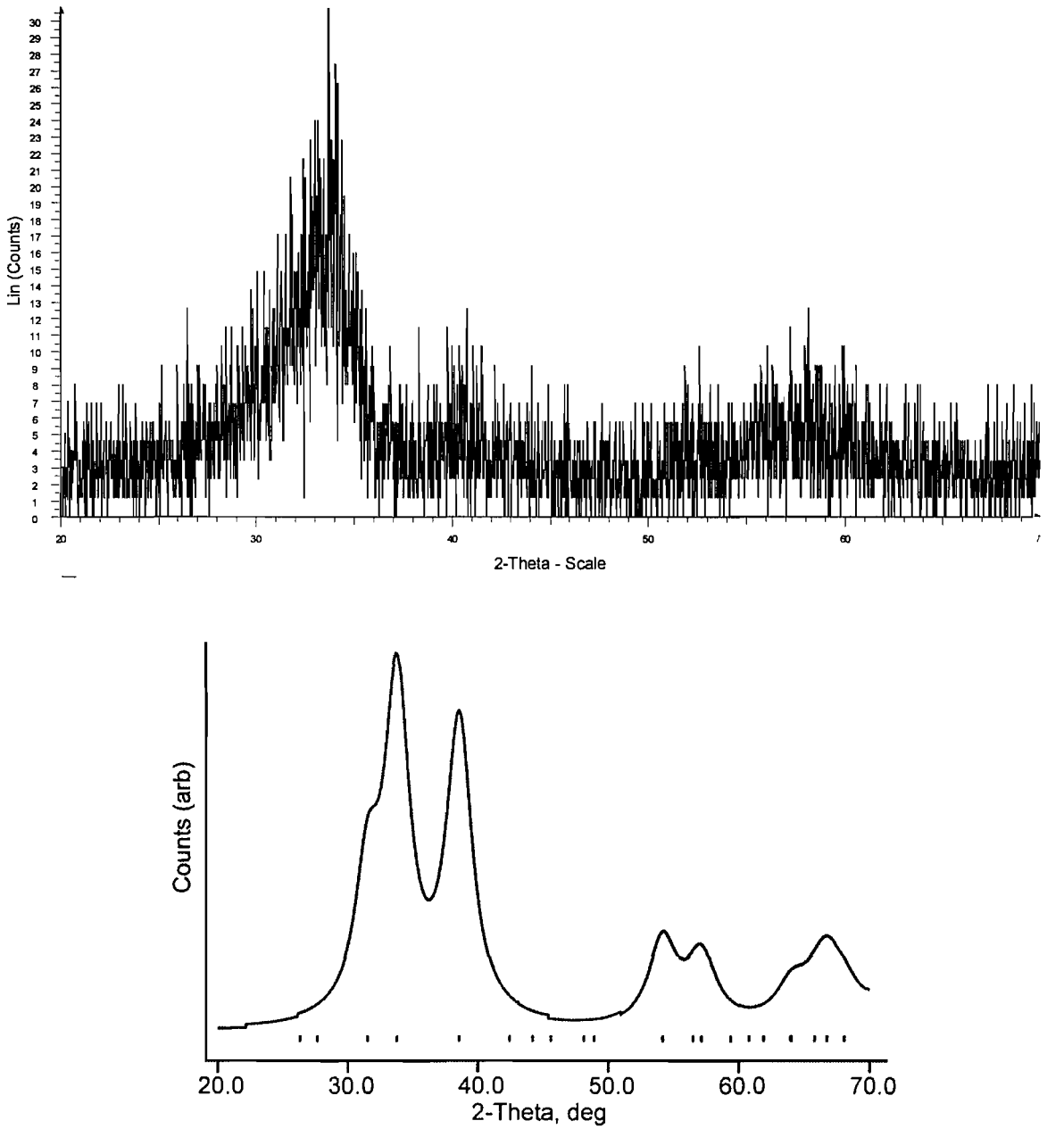

Figure 6.8 PXD profile of the monolithic hafnium nitride precursor, annealed at 800°C under ammonia (top), which resembles a rhombohedral-type template (bottom).

6.3.4 Zirconium

Gelation Results

The gelation which, with the previous amides, had been observed to occur over the course of 24 to 72 hours, apparently occurred in less than 20 hours for the Zirconium based gels. Upon inspecting the gel after approximately 18 hour from the addition of the ammonia fragments of gel possessing shear faces were seen in the reaction vessel. This was not thought to be powder as the product didn't have the appearance of either finely divided or highly agglomerated precipitate. The appearance was very similar to the fragmented pieces of gel which were observed upon the agitation of the previous systems. The solvent was removed via reduced pressure and the solid material was annealed under an ammonia atmosphere to 800 °C and then analysed via PXD.

PXD Results

Due to the unfeasibly low quantity of zirconium-based product used for analysis, the diffraction pattern was worse than that which had previously been seen for the hafnium-based product.

Due to the lack of material available for analysis, definite conclusions as to the structure and composition of the material were tenuous at best.

However, due to the chemical similarities of zirconium and hafnium in terms of oxophilicity and structure, post annealing parallels could be drawn between the similarities in shape of the Zr pattern to the Hf pattern and therefore the potential match it could possess towards an oxide-based material.

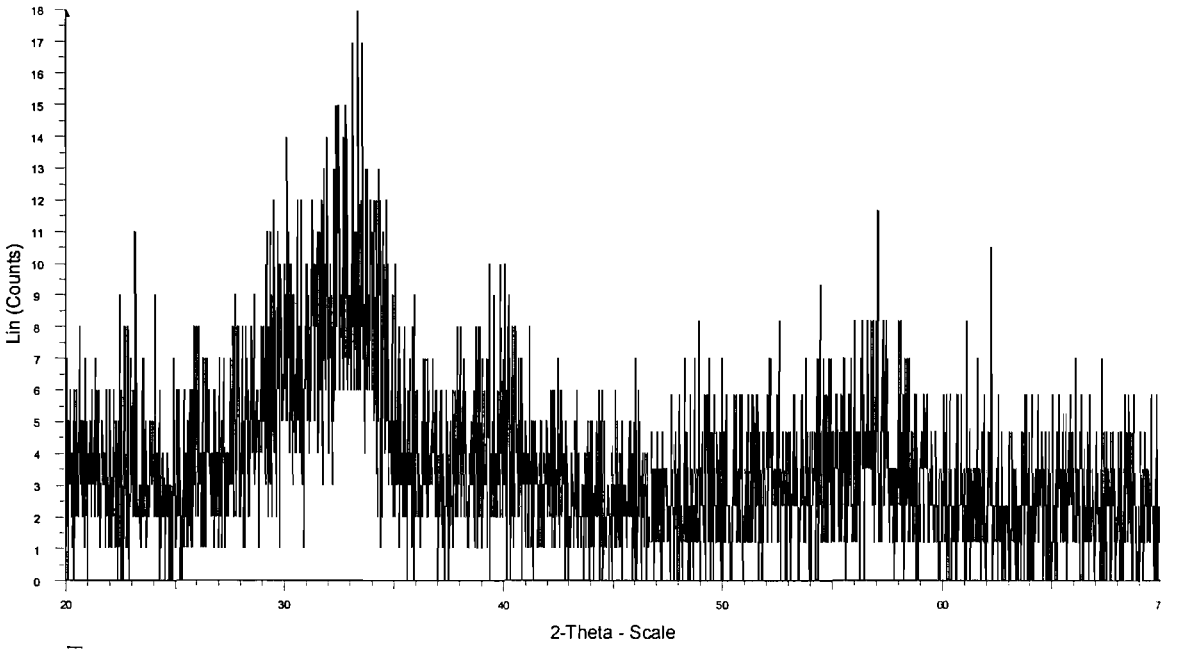

Figure 6.9: Diffraction pattern of zirconium product which resembles the hafnium product.

6.3.5 Super-critical Extraction of THF

Supercritical Fluid Extraction (SFE) was attempted due to the potential for the production of aerogels. As normal reduced pressure 'drying' methods causes the collapse and densification of precursors' pore structure; due to the phase change of liquid solvent to a gas, under reduced pressure at room temperature, the solvent is liable to expand whilst inside the monolithic species and consequently destroy the extended structure due to internal pressures being too great for the structure.

By using a supercritical extraction technique the vapour pressure build-up that would occur, causing the destruction of the pore network within the gel could be avoided and could potentially lead to the preservation of the internal structure of the precursor and hence give a monolithic aerogel.

Removal of supercritical THF from the hafnium and zirconium-based precursors gave mixed results. The hafnium-based experiments appeared to work well, with a monolithic material being extracted from solution with little visual damage. The precursor was heated under ammonia to 800 °C at a slow ramp rate of 1 °C per minute to 400 °C and then 2.5 °C from 400 to 800 °C. This was done in an attempt to safeguard the pore structure and retain

any higher surface area. However, it was discovered that the surface area of the material was no different to the hafnium xerogel material.

Zirconium was also attempted but unfortunately the monolithic material could not be protected from collapsing during the process of supercritical extraction. The extraction technique was repeated several times with careful monitoring of the temperature, pressure release and general technique of the process but the results remained the same.

6.4 Conclusions

The outstanding achievement of this chapter has been the successful creation of a set of conditions which are able to produce monolithic nitride materials from amides containing the group IV metal titanium, via a procedure involving the gelation of amide reagents with nothing more than stoichiometric amounts of ammonia; an achievement which has been previously assumed to be impossible[13]. Hafnium- and zirconium-based materials showed signs of potential, with gelation being facile, although the syneresis was so aggressive that the gel was self damaging. The refinement of its specific annealing process was also needed in order to successfully translate the monolithic gels produced into nitrides rather than oxides.

Developing conditions to synthesise monolithic gels of group IV binary nitrides is a major achievement and will provide a foundation for a methodology which can return high-purity monolithic materials tailored to specific dimensions and pore sizes. However the unidentified white 'crust' which was observed on all of the samples (particularly those based on hafnium and zirconium) after annealing in ammonia, was thought to be due to the quality of the ammonia used throughout all stages of ammonolysis; it was possible that the gas was not sufficiently oxygen-free and the layer was potentially oxide-containing, especially when considering that the increased moisture/oxygen sensitivity of the zirconium and hafnium, in comparison to the titanium-based analogue, could potentially amplify the effect of any ingress of oxygen or moisture into the reaction mixture.

Evidence to support the theory that the oxidation was only superficial to the sample presented itself upon splitting the annealed material open. The white/grey layer penetrated

the samples by less than 1 mm with the remaining ceramic material possessing a colouration associated with its nitride form: brown for the titanium nitride material; yellow/ ivory for the hafnium nitride material. EDX analysis of this material revealed that in the areas that were not a grey/white colour, the sample did not possess oxygen.

The annealed titanium-based compounds were found to resemble TiN when analysed by PXD, the annealed hafnium- and zirconium-based compounds indicated a similarities to both distorted rocksalt-phase nitride materials and orthorhombic oxides. It was found upon the modelling of the diffraction pattern for the hafnium-containing material that a fit could be generated when modelling the patterns against the distorted rocksalt variant of Hf_3N_4 or an orthorhombic HfO_2 structure. Additional information from EDX analysis indicated that the hafnium-containing materials produced did not possess any oxygen in its composition, which leads to the possibility that parts of the compound could be the orthorhombic HfO_2 as the diffraction pattern also resembled orthorhombic HfO_2 whilst other areas were some form of hafnium nitride.

As previous experiments were conducted using the titanium-based amide, which is less oxophilic, it would seem feasible that minute quantities of oxygen could have been present in the gas and that the 'drying' of the ammonia, using a lithium amide drying column was not sufficient.

A final factor is the notion that the amides themselves had been stored in a glovebox whose atmosphere purity had come into question on a number of occasions and therefore could have been a source of contamination for any of the glassware, precursors or pre-annealed monoliths. As the monolithic precursors showed no visual signs of oxidation when being synthesised and the materials produced were of a nitride species internally, the oxidation of the amide precursors can rationally be ruled out.

The suspicion that the reactive gas, used in the annealing process, was responsible for the oxidation is seemingly vindicated as the surface of the precursor monolith was oxidised whilst internally it was not, suggesting that the oxidising source was external to the precursor material rather than the material itself intrinsically possessing a source of oxygen.

Additional characterisation would have been desirable to establish the source of the erroneous white coating on the products. Unfortunately due to equipment failures and the unsuitability of replacement chemicals, this was not possible. However, the results gained so far, indicate that for titanium- and hafnium-containing materials the purported oxidation is not a major issue and monolithic nitrides can definitely be produced.

7 CONCLUSIONS

The significant aims of this research were to develop a sol-based coating method that could successfully deposit a coating sol onto a substrate, which could in turn, be cured to produce a continuous, well-adhered film; and also to explore the potential for the synthesis of transition metal nitride monoliths from transition metal amide precursors and their subsequent drying to produce xero- and aerogels.

In essence the research was a great success as not only were two discrete routes to the generation of functioning coating sols developed, but also it was proven that there is great potential for the development of sol-gel routes to monolithic nitride products.

Basic control of film thickness was achieved through the control of the amides used. By transaminating the amides with different length amines the viscosity of the coating sols could be modified (longer chain lengths resulted in higher viscosities). This directly related to the overall thickness of the annealed coatings and also the quality as well, as it was noted that higher concentration/viscosity coatings of *any* of the coatings sols produced usually possessed fewer defects.

In hindsight, three significant areas, throughout the course of research, have served to offer direction for future development of the techniques that have been developed in this thesis.

Firstly, during the characterisation of the precipitous material from the initial ammonolysis reactions, the ability to characterise the exhaust gases being ejected by mass spectroscopy from the precursor material during their thermogravimetric analysis would have been invaluable. The ability to characterise the thermolysed fragments as they were exhausted from the specimen being heated would have allowed the identification of the atomic constituents, their relative ratios and the overall mass of the fragments in question, at any given point during the course of thermolysis. This would have allowed far more accurate modelling of the actual reaction pathway during the heating of the precursor. It would also have served to assist in the elucidation of the role of the annealing gas used and how significant a contribution it makes to the end product.

Secondly, the further refinement of the coating method, possibly through the use of a portable dip- or spin-coater inside a nitrogen filled glove box, could allow for advances in coating quality as the developed coating method was not without limitations. One such limitation being the need to canulate the solution every time a coating was to be performed, and consequently, the potential for oxygen contamination that was associated with it.

Finally, the further development of the synthetic route to the monolithic products and the drying techniques that were employed in order to produce aero- and xerogels is by far the most interesting and potentially most fruitful area. Problems were encountered with the apparent ingress of oxygen into the system, caused by either contaminated reagents or sub-standard ammonia gas, used for the annealing of the monolith. If the source of this contamination were to be eliminated, something which a combination of mass spectroscopy and thermogravimetric analysis would be able to assist in isolating, the only issue confronting a reproducible and reliable synthesis of monolithic nitrides would be the refinement of the drying procedures. In particular, the area of supercritical extraction showed great potential, results were varied but definitely showed potential. If the conditions were to be refined in order to extract the solvent without causing stress fractures within the monolith, then the potential for further research and application could be huge.

8 BIBLIOGRAPHY

[1] F. Cheng, S. Clarke, S. M. Kelly, J. S. Bradley, *J. Am. Ceram.*, 2004, **87** [8], 1413.

[2] L. Jinwang, D. Dzivenko, A. Zerr, C. Fasel, Y Zhou, R. Riedel, *Z. Anorg. Allg. Chem.*, 2005, **631**, 1449.

[3] F. Cheng, S. M. Kelly, N. A. Young, S. Clark, M. G. Francesconi, F. Lefebvre, J. S. Bradley, *Chem. Commun.*, 2005, 5662.

[4] R. Marchand, F. Tessier, F. J. DiSalvo, *J. Mater. Chem.*, 1999, **9,** 297.

[5] M. Jansen, P. Baldus, D. Sporn., *Science*, 1999, **285**, 699.

[6] G. M. Brown, L. Maya, *J. Am. Ceram. Soc.*, 1988, **71**, 78.

[7] F. Levy, P.Hones, P.E. Schmid, R Sanjines, M. Diserens, C. Wiemer, *Surf. Coat. Technol.*, 1999, **120-121**, 284.

[8] D. C. Bradley, I. M. Thomas, *Can. J. Chem.*, 1962, **40**, 1355

[9] D. C. Bradley, E. G. Torrible, *Can. J. Chem.*, 1963, **41**, 131

[10] K. Sugiyama, S. Pac, Y. Takahashi, and S Motojima, *J. Electrochem. Soc.,* 1975, **122** [11], 1545.

[11] L. M. Dyagileva, V. P. Mar'in, E. I. Tsyganova, I. L. Gaidym and Y. A. Aleksandrov, *J. Gen. Chem. USSR (Engl. Transl.)* 1984, **54** [3], 538.

[12] G. M. Brown and L. Maya, *J. Am. Ceram. Soc.*, 1988, **71**, 78

[13]D. V. Baxter, M. H. Chisholm, G. J. Gama, V. F. Distasi, *Chem. Mater.*, 1996, **8**, 1222.

[14] W. Y. Ching, S. Mo, L. Ouyang, I Tanaka, M. Yoshiya, *Physical Review B*, 2000, **61**, 609.

[15] A. Zerr, G. Miehe, G. Serghiou, M. Schwarz, E. Kroke, R. Riedel, H. Fue, P. Kroll, R. Boehler,., *Nature*, 1999, **400**, 340.

[16] K. Leinenweber, *et al.*, *Chem. Euro. J.*, 1999, **5**, 3076.

[17] A. Zerr, R. Riedel, G. Miehe, *Nature Materials,* 2003, **2**, 185.

[18] A. Zerr, G. Serghiou, R. Boehler, *Hard Materials*, Wiley-VCH, Weinheim, 2000.

[19] N. T. Kuznetsov in *Precursors for carbide, nitride and boride synthesis, Vol. 68* (edited by R. A. Andrievski and Y.G. Gogotsi), Kluwer academic publishers, 1999, pp. 223-245.

[20] K. S. Weil, M. A. Sriram, P. N. Kumta, *App. Org. Chem.,* 1997, **11**, 163.

[21] S. J. Archibald, F. Cheng, S. Clark, B. Toury, S. M. Kelly, J. S. Bradley, *Chem. Mater.*, 2003, **15**, 4651.

[22] P. Afanasiev, *Inorg. Chem. Comm.* 2002, **41**, 5317.

[23] J. Löffelholz, M. Jansen, J. Engering, *Z. Anorg. Allg. Chem.*, 2000, **626**, 963.

[24] R. G. Gordon, D. M. Hoffman, R. Fix, *Chem. Mater.*, 1991, **3**, 1138.

[25] L. H. Dubois, *Polyhedra*, 1994, **13**, 1329.

[26] R. G. Gordon, J. N. Musher, *J. Electrochem. Soc.*, 1996, **143**, 736.

[27] H. K. Shin, H. J. Shin, *Chem. Mater.*, 1997, **9**, 76.

[28] http://www.azom.com/details.asp?ArticleID=2620#_Motorsports

[29] http://www.amfmotorsports.com/ohlinsmcguide.htm

[30] W. Schintlmeister, O. Pacher, K. Pfaffinger, T. Raine, *J. Electrochem. Soc.*, 1976, **123**, 924.

[31] *Timeline of Art History*. New York: The Metropolitan Museum of Art, 2000.

[32] Genesis 11 v.3

[33] P.B. Vandiver, *Scientific American,* 1990, **262**, 106

[34] J. Smeaton, "Narrative of the building etc. of the Eddystone lighthouse", London, 1791.

[35] J.B. von Helmot , *De Lithiase, Amsterlodami,* 1644, 28.

[36] T. Bergman, "De terra silicea", *Upsala,* 1779.

[37] L.N. Vauquelin, *Ann. Chim. Phys.*, 1832, **50**, 362.

[38] W.A. Patrick "Silica gel and process of making same" U.S. Patent 1, 1919, **297**,724.

[39] J.D. Wright, A.J.M. Sommerdijk, "Sol-gel materials: chemistry and application", Published by CRC Press, 2001, 8-13.

[40] U. Schubert, N. Hüsing, Synthesis of Inorganic Materials 2nd edition, Wiley-VCH, Weinheim, 2005, 192-221

[41] J. Patscheider, *MRS Bull.*, 2003, 180.

[42] K. Nakane, N. Ogata, Y. Kurokawa, *J. Appl. Polym. Sci.*, 2006, **100**, 4320.

[43] K. W. Völger, E. Kroke, C. Gervais, T. Saito, F. Babonneau, R. Riedel, Y. Iwamoto, T. Hirayama, *Chem. Mater.*, 2003, **15**, 755.

[44] J. J. Baumberg, *Nature Mater.* 2006, **5**, 2.

[45] N. Binstead, Program for the Analysis of X-ray Absorption Spectra, version 3.33, University of Southampton, UK, 1998.

[46] K. Nakamoto, *Infrared and Raman Spectra of Inorganic Compounds, Theory and Applications in Inorganic Chemistry*, Wiley-Interscience, 1997.

[47] C. H. Winter, *Aldrich. Chim. Acta.*, 2000, **3**, 33

[48] H. C. Chen, B. H. Tseng, M. P. Houng, W. H. Wang, *Thin Solid Films*, 2003, **445**, 112.

[49] C. Mitterer, P. H. Mayrhofer, *Key Eng. Mater.*, 2004.

[50] D. J. Blackwood, *J. Corros. Rev.*, 2003, **21**, 97.

[51] G. B. Smith, A. Ben-David, P. D. Swift, *Renew. Energy*, 2001, **22**, 79.

[52] K. Leinenweber, M. O'Keefe, M. Somayazulu, H. Hubert, P. F. McMillan, G. W. Wolf, *Chem. Eur. J.*, 1999, **5**, 3076.

[53] E. Soignard, P. F. McMillan, *Chem. Mater.*, 2004, **16**, 3533.

[54] N. Binstead, Excurve 9.271, University of Southampton, UK, 2003.

[55] H. J. Holleck, *Vac. Sci. Technol. A*, 1986, **4**, 2661.

[56] Powder Diffraction File, version 2.4, International Centre for Diffraction Data, Swarthmore, PA 19073, USA, 2004.

[57] W. Spengler, R. Kaiser, A. N. Christensen, G. Müller-Vogt, *Phys. Rev. B*, 1978, **17**, 1095.

[58] G. E. Brown Jr., G. Calas, G. A. Waychunas, J. Petiau, *Rev. Miner. Geochem.*, 1988, **18**, 431.

[59] M. M. Banazak Holl, P. T. Wolczanski, G. D. Van Duyne, *J. Am. Chem. Soc.*, 1990, **112**, 7989.

[60] C. J. Carmalt, A. Newport, I. P. Parkin, P. Mountford, A. J. Sealey, S. R. Dubberley, *J. Mater. Chem.* 2003, **13**, 84.

[61] H.O. Pierson, *Handbook of Chemical Vapour Deposition: Principles, Technology, and Applications*, Noyes Publications, Park Ridge, NJ, 1992.

[62] K. H. Kim, S. H. Lee, *Thin Solid Films* 1996, **283**, 165.

[63] J. J. Baumberg, *Nature Mater.* 2006, **5**, 2.

[64] R. Rovai, C. W. Lehmann, J. S. Bradley, *Angew. Chem. Intl. Ed.* 1999, **38**, 2036.

[65] Cheng F., Kelly S. M., Clark S., Bradley J. S., Baumbach M., Schütze A., *J. Memb. Sci.*, 2006, **280**, 530.

[66] S. Kaskel, C. W. Lehmann, G. Chaplais, K. Schlichte, M. Khana, *Eur. J. Inorg. Chem.*, 2003, 1193.

[67] G. Chaplais, S. Kaskel, *J. Mater. Chem.*, 2004, **14**, 1017.

[68] A. Vioux, *Chem. Mater.* 1997, **9**, 2292.

[69] "Generalised structure analysis system", R.B. Von Dreele and A.C. Larson, Los Alamos National Laboratory, NM87545, USA (December 2002 release)

[70] GSAS manual, A.C. Larson and R.B. Von Dreele, LANSCE MS-H805, Los Alamos National Laboratory, Los Alamos NM, NM 87545, 2000

[71] "Powder Diffraction File", version 2.4, International Centre for Diffraction Data, Swarthmore, PA 19073, USA (2004).

[72] A. W. Jackson, O. Shebanova, A. L. Hector, P. F. McMillan, *J. Solid State Chem.*, 2006, **179**, 1383.

[73] K. Kohno, *J. Mater. Sci.*, 2006, **27**, 658.

[74] ; L. Wicikowski, B. Kusz, L. Murawski, K. Szaniawska, B. Susla, *Vacuum*, 1999, **54**, 221.

[75] K. Kamiya, T. Yoko, M. Bessho, *J. Mater Sci.*, 1987, **22**, 937.

[76] S. J. Henderson, A. L. Hector, *J. Solid State Chem.*, 2006, **179**, 3518.

[77] D. Farrusseng, K. Schlichte, B. Spliethoff, A. Wingen, S. Kaskel, J.S. Bradley, F. Schüth, *Angew. Chem. Intl. Ed.*, 2001, **40**, 4204.

[78] J,. G. Stark, H. G. Wallace, *Chemistry Data Book (2nd Edition)*, John Murray Publishers Ltd., 1982.

[79] D. C. Bradley, I. M. Thomas, *J. Chem. Soc.*, 1960, 3857.

[80] D. Mckay. D. H. Gregory, J. S. J. Hargreaves, S. M. Hunter, X. Sun, *Chem. Comm.*, 2007, 3051.

[81] F. Cheng, S. M. Kelly, S. Clark, J. S. Bradley, M. Baumbach, A. Schütze, *J. Membrane Sci.*, 2006, **280**, 530.

[82] L. Volpe, M. Boudart, *J. Solid State Chem.*, 1985, **59**, 332.